

Fatigue design investigation of the main- to cross-girder connection in steel railway bridges

A study on the beam railway bridges of the Oostertoegang in Amsterdam

MSc. Thesis

Kasja Romijn



Fatigue design investigation of the main- to cross-girder connection in steel railway bridges

A study on the beam railway bridges of the Oostertoegang in Amsterdam

by

Kasja Romijn

to obtain the degree of Master of Science
at the Delft University of Technology,
in Civil Engineering.

Student number: 4852281
Project duration: February, 2023 – October, 2023
Thesis committee: Prof. dr. ir. M. Veljkovic, TU Delft, Chair
Ir. D. H. Malschaert, TU Delft, Daily supervisor
Dr. ir. J. H. den Besten, TU Delft
Ir. W. P. J. Langedijk, Iv-Infra, Daily supervisor

Cover: Render of the Oostertoegang in Amsterdam [1]

An electronic version of this thesis is available at <http://repository.tudelft.nl/>.



Preface

This thesis represents my final delivery to obtain the degree of Master of Science in Civil Engineering at Delft University of Technology. It concludes my academic journey within the Structural Engineering master's program, specializing in Steel and Timber Construction. I would like to express my sincere appreciation to those who have consistently motivated me and provided guidance throughout the process of writing this thesis.

I would like to express my gratitude to the members of my graduation committee which has been composed of people from TU Delft and Iv-Infra. Firstly, I want to thank the chair of the committee, Milan Veljkovic, for the feedback and guidance during the research process. I want to express my appreciation to Henk den Besten for the insightful feedback on the report. And a special thanks to my daily supervisors David Malschaert and Walter Langedijk for creating a low threshold to ask questions, sharing their expertise, and providing feedback.

Also, I want to thank Iv-Infra for giving me the opportunity to conduct my thesis research at such a great engineering company. Thank you to my colleagues who have been instrumental in my learning journey.

Finally, I would like to acknowledge my family, boyfriend, and friends for their unconditional love and support.

Kasja Romijn
Haarlem, October 2023

Summary

Over the past few decades, the Netherlands has built numerous steel railway bridges to improve its infrastructure. The repeated loading from railway traffic makes steel bridges susceptible to fatigue damage. This may result in the premature need for either repairing or replacing the structure. The stress ranges at fatigue-prone locations are generally higher in railway bridges than in road traffic bridges [2]. Due to the limited space available due to road and rail alignment, the connection between the main girder and cross-girder is often identified as a critical fatigue location.

The main- to cross-girder connection can be designed for fatigue using different design principles. Designing the connection with a certain rotational stiffness leads to higher fatigue stresses at this location. Meeting the fatigue requirements at the connection can often be achieved by local adjustments, such as welding extra steel plates to the fatigue-induced location to evenly distribute stresses from the cross-girder to the main girder. This can be a costly solution. Designing a connection that is flexible could reduce stresses at the main- to cross-girder connection. Solving fatigue issues can be done by making global adaptations to the structure. The question arises: which aspects can be adjusted such that slight changes can notably improve fatigue resistance in a cost-effective manner?

This report focuses on the following research question: *How can the design of the connection between the main girder and cross-girder of a railway bridge be optimized for fatigue?*

To answer the research question, a literature study and a finite element investigation of the main- to cross-girder connection are performed. A reference model is made after which parameters are altered to investigate their impact on the fatigue response of the connection. The reference model is based on the design of the bridges from *project Oostertoegang*. However, instead of considering a connection with a certain rotational stiffness, the design is made more flexible for this study. *Ansys 2022 R2* [3] is used to create a finite element model of the bridge with shell elements. The hot spot stress method is used to conduct the fatigue assessment. In total four critical fatigue locations are researched for six parameters. The parameters researched are: the center-to-center distance between the cross-girders, the height of the cross-girder and main girder, the thickness of the inner web plate of the main girder, the diaphragm, and the steel deck plate.

From the analysis, it can be concluded that for one detail (M3) local measures should be applied to meet fatigue criteria. The three other details can satisfy requirements within feasible limits. The most cost-effective and realistic way is to increase the thickness of the inner web of the main girder. Other cost-effective but less feasible solutions to optimize the flexible design for fatigue are: decreasing the thickness of the diaphragm and increasing the height of the cross-girder. These parameters show the best ratio between the costs needed to alter the parameter and the total fatigue damage change of the critical detail. It is important to mention that this study exclusively examines four specific structural hot spot locations. Modifying the design for one fatigue location can be detrimental to the other.

Furthermore, it is determined that the fatigue assessment using finite element analysis with shell elements can be optimized by using the hot spot stress method in combination with modeling the weld using an increased thickness, especially according to prTS1993-1-901 guidelines [4]. This type of modeling technique shows a close resemblance to a solid model, which is the best representation of reality. Not incorporating the weld could overestimate the stresses.

Contents

Preface	i
Summary	ii
Nomenclature	v
1 Introduction	1
1.1 Background information	1
1.2 Problem statement	3
1.3 Research objectives	3
1.4 Scope	4
1.5 Methodology	4
1.6 Report outline	5
2 Literature study	6
2.1 Introduction to fatigue	6
2.2 The S-N curve	7
2.2.1 Detail categories	7
2.2.2 Cycle counting methods	9
2.2.3 Damage calculation	10
2.3 Fatigue assessment methods	10
2.3.1 Nominal stress method	11
2.3.2 Hot spot stress method	11
2.3.3 Effective notch method	14
2.4 Finite element analysis	14
2.4.1 Shell elements	15
2.4.2 Solid elements	18
2.5 Design of railway bridges	18
2.6 Fatigue load models railway bridges	22
2.6.1 Load model 71	24
2.6.2 Annex D model	25
2.7 Rotational stiffness	26
3 Methodology for parametric study	28
3.1 Reference model configuration	28
3.2 Finite element model	30
3.3 Fatigue assessment method	35
3.4 Parameters	38
3.5 Costs	41
4 Method validation and results	43
4.1 Validation of the method for parametric study	43
4.1.1 Weld modeling technique	43
4.1.2 Hand calculation versus Iv-Tool	44
4.2 Results of the parametric study	44
4.2.1 The type and location of the diaphragm	44
4.2.2 The center-to-center distance between the cross-girders	45
4.2.3 The height of the cross-girder	49
4.2.4 The height of the main girder	50
4.2.5 The thickness of the inner web of the main girder	53
4.2.6 The thickness of the diaphragm	55
4.2.7 The thickness of the steel deck plate	56

4.3	Results of additional fatigue detail	58
4.4	Design recommendations for bridges project Oostertoegang	58
5	Conclusion and recommendations	60
5.1	Conclusion	60
5.2	Recommendations for further research	61
	References	62
A	Fatigue detail categories	65
B	Rainflow counting Iv-Tool	68
C	Verification modeling technique	70
D	Hand calculation versus Iv-Tool	78
E	Deformed shapes	83
F	Results fatigue detail M3	98

Nomenclature

Abbreviations

Abbreviation	Definition
2D	Two-dimensional
3D	Three-dimensional
APDL	Ansys Parametric Design Language
CAFL	Constant Amplitude Fatigue Limit
COL	Cut-Off-Limit
C-T-C	Center-To-Center
FE	Finite Element
FEA	Finite Element Analysis
FEM	Finite Element Method
HSS	Hot Spot Stress
IIW	International Institute of Welding
LM71	Load Model 71
NB	Nationale Bijlage; National Annex
OSD	Orthotropic Steel Deck
OVS	Ontwerpvoorschriften Prorail
ROK	Richtlijnen Ontwerp Kunstwerken
SSR	Sum Squared Regression
SST	Total Sum of Squares

Symbols

Symbol	Definition
a	The distance between rail support points
D	The total damage value
E	The elastic modulus
I_b	The second moment of area of the beam
I_c	The second moment of area of the column
K_b	The mean value of I_b/L_b for all beams at the top of that "storey"
K_c	The mean value of I_c/L_c for all columns in that "storey"
k_f	A stress concentration factor
L	The span length
L_ϕ	The determinant length
L_b	The span of the beam
L_c	The storey height of a column
m	The slope of the curve
N	The number of load cycles
n_0	The first natural bending frequency of the bridge loaded by permanent actions
n_i	The design number of cycles applied at the i^{th} stress level $\Delta\sigma_i$
N_i	The number of load cycles to failure corresponding to $\Delta\sigma_i$
n_r	The first natural torsional frequency of the bridge loaded by permanent actions
Q_{vi}	The point force on each rail due to LM71 or a wheel load of a Fatigue Train
r	The effective notch radius
R^2	The coefficient of determination
$S_{j,ini}$	The initial rotational stiffness
t	The thickness of the plate
V	The maximum line speed at the site
v	The maximum permitted vehicle speed
γ_{Ff}	The partial factor for equivalent constant amplitude stress ranges
γ_{Mf}	The partial factor for fatigue strength $\Delta\sigma_C$
δ	The element size
δ_0	The deflection at midspan due to permanent actions
$\Delta\sigma$	The stress range (direct stress)
$\Delta\sigma_{71}$	The stress range caused by Load Model 71 without the α -factor
$\Delta\sigma_{hs}$	The hot spot stress
$\Delta\sigma_{nlp}$	The non-linear peak stress
$\Delta\sigma_x$	The normal stress in local x-direction
$\Delta\sigma_b$	The bending stress
$\Delta\sigma_C, \tau_C$	The reference value of the fatigue strength at $N_c = 2 \cdot 10^6$ cycles
$\Delta\sigma_D$	The constant amplitude fatigue limit at the number of cycles N_D
$\Delta\sigma_i$	The design stress range
$\Delta\sigma_L, \tau_L$	The cut-off limit at the number of cycles N_L
$\Delta\sigma_m$	The membrane stress
λ	The damage equivalence factor for fatigue
λ_{max}	The maximum value taking account of the fatigue limit
λ_1	The factor for the damage effect of traffic
λ_2	The factor for the traffic volume
λ_3	The factor for the design life of the bridge
λ_4	The factor for the structural element is loaded by more than one track
τ_{xy}	The shear stress
ϕ	The dynamic factor

1

Introduction

This chapter is comprised of an introduction to fatigue at railway bridges and fatigue assessment methods. Moreover, the problem statement, research objectives, scope, methodology, and outline of the report are described.

1.1. Background information

In recent decades, the Netherlands has constructed several steel railway bridges to enhance its infrastructure. Examples of recently built railway bridges are the Zandhazenbrug (2016), Bert Swartbrug (2017), Vleutensespoorbrug 2 (2018), and the two railway bridges part of Theemswegtracé (2020).

The repetitive loading from road and/or railway traffic makes steel bridges vulnerable to fatigue-induced damage. Fatigue is a phenomenon whereby cyclic loading induces cracking or even fracture within steel structures [5]. This can lead to the early repair or replacement of the structure. The stress range within joints in the structure is often a major factor. The stress range in railway bridges is generally higher than in road bridges [2]. Haghani et al. [6] collected a total of more than 100 fatigue damage cases in existing steel bridges and categorized it on detail type, see Figure 1.1. It can be concluded that the connection between the main girder and the cross-girder followed by the diaphragm are common areas prone to fatigue-related issues in steel bridges. Diaphragms, in this report, are stiffener plates positioned within the main girders to transform shear forces from the cross-girders into torsional forces and contribute to the stability of the main girders.

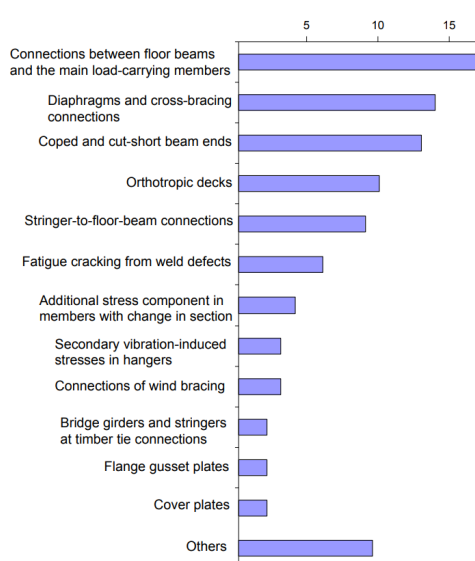


Figure 1.1: Fatigue damage cases categorized on detail type [6]

Furthermore, in the design of the Zandhazenbrug and the Vleutensespoorbrug 2, the welded connection between the main girder and the cross-girder has been identified as a critical fatigue detail [7][8]. Figure 1.2 and Figure 1.3 exhibit technical drawings of the Zandhazenbrug and Figure 1.4 and Figure 1.5 of the Vleutensespoorbrug 2. Both railway bridges are arch bridges, however, the Zandhazenbrug has diagonal hangers while the Vleutensespoorbrug 2 has vertical hangers, which results in different behaviors. Both bridges consist of two railway tracks and a steel-concrete deck in combination with a ballast bed. The thickness of the steel-concrete deck is 400 [mm] and 370 [mm] for the Zandhazenbrug and Vleutensespoorbrug 2, respectively. The cross-girders of the Zandhazenbrug span 11.5 meters and have a center-to-center distance of 1.6 [m]. For the Vleutensespoorbrug 2, the cross-girder span is 9 meters and the center-to-center distance is 3.5 [m].

The connection between the main girder and cross-girder of the Zandhazenbrug is designed with other principles than the Vleutensespoorbrug 2 to meet specific fatigue criteria. For the Zandhazenbrug, the height of the steel-concrete deck was restricted due to road and rail alignment. High local stress ranges are measured at the main- to cross-girder connection. To reduce those stresses, the center-to-center distance between the cross-girders is made smaller. Furthermore, an additional plate is welded into the main girder in alignment with the upper flange of the cross-girders to satisfy fatigue requirements. As a result, the connection has a certain rotational stiffness. On the contrary, the main- to cross-girder connection of the Vleutensespoorbrug 2 is made as flexible as possible to reduce the clamping moments. These moments influence the fatigue stresses at the connection. To enhance the flexibility of the connection, the diaphragms are designed with a specific configuration. The extent to which the diaphragm is attached to the inner web of the main girder is restricted in length. In addition, the height of the main girder is increased and the main girder inner web plate is decreased to 15 [mm], to gain more flexibility and meet fatigue criteria.

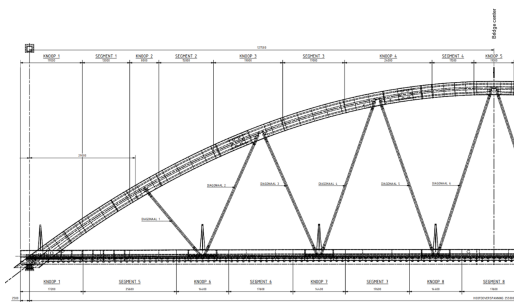


Figure 1.2: Overview Zandhazenbrug, half of the bridge [mm] [lv-Infra]

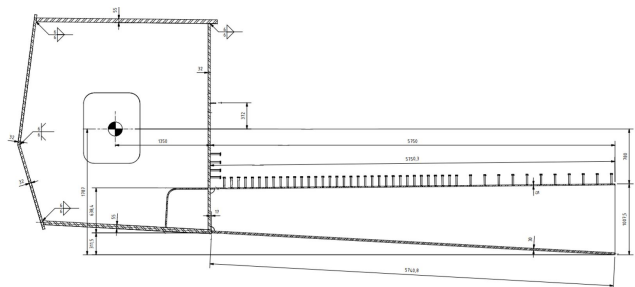


Figure 1.3: Cross-section Zandhazenbrug (half) [mm] [lv-Infra]

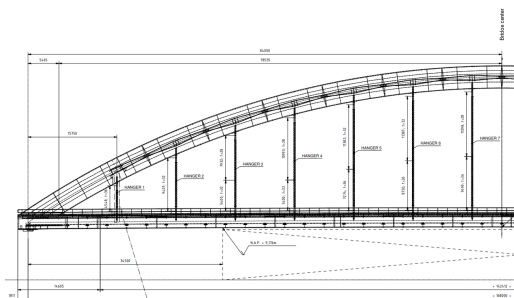


Figure 1.4: Overview Vleutensespoorbrug 2, half of the bridge [mm] [lv-Infra]

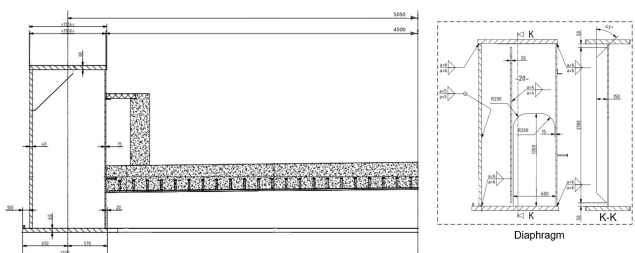


Figure 1.5: Cross-section Vleutensespoorbrug 2 (half) [mm] [lv-Infra]

Multiple guidelines and standards are available for fatigue assessment, including Eurocode 3 part 1-9 [9] and the International Institute of Welding (IIW) [10]. These guidelines are created based on an extensive series of experiments performed on multiple connection details. These details are assigned to detail categories which are used in combination with so-called S-N curves to determine the expected

fatigue life of the structure. Detail categories are created for basic connection types.

In the Netherlands, ProRail defined additions to Eurocode for railway structures, called the OVS [11]. Similarly, Rijkswaterstaat created a document with additional guidelines to Eurocode for civil artworks, ROK2.0 [12]. Should ROK be found applicable to railway bridges and be in contradiction with the OVS, precedence is granted to the OVS guidelines [11]. While there is freedom in the structural design of railway bridges, ProRail often mandates the integration of a ballast bed in railway bridge designs. This reduces sound emissions and in the event of damage to the railway bridge, the track can be restored through adjustments to the ballast bed. For this reason, a supporting deck is needed beneath the ballast which can be made from e.g. concrete or steel.

To ascertain the stresses in structural elements, finite element (FE) models are commonly used. Diverse methodologies for fatigue assessment have been established to determine the stress ranges in (complex) details: (modified) nominal stress method, hot spot stress method, and the effective notch method. Each methodology has its advantages and disadvantages. The modeling technique does also influence the results. Engineering firms often use the nominal stress or hot spot stress method because fatigue assessment can be relatively fast achieved with an acceptable level of accuracy.

1.2. Problem statement

During the design process of the Zandhazenbrug and the Vleutensespoorbrug 2, the engineering company Iv-Infra noticed that the connection between the main girder and the cross-girder is often a critical fatigue detail (see Figure 1.3 and Figure 1.5). Train passages cause large stress ranges in the connection and in addition substantial dynamic factors should be accounted for. Almost all conceivable structural design parameters could affect the stress distribution between fatigue-prone details.

Often, during the design process of a (railway) bridge, it turns out to be necessary to incorporate specialized detailing at the main- to cross-girder connection to meet fatigue requirements. For example, this can be achieved by incorporating additional plates at the connection. These additional plates are welded at critical fatigue locations to evenly distribute stresses from the cross-girder to the main girder. However, the extra welding involved is costly and introduces additional fatigue-prone areas in the bridge's structure. Moreover, the addition of extra plates and thicknesses at the connection makes the connection more stiff. A stiffer connection attracts more force and deforms less, which is not always beneficial for fatigue.

Iv-Infra is intrigued by the prospect of developing a main- to cross-girder connection that minimizes the need for additional welded plates to reduce costs. This can be achieved by the creation of a more flexible connection design, as is accomplished in the design of the Vleutensespoorbrug 2 [8]. Flexible connections take a minimum of bending moments and only transfer shear forces, so stresses at the main- to cross-girder connection can be reduced. However, to create a flexible connection that satisfies fatigue requirements, sometimes additional adjustments should be made to the design of bridge elements to influence the stress distribution within the connection. A challenge occurs due to the limited space available caused by road and railway alignment. So, if the fatigue strength of a "flexible" design is insufficient, the question arises: which design aspects can be adjusted such that slight changes can notably improve fatigue resistance in a cost-effective manner?

1.3. Research objectives

The primary objective of the research is to determine which design considerations can increase the estimated fatigue life of a flexible connection while minimizing the necessity of adding extra welded plates to the connection. In this way, in the early design phase, parties who design railway bridges can determine if it is feasible within the physical restrictions to achieve a flexible connection. Such a connection requires less welding, which is cost-advantageous when you consider that this detail occurs more frequently in the design of a bridge.

The main research question is:

- *How can the design of the connection between the main girder and cross-girder of a railway bridge be optimized for fatigue?*

The main research question will be answered with the following sub-questions:

- *What fatigue assessment method is most suitable to use with finite element modeling using shell elements?*
- *What are critical fatigue locations of a welded main- to cross-girder connection?*
- *Which design considerations (parameters) are cost-effective in improving the fatigue performance of the main- to cross-girder connection of a railway bridge?*

1.4. Scope

The research focuses on the fatigue assessment of the connection between the main girder and cross-girder in steel railway bridges. Only beam bridges whose design is based on cross-girders attached to main girders with a weld are considered. The most critical fatigue details of the connection will be determined and focused on. Other potential fatigue-prone details in the bridge will be disregarded in the study, even though these can be critical.

Furthermore, the study exclusively examines the fatigue response of the beam railway bridges designed for *project Oostertoegang* at Amsterdam Central Station by Iv-Infra. Originally, these bridges were designed with a main- to cross-girder connection with a certain rotational stiffness and it will be researched how the bridge responds to a flexible connection design. This limits the research to a steel railway bridge with rectangular box main girders and I-profile cross-girders with an orthotropic steel deck. Moreover, this bridge does not contain an arch or truss structure.

The scope will be exclusively on the fatigue assessment. The strength and stability of the bridge will be disregarded within the scope. The fatigue assessment is based on European guidelines and Dutch national regulations and will be performed using finite element analysis, no experiments will be conducted.

1.5. Methodology

To answer the research question a literature study and a finite element assessment of the main- to cross-girder will be performed. The literature study will be conducted to gather relevant background information. This encompasses details regarding fatigue assessment, finite element analysis, and fatigue in railway bridges. Thereafter, a reference model is determined after which parameters will be altered to investigate their impact on the fatigue response of the main- to cross-girder connection. This reference model will be based on the bridges for *project Oostertoegang*. Currently, Iv-infra is working on project Oostertoegang. Within the project, the 15 railway bridges on the eastern side of Amsterdam Central Station will be replaced one by one from 2024 onwards [1]. *Ansys® 2022 R2* [3] will be used to create a finite element model of the bridge with shell elements. A pre-existing study performed by Pandit [13] will be used to validate the (weld) modeling technique used. It will be determined which fatigue locations at the connection are most critical and which parameters could influence the stresses at these locations. The hot spot stress method will be used to conduct the fatigue assessment. The parametric study will ascertain the impact of the identified parameters on the fatigue damage at the identified critical locations. Moreover, the parameters are compared on the costs associated with improving fatigue performance.

1.6. Report outline

The report is structured into several chapters. The contents of the chapters are outlined below.

- **Chapter 1:** Provides an introduction to the master thesis.
- **Chapter 2:** Presents the literature study for the thesis, offering relevant background information and previous research. It covers an introduction to fatigue and the S-N curve, discusses various fatigue assessment methods, and provides insights into finite element analysis. In addition, the design of railway bridges and fatigue in railway bridges will be focused on. Lastly, the determination of the rotational stiffness will be discussed.
- **Chapter 3:** Describes the methodology to answer the research questions of the report. A parametric study based on a reference model will be done. The reference model is based on the design of the bridges of *project Oostertoegang*. Parameters that will influence fatigue critical details at the connection between the main girder and cross-girder will be researched. A finite element model of the reference design is made in *Ansys® 2022 R2* [3] for conducting the fatigue assessment. The fatigue assessment will be performed with the hot spot stress method.
- **Chapter 4:** The methodology of the parametric study is validated for certain choices made, and the results of the fatigue assessment for all parameters are provided and discussed. In addition, recommendations for the fatigue design of the bridges from project Oostertoegang are provided.
- **Chapter 5:** Answers the research question based on the research performed. In addition, it offers recommendations for further research.
- **Appendices A-F:** Contains additional information to the content of the chapters.

2

Literature study

In this chapter, a literature study is performed covering an introduction to fatigue, the S-N curve, fatigue assessment methods, finite element analysis, design of railway bridges, fatigue load models for railway bridges, and rotational stiffness.

2.1. Introduction to fatigue

Fatigue is the phenomenon that causes cracking or fracture in steel structures due to cyclic loading. In steel bridges, this repetitive loading is caused by traffic. The magnitude of the stress range is an important factor for fatigue. Generally, the stress ranges in railway bridges are higher than those found in road bridges [2].

The ASM Handbook gives the following definition of fatigue:

”Fatigue is the progressive, localized, and permanent structural change that occurs in a material subjected to repeated or fluctuating strains at nominal stresses that have maximum values less than (and often much less than) the tensile strength of the material. Fatigue may culminate into cracks and cause fracture after a sufficient number of fluctuations.” [5]

Fatigue can be divided into three crack development stages: the crack initiation period, the crack propagation period, and the final fracture. An overview of the fatigue phases is shown in Figure 2.1. During the crack initiation period, inconspicuous microscopic cracks start to form in slip bands at stress levels below the yield limit [14]. The cracks are formed due to an increase in stress concentration caused by the presence of geometric irregularities in the detail, the geometry of the weld, and local weld effects [15]. In the crack propagation period, the microscopic cracks proceed with growing until failure, on a macroscopic scale [14]. Influencing factors are material quality and environmental conditions. At the point of final failure, the crack will grow unstable.

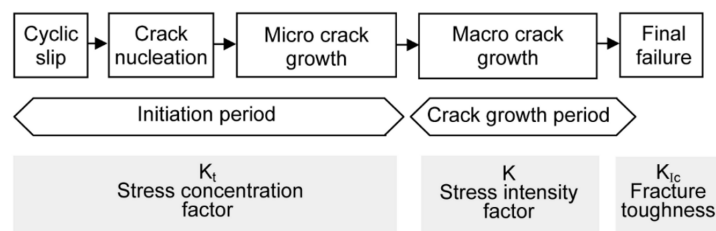


Figure 2.1: Phases of fatigue life [14]

2.2. The S-N curve

To determine the fatigue performance of a steel structure, the fatigue life of every structural detail must be evaluated [16]. The resistance of a detail is represented by the S-N curve or Wöhler curve. The S-N curve is based on the experimental results in which specimens are tested under constant amplitude loading [17]. To derive the fatigue curve, the number of cycles until failure for each specimen is measured and plotted on a double logarithm scale. On the horizontal axis the number of cycles until failure (N) is shown and on the vertical axis the stress range ($\Delta\sigma$). The experimental result shows a large scatter of data, e.g. see Figure 2.2. A survival probability of 95% is set by Eurocode 3 part 1-9, based on the mean value, to determine the characteristic curve.

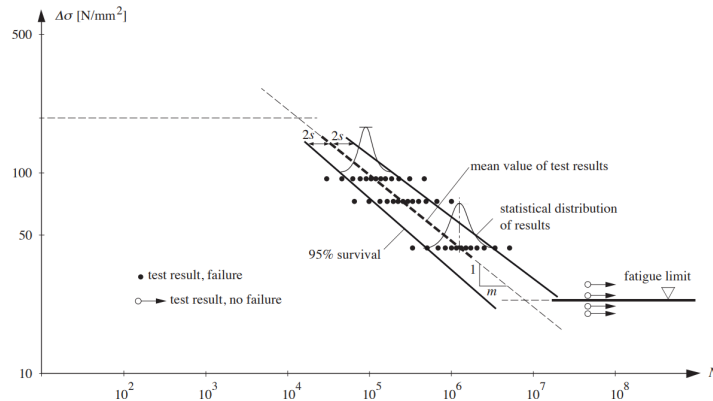


Figure 2.2: S-N curve from fatigue test results, plotted in double logarithm scale, by constant amplitude loading [17]

2.2.1. Detail categories

NEN-EN 1993-1-9 [9] and International Institute of Welding (IIW) [18] defined detail categories based on the characteristic curve of experimental results. Detail categories are determined for standardized commonly used joints. A fatigue detail category illustrates the stress range of failure when $N = 2 \cdot 10^6$ load cycles are applied.

The detail category accounts for several influencing factors that are not considered in the design stress of the fatigue assessment. Two of these effects are weld imperfections and the residual stresses due to welding. In addition, the effect of the geometry of the detail and the weld geometry can be incorporated into the detail category. It depends on the fatigue assessment method used if these are considered in the design stress or the detail category, see Section 2.3.

Direct stresses

Figure 2.3 shows the S-N curve for several (nominal stress) detail categories [9]. In this figure, three points are highlighted, namely:

1. The fatigue detail category $\Delta\sigma_C$ corresponding with $N_C = 2 \cdot 10^6$ load cycles
2. The constant amplitude fatigue limit (CAFL) $\Delta\sigma_D$ corresponding with $N_D = 5 \cdot 10^6$ load cycles
3. The cut-off-limit (COL) $\Delta\sigma_L$ corresponding with $N_L = 10^8$ load cycles

The fatigue life of a detail is infinite if stress ranges with a constant amplitude are applied and are below the CAFL. If the stress ranges applied have a non-constant amplitude, the fatigue life is infinite if the stress ranges are below the COL.

For nominal stress ranges, the slope of the curve between point 1 ($\Delta\sigma_C$) and point 2 ($\Delta\sigma_D$) is equal to $m = 3$ and between point 2 and point 3 ($\Delta\sigma_L$) is equal to $m = 5$. The constant amplitude fatigue limit can be calculated with Formula 2.1 and the cut-off-limit with Formula 2.2 [9].

$$\Delta\sigma_D = \left(\frac{2}{5}\right)^{\frac{1}{3}} \cdot \Delta\sigma_C \quad (2.1)$$

$$\Delta\sigma_L = \left(\frac{5}{100}\right)^{\frac{1}{5}} \cdot \Delta\sigma_D \quad (2.2)$$

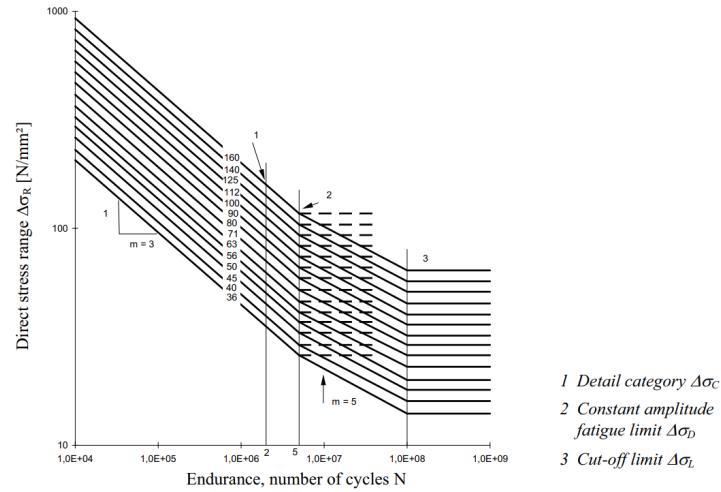


Figure 2.3: Fatigue strength curve for direct stress ranges according to NEN-EN 1993-1-9 [9]

The design number of load cycles until failure (N_i) for a certain design stress range $\Delta\sigma_i$ can be determined with Formula 2.3.

$$N_i = \begin{cases} 2 \cdot 10^6 \cdot \left(\frac{\Delta\sigma_C}{\Delta\sigma_i}\right)^3 & \text{if } \Delta\sigma_i \geq \Delta\sigma_D \\ 5 \cdot 10^6 \cdot \left(\frac{\Delta\sigma_D}{\Delta\sigma_i}\right)^5 & \text{if } \Delta\sigma_D > \Delta\sigma_i \geq \Delta\sigma_L \\ \infty & \text{otherwise} \end{cases} \quad (2.3)$$

Shear stresses

The fatigue strength curve for shear stresses for two detail categories is shown in Figure 2.4 [9]. The slope of the curve between point 1 (τ_C) and point 2 (τ_L) is equal to $m = 5$. The cut-off-limit ($\Delta\tau_L$) at $N_L = 10^8$ load cycles can be calculated with Formula 2.4.

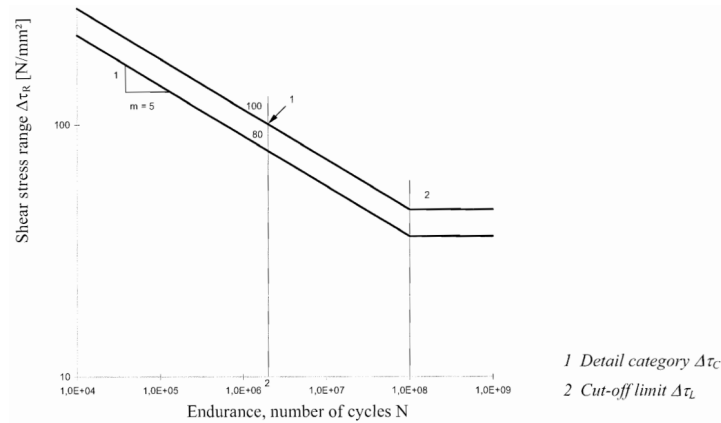


Figure 2.4: Fatigue strength curve for shear stress ranges according to NEN-EN 1993-1-9 [9]

$$\Delta\tau_L = \left(\frac{2}{100}\right)^{\frac{1}{5}} \cdot \Delta\tau_C \quad (2.4)$$

The design number of load cycles until failure (N_i) for a certain design shear stress range $\Delta\tau_i$ can be determined with Formula 2.5.

$$N_i = \begin{cases} 2 \cdot 10^6 \cdot \left(\frac{\Delta\tau_C}{\Delta\tau_i}\right)^5 & \text{if } \Delta\tau_i \geq \Delta\tau_L \\ \infty & \text{otherwise} \end{cases} \quad (2.5)$$

2.2.2. Cycle counting methods

Real structures rarely experience constant amplitude loading. In order to use the S-N curve, a cycle counting method must be applied to reduce the complex irregular loading history to a series of regular load cycles organized by amplitude [19]. There are different types of cycle counting methods. According to NEN-EN 1993-1-9 [9], the rainflow method and the reservoir method are recommended to count the cycles for welded components. Other methods are, for example, peak counting, level-crossing counting, and range-pair counting [20]. The rainflow method and the reservoir method will be discussed in further detail. The results for those methods are the same if the methods are used in the right manner [10].

Rainflow method

Matsuishi, M. and Endo, T. first introduced the rainflow method in 1968 [21]. In 1982, S.D. Downing and D.F. Socie published a version of the rainflow counting algorithm which is utilized more widely [19]. I. Rychlik defined a new mathematical definition of the rainflow cycle algorithm, in 1987 [22].

The rainflow method is based on the principle of rain dripping from a pagoda roof. The load history is rotated by 90 degrees. The first extreme (maximum/minimum) point is defined as point A, see example Figure 2.5. A half-cycle can be counted each time the water stream:

- Falls from a maximum point (e.g. Figure 2.5: Stream A-D)
- Falls from a minimum point (e.g. Figure 2.5: Stream B-C)
- Is interfered by another water stream from above (e.g. Figure 2.5: Stream C-B)
- Is at the end of the cycle history (e.g. Figure 2.5: Stream D-A)

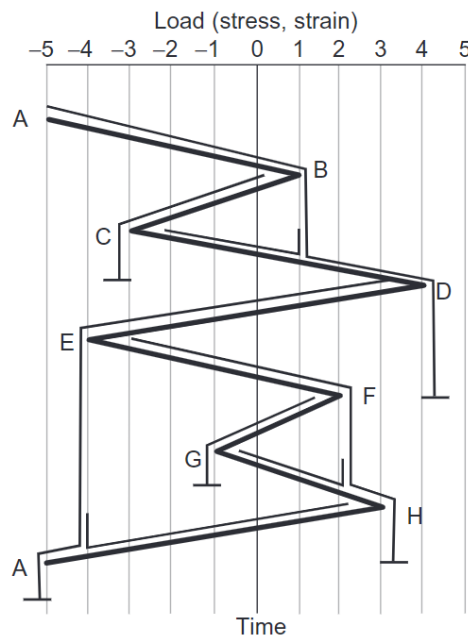


Figure 2.5: Illustration of the rainflow cycle counting method [23]

The counted cycles from Figure 2.5 are shown in Table 2.1.

Table 2.1: Rainflow cycle counts based on Figure 2.5 [23]

No. of full cycles	From	To	Range	Mean
1	A	D	9	-0.5
1	B	C	4	-1
1	E	H	7	-0.5
1	F	G	3	0.5

Reservoir method

The reservoir counting method is based on the principle of the flow of water from a reservoir [10]. First, the "reservoir" is filled with "water", where the greatest depth is the largest load cycle. To determine the second load cycle, the second largest depth is drained. The process is repeated until all water is drained.

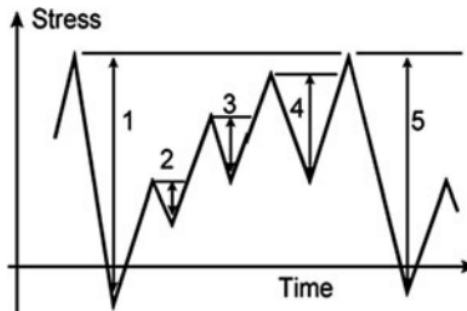


Figure 2.6: Illustration of the reservoir cycle counting method [10]

2.2.3. Damage calculation

The Palmgren-Miner cumulative damage rule is used to determine the total damage (D) of load cases with different amplitudes. The damage can be calculated with Formula 2.6 [9]. The damage value differs from 0 to 1, where 0 refers to the undamaged situation and 1 to the damaged situation. If the damage value is larger than 1, it is expected that fatigue damage will occur.

$$D = \sum_{i=1}^n \frac{n_i}{N_i} \leq 1 \quad (2.6)$$

where:

D = the total damage value

n_i = the design number of cycles applied at the i^{th} stress level $\Delta\sigma_i$

N_i = the number of load cycles to failure corresponding to $\Delta\sigma_i$

i = the number of stress levels in the spectrum

2.3. Fatigue assessment methods

Different fatigue assessment methods are established to determine the stress range which can be used to determine the fatigue resistance based on S-N curves. These methods are: the (modified) nominal stress method, the hot spot stress method, and the effective notch method [10]. Eurocode 3 part 1-9 describes the (modified) nominal stress method and the hot spot stress method [9]. The nominal stress method is commonly applied to determine the fatigue life of a simple detail. If the detail is more complicated, it is recommended to use the hot spot stress method [24]. The effective notch method is not included in NEN-EN 1993-1-9 but is described by the document of the International Institute of Welding [10].

Figure 2.7 shows the distribution of the stress for different methods. Each method considers different factors in the design stress. If an influencing factor is not considered in the stress, it is considered in the detail category.

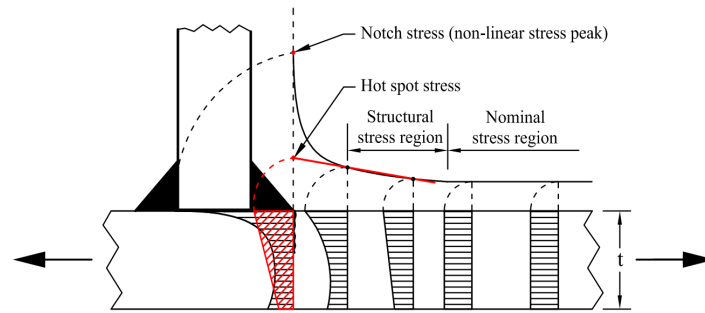


Figure 2.7: Stresses for different fatigue assessment methods [25]

2.3.1. Nominal stress method

The nominal stress method considers only the nominal stresses to determine the fatigue life of the considered detail. This method considers the macro geometrical effects due to the design of the connection but does not include the effects of the weld geometry and the notch effect due to the weld toe transition [10]. The residual stresses due to welding and the weld imperfections are included in the detail category, which is also the case for the other assessment methods.

Axial or angular misalignments that influence stress concentrations should be considered. These are already partly covered in the detail category. However, if these misalignments exceed the already covered amount, an additional stress concentration factor k_f should be applied. This factor should be multiplied by the nominal stress to determine the modified nominal stress [9].

2.3.2. Hot spot stress method

The hot spot stress (HSS) is determined by the extrapolation of stresses, using reference points, to the weld toe. The HSS method is restricted to the fatigue analysis of the weld toe. The method is not suitable for cases where the crack will grow from the weld root and propagate in the weld throat [26]. The hot spot stress method considers besides the macro geometrical effects of the connection design, the discontinuities due to the weld geometry [10]. The notch effect due to the weld toe transition is not taken into account in the design stress but it is in the detail category. NEN-EN 1993-1-9 [9] includes hand calculation of the HSS. When finite element modeling is used, the IIW provides recommendations [18].

Figure 2.8 shows the non-linear stress distribution along the plate thickness at the weld joint. The stress can be separated into three stress elements: the membrane stress (σ_m), the shell bending stress (σ_b), and the non-linear peak stress (σ_{nlp}). The hot spot stress accounts only for the geometry of the connection, σ_m and σ_b , and not for the local weld effects σ_{nlp} [18].

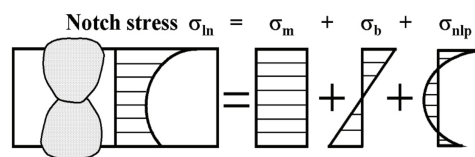


Figure 2.8: Non-linear stress distribution across the plate thickness [26]

If finite element modeling is used, very high stresses are measured at the location of the weld toe due to singularities. These singularities are unrealistic, so extrapolation at defined points from the weld notch is used to determine the hot spot stress. The local effect at the notch is negligible at a distance of approximately $0.4t$ from the weld toe [18].

There are two different types of hot spots: type a and type b. For type a, the weld is located on the plate surface, and for type b, the weld is located on the plate edge. For type a weld, the reference points to determine the HSS are dependent on the plate thickness. For type b welds, the thickness of the plate is not relevant to determine the HSS, so fixed reference points are defined [18]. This is illustrated in

Figure 2.9.

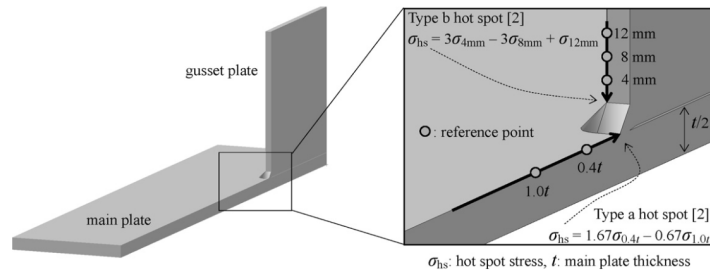


Figure 2.9: Definitions of hot spot stresses [27]

The IIW gives recommendations to use the hot spot method in combination with finite element modeling, see Table 2.2. The mesh size and extrapolation points can be determined, based on the element types used, shell or solid, and the weld type, a or b. If a coarse mesh is applied, linear extrapolation is used. When a fine mesh is applied, both linear and quadratic extrapolation is possible, dependent on the weld type [18]. An overview of the extrapolation formulas is shown in Table 2.3.

Table 2.2: Recommendations hot spot method, mesh and extrapolation points [10]

Type of model and weld toe		Relatively coarse models		Relatively fine models	
		Type a	Type b	Type a	Type b
Element size	Shells	t x t max t x w/2 ^{*)}	10 x 10 mm	≤ 0.4 t x t or ≤ 0.4 t x w/2	≤ 4 x 4 mm
	Solids	t x t max t x w	10 x 10 mm	≤ 0.4 t x t or ≤ 0.4 t x w/2	≤ 4 x 4 mm
Extrapolation points	Shells	0.5 t and 1.5 t mid-side points ^{**)}	5 and 15 mm mid-side points	0.4 t and 1.0 t nodal points	4, 8 and 12 mm nodal points
	Solids	0.5 and 1.5 t surface center	5 and 15 mm surface center	0.4 t and 1.0 t nodal points	4, 8 and 12 mm nodal points

^{*)} w = longitudinal attachment thickness + 2 weld leg lengths
^{**)} surface center at transverse welds, if the weld below the plate is not modelled (see left part of fig. 2.2-11)

Table 2.3: Hot spot stress extrapolation formulas [10]

	Relatively coarse models	Relatively fine models
Type a	$\sigma_{hs} = 1.50 \cdot \sigma_{0.5(t)} - 0.50 \cdot \sigma_{1.5t}$	$\sigma_{hs} = 1.67 \cdot \sigma_{0.4t} - 0.67 \cdot \sigma_{1.0t}$
Type b	$\sigma_{hs} = 1.50 \cdot \sigma_5 - 0.50 \cdot \sigma_{15}$	$\sigma_{hs} = 3 \cdot \sigma_4 - 3 \cdot \sigma_8 + \sigma_{12}$

Other structural stress methods

In literature, other structural stress methods are proposed and some will be discussed below.

One-point hot spot stress method

Another more simplified, structural stress method is suggested by Fricke [28], called the one-point hot spot stress method. With this method, the hot spot stress is determined at 0.5t from the weld toe. No extrapolation is needed. Several studies show promising results when this method is evaluated to other fatigue testing methods [28][29]. However, to get a value that match fatigue test results more, the HSS stress gathered from the one-point hot spot stress method should be multiplied by 1.12, see Figure 2.10.

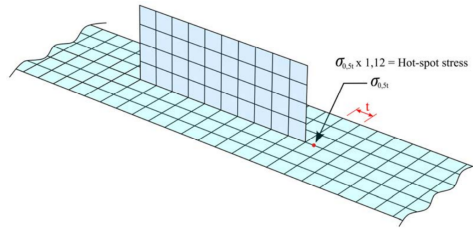


Figure 2.10: One-point hot spot stress method [30]

One-millimeter stress method

Xiao and Yamada [31] presented a method to determine the geometric stress, the one-millimeter stress method. This method is based on the stress 1 [mm] below the surface of the weld toe. Both, the geometry and the local effect of the weld are considered. However, there are some limitations to this method. One is that it can only be used with a solid element model (Section 2.4.2) because the thickness of the plate must be modeled. Furthermore, it cannot be applied to a combination of normal and bending stresses. The method can only be used when exclusively normal stresses are present.

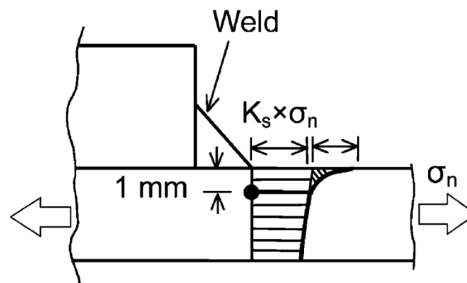


Figure 2.11: One-millimeter stress method [31]

Traction force method by Dong

Dong [32] proposed another method to determine the stress at the weld toe location. As stated before (Figure 2.8), the structural stress consists of a membrane component σ_m and a bending component σ_b . Two reference planes are defined: section A-A in the local y -direction at the location of the weld toe and section B-B in the local y -direction at the distance δ in the x -direction of the weld toe, see Figure 2.12. At the location of section B-B, the singularity at the location of the weld toe is of less influence. Considering equilibrium between the sections A-A and B-B, the structural stress components can be determined with Formula 2.7 for plane B-B (force equilibrium) and Formula 2.8 for plane A-A (moment equilibrium). If δ is small or transverse shear is negligible, σ_m and σ_b can be determined directly at section A-A. This method is claimed to be mesh-sensitive.

$$\sigma_m = \frac{1}{t} \int_0^t \sigma_x(y) \cdot dy \quad (2.7)$$

$$\sigma_m \cdot \frac{t^2}{2} + \sigma_b \cdot \frac{t^2}{6} = \int_0^t \sigma_x(y) \cdot y \cdot dy + \delta \int_0^t \tau_{xy}(y) \cdot dy \quad (2.8)$$

where:

- t = the thickness of the plate
- δ = the element size
- τ_{xy} = the shear stress
- σ_x = the normal stress in local x -direction

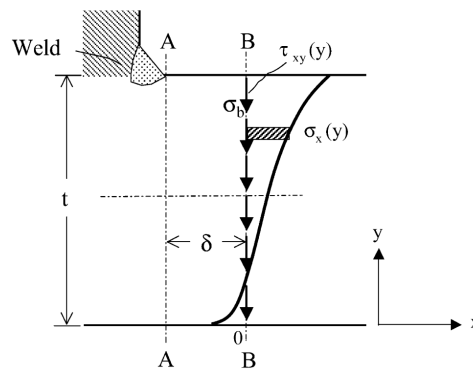


Figure 2.12: Dong method [32]

2.3.3. Effective notch method

The effective notch method does include the geometrical effects of the connection, the weld geometry, and the notch effect due to the weld toe transition in the determination of the design stress. The assessment method can be used for both cracks propagating from the weld root and weld toe. The effective notch method is not included in Eurocode, but the IIW gives recommendations. If finite element modeling is used, stress singularities occur at the location of the weld toe and weld root transitions. An effective notch radius of $r = 1$ [mm] is applied at these locations, see Figure 2.13. The effective notch stress is compared with a single S-N curve to determine the fatigue strength of any detail [10].

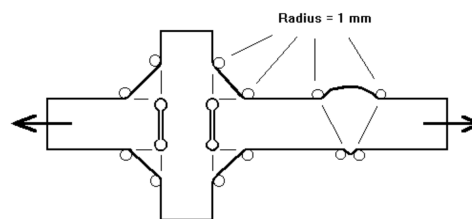


Figure 2.13: Effective notch method radius [10]

The effective notch method recommendations described by IIW are limited to a plate thickness of $t \geq 5$ [mm]. It is recommended to model the weld with a flank angle of 30° for butt welds and 45° for fillet welds. Table 2.4 shows the recommended element sizes around the notch when using finite element modeling for a notch radius of $r = 1$ [mm]. The effective notch stress is compared with one single detail category of 225 [MPa]. The slope from the S-N curve has a constant value of $m = 3$ until $N = 10^7$ cycles. Thereafter, the slope is $m = 22$ [10].

Table 2.4: Effective notch element size around the notch [10]

Element type	Element size [mm]
Quadratic	≤ 0.25
Linear	≤ 0.15

2.4. Finite element analysis

A Finite Element Analysis (FEA) is performed to approximate the behavior of an object under various physical conditions. Finite Element Method (FEM) is a numerical method for solving partial differential equations. The finite element program solves a problem by dividing the object into small parts, finite elements [33]. The results are, for example, the stress or displacement of the element under considered physical conditions. The element size used for the model is important when fatigue assessment is performed, as mentioned in 2.3. Different element types can be used to perform the analysis: shell and solid elements. These element types will be further investigated.

2.4.1. Shell elements

Shell or plate elements are two-dimensional (2D) elements that give a good approximation of the results if the thickness-to-length ratio of the element is substantially small. When a finite element model is created with shell elements, the mid-plane of the structural element is modeled. The thickness of the element is inserted as a property. In this case, it is assumed that transverse shear deformation is not important. Because fewer mesh elements are modeled, the computational time will decrease. However, the results do not consider the influence of the variation throughout the thickness of the element, which can give inadequate results [10].

Shell elements can be triangular or quadrilateral. If the shape of the element is irregular or curved, triangular elements are beneficial. First-order triangular elements have 3 nodes, one at each corner, while quadrilateral elements have 4 nodes. A second-order shell element (quadratic) has midpoints on each side. Resulting in 6 and 8 nodes for triangular and quadrilateral elements, respectively. Higher-order elements are also possible. Higher-order elements will result in a more accurate approximation [34].

For simplification of the model, the welds are not modeled in all cases. However, in some cases, it might be important. For example, when the results are affected by local bending [10]. Some modeling techniques to represent the stiffness of the weld that is developed will be discussed below.

Increased thickness

In the IIW recommendations for the structural hot spot stress approach, a modeling technique to include the weld in a shell model is described [18]. With this method, the thickness of the plate at the location of the weld is increased by the weld leg length. The height of the region which has an increased thickness corresponds to the sum of the weld leg length and half the thickness of the plate. Also, the weld ends are modeled. The method is visualized in Figure 2.14.

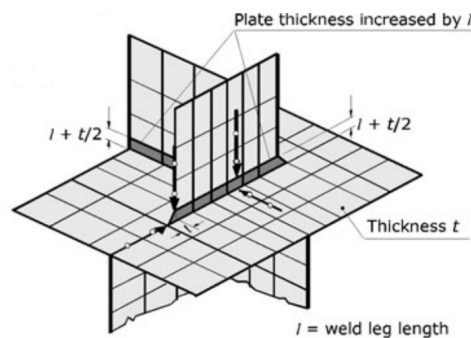


Figure 2.14: Welds modeled with reinforced plate strips with inclined ends [18]

In addition, Eriksson et al. [35] proposed a modeling technique where the thickness is increased at the location of the weld when a double-sided fillet weld is considered. Figure 2.15 shows the approach for a cruciform joint. The thickness is increased by the throat thickness of the weld. The height of the region is equivalent to the sum of the weld leg length and half the thickness of the plate. The thickness of both plates at the welded location is increased.

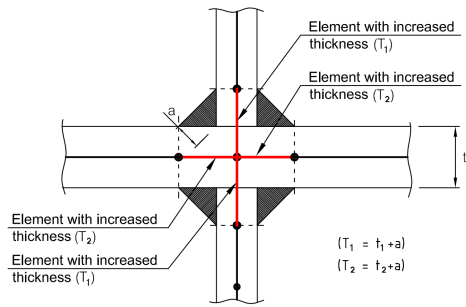


Figure 2.15: Weld modeling technique with increased thickness [35]

Moreover, prTS 1993-1-901 (draft) [4] provides guidelines for the design of orthotropic steel decks (OSD) against fatigue using the hot spot stress method. If shell elements are used in the model, the thickness can be increased at the location of the weld to include the weld effects, see Figure 2.16. This modeling method is also included in ROK2.0 [12]. At the weld intersection, the thickness of both plates is increased by the weld leg length. Also, weld ends are included with an inclined geometry. The method is a combination of the IIW method [18] and the method proposed by Eriksson [35], however, the weld leg length is considered instead of the throat thickness of the weld. TS 1992-1-901 provides guidelines for different types of welds.

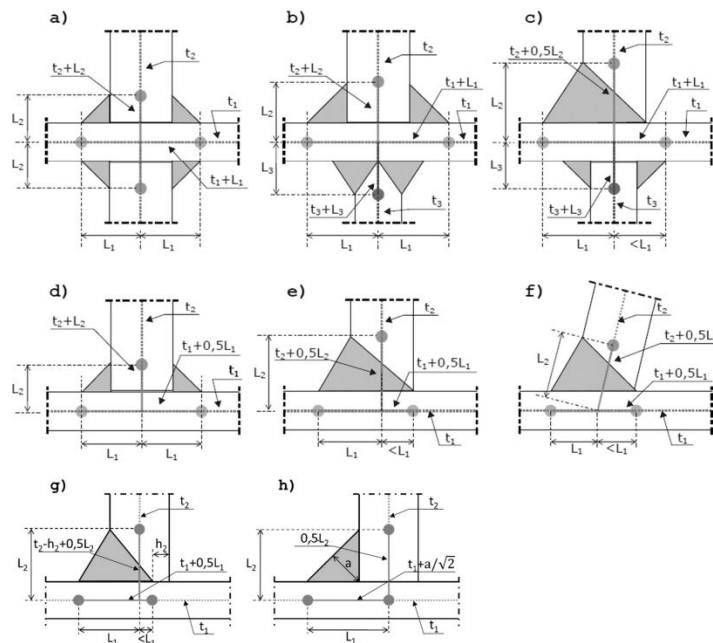


Figure 2.16: Increased thickness of shell elements at the location of the weld [12][4]

The increased thickness modeling techniques are summarised in Table 2.5.

Table 2.5: Comparison increased thickness modeling techniques

Modeling technique	Plates with increased thickness	Amount of increased thickness	Weld ends included (Yes/No)
IIW	Attached plate	Weld leg length	Yes
Eriksson	Attached plate + bottom plate	Weld throat thickness	No
IIW + Eriksson	Attached plate + bottom plate	Weld throat thickness	Yes
prTS 1993-1-901	Attached plate + bottom plate	Weld leg length	Yes

Comparison of increased thickness methods

Pandit [13] compared different numerical models of transverse and longitudinal fillet welded cruciform joints. In total five modeling techniques are compared for different load cases (in-plane bending, in-plane torsion, out-of-plane torsion, and combinations of those). The modeling techniques compared

are: solid, shell without weld, shell with weld according to IIW, shell with weld according to Eriksson, and shell with weld according to a combination of IIW and Eriksson. It is concluded that the shell element models without considering the weld overestimate the hot spot stress at the hot spot location, compared to the hot spot stress determined with the solid model. The overestimation is maximal 25% and 16%, for the transverse and longitudinal cruciform joints, respectively. If the weld is not modeled, it is recommended to determine the hot spot stress by extrapolating to the plate intersection point, according to IIW [10]. When the weld is included in the model, the hot spot stress should be extrapolated to the weld toe location. All weld modeling techniques for shell elements show equivalent hot spot stress with the solid element model for the considered load cases.

In addition, Nikraftar [36] researched the effect of modeling techniques for a simple T-joint. The same (weld) modeling alternatives, as considered in the research of Pandit [13], are considered. The load cases in-plane bending and out-of-plane bending are considered. From this study is concluded that the weld modeling technique which is a combination of the IIW and the Eriksson approach fits the results of the solid model the best if the hot spot method is used.

Oblique shell elements

Niemi [37] recommended in 1995 the use of oblique shell elements to represent the weld in shell element models. Both weld stiffness and geometry are represented with this modeling technique. However, this is an approximation, so this technique is not suitable for weld root fatigue failure because for this failure mode the representation of the stiffness and geometry of the weld are more important. At the intersection, the main plate is connected to the attached plate, see Figure 2.17. The thickness of the oblique shell elements is taken equal to the throat thickness of the weld [25].

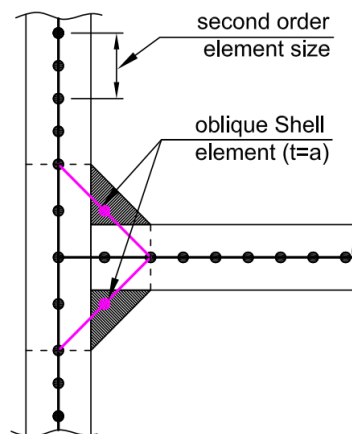


Figure 2.17: Weld modeling technique with oblique shell elements [25]

Rigid links

Fayard et al. [38] suggested in 1996 the use of rigid links to model the weld in shell element models. The goal was to create a technique to determine the hot spot stress at the weld toe. With this modeling technique, the HSS can be read directly from the center of gravity, so extrapolation is not needed. The local rigidity caused by the weld is represented by rigid links, see Figure 2.18. The length of E1 and E2 should be chosen correctly to represent the local rigidity. The two adjacent plates are not connected to each other at the location of the joint [25].

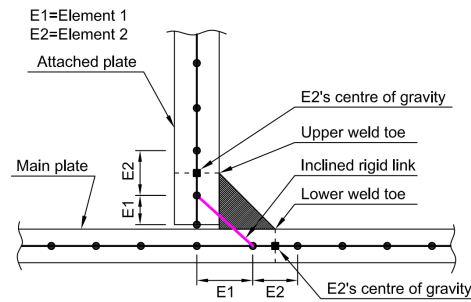


Figure 2.18: Weld modeling technique with rigid links [25], adapted from [38]

2.4.2. Solid elements

Solid elements are three-dimensional (3D) elements that represent the structure. The elements take the variation throughout the thickness into account because the thickness is modeled. The results most closely resemble reality. In addition, the geometry of the weld can be modeled. This led to more realistic results compared to shell elements. However, the computational time will increase because more elements are modeled when using solid elements.

Solid elements can be tetrahedral or hexahedral. First-order tetrahedral elements have 4 nodes, and hexahedral elements have 8 nodes. Also, higher-order elements are possible [34].

2.5. Design of railway bridges

In the 19th century, the train became part of the infrastructural network. In the second part of this century, the railway network was expanded, and many steel railway bridges were built in the Netherlands. In the period of the second world war (1940-1945), some railway bridges were destroyed and needed to be repaired or rebuilt. Until 1975, not many new bridges were built. Thereafter, the question was raised if the bridges built around 1900 could still withstand the increased train intensity. From then, old railway bridges were replaced by newly built ones [39]. The design of railway structures developed over time, see Figure 2.19. In addition, the joint methodology changed from rivets to bolts and welds, from 1940 onwards, because of advantages such as higher production speed and the possibility of automatization [39].

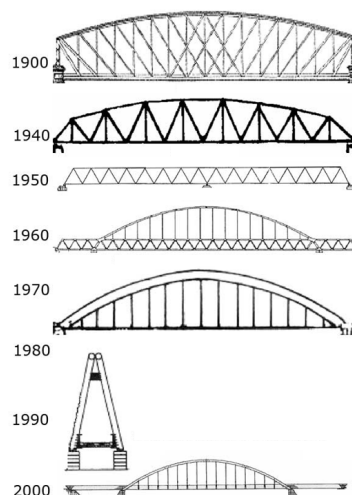


Figure 2.19: Development of types of steel railway bridges in chronological order [40]

Currently, railway bridges are still mainly built from steel and sometimes in combination with (reinforced) concrete, which made their entry around 1950 [39]. Concrete bridge decks can be preferable to reduce sound emissions (large own weight), for example. Also, the cross-section of bridge elements can be designed in different ways, for example with box girders or plate girders. Eurocode provides guidelines

for railway bridge design. In addition, Prorail [11] and Rijkswaterstaat [12] defined additional guidelines to Eurocode in the Netherlands. A ballast bed on bridges could be used to reduce sound emissions even more and in case of e.g. deformations of the bridge the ballast can be adapted to repair the track. For this reason, Prorail often demands to realize a track in ballast bed for newly built bridges. A drawback is that a higher construction height is needed, compared to cast-in railway tracks.

Reference projects

The design of some railway bridges that have been built in the recent decade will be briefly discussed and thereafter compared on relevant design aspects for this research.

Zandhazenbrug: The Zandhazenbrug was opened in 2016 and is located in Muiderberg in the Netherlands, see Figure 2.20. The railway bridge replaces a concrete viaduct to make widening of the Highway A1 possible. The cross-section of the Zandhazenbrug is shown in Figure 1.3. The connection between the main- and cross-girder has a certain rotational stiffness, as discussed in Chapter 1. The main girder has a kink in the outer web to reduce sound frequencies. The main girder and the arches are made from steel grade S460 and the cross-girders are from S355 [7]. In general, high-strength steels are less robust and more prone to welding errors. One factor influencing weldability is the carbon equivalent. High-strength steel contains often higher carbon concentrations. For this reason, strict requirements are often imposed on steels with high-strength grades. To maintain quality and prevent issues like cold cracking, additional measures, such as pre-heating, could be taken [41].



Figure 2.20: Zandhazenbrug [42]

Bert Swartbrug: The Bert Swartbrug was opened in 2017 and is located in Zuidhorn, the Netherlands (see Figure 2.21). The railway bridge replaces an old steel bridge to make the widening of the river underneath possible [43]. A technical drawing of the cross-section of the Bert Swartbrug is shown in Figure 2.22.



Figure 2.21: Bert Swartbrug [43]

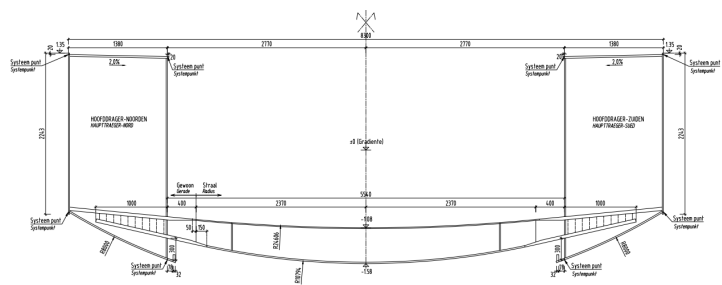


Figure 2.22: Cross-section Bert Swartbrug [43]

Vleutensespoorbrug 2: The Vleutensespoorbrug 2 is located next to Vleutensespoorbrug and is part of project UtARK (Utrecht Amsterdam-Rijnkanaal). In Figure 2.23, the bridge is shown. The bridge was opened in 2018 and is part of the expansion of the railway network Utrecht Centraal - Leidsche Rijn [8]. The cross-section is shown in Figure 1.5. The foundation of the design process was to create an as flexible as possible connection between the main girders and cross-girders. This was accomplished

by configuring the inner web of the main girder to allow for deformation freedom. The diaphragm is designed to minimize its attachment length to the inner web of the main girder as much as possible. Moreover, the inner web has a different thickness compared to the outer web, and the height of the main girder has been increased to enhance flexibility.



Figure 2.23: Vleutenspoorbrug 2 (middle one) [44]

Theemswegtracé: Two comparable arch railway bridges have been built for the new railway network Theemswegtracé in the Netherlands. One is constructed across the Thomassentunnel, and the other spans the Rozenburgsesluis. This section includes information from the bridge crossing Rozenburgsesluis (see Figure 2.24). These bridges are part of a new railway route which makes it possible that freight trains from Rotterdam can go to Europe without crossing the Calandbrug. The Calandbrug is used for both rail- and road traffic and has to be opened once in a while for shipping traffic [45]. The cross-section of the railway bridge across Rozenbrugsesluis is shown in Figure 2.25.



Figure 2.24: Rozenburgsesluis, Theemswegtracé [46]

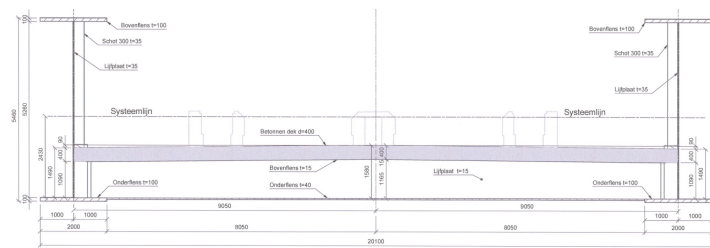


Figure 2.25: Cross-section Rozenburgsesluis, Theemswegtracé [lv-Infra]

Herentals: Railway bridge Herentals is a bridge in Herentals, Belgium (see Figure 2.26). This bridge is built to replace an existing bridge so that the clearance height for shipping traffic can be increased and the Albertkanaal can be widened. Construction started in March 2023 [47]. A drawing of the cross-section design is shown in Figure 2.27.



Figure 2.26: Herentals [48]

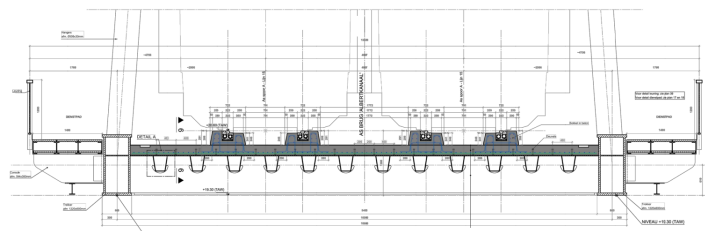


Figure 2.27: Cross-section Herentals [Infrabel]

Kuringen: The railway bridge in Kuringen (Belgium) replaces two existing railway bridges. The bridge is shown in Figure 2.28. It is part of the same project as the railway bridge in Herentals. The widening of the Albertkanaal and increasing the clearance height. The bridge was opened in 2021 [49]. The cross-section of the Kuringen railway bridge is shown in Figure 2.29. The rail is constructed in concrete

blocks without a ballast, as can be seen in Figure 2.30.



Figure 2.28: Kuringen [49]

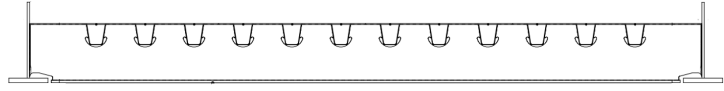


Figure 2.29: Cross-section Kuringen [Infrabel]



Figure 2.30: Construction of the rail, Kuringen [50]

An overview of the different technical characteristics of the above-described railway bridges is shown in Table 2.6. Unknown values are not filled in. All bridges are arch bridges with span lengths between 123 and 255 meters. Half of the bridges discussed have diagonal (Nielsen-type) hangers and the other half have a vertical hanger configuration. The force distribution in the bridge is for both types different. With Nielsen-type hangers, better lateral resistance can be achieved. Diagonal hangers serve as structural braces that can take lateral forces (e.g. wind load). Furthermore, bridges with these hangers typically exhibit less flexibility, which could minimize deflection within the vertical plane and enhance overall stability. All considered bridges have a steel-concrete deck that is connected to the steel structure with shear studs, except the railway bridge Kuringen, this bridge has an orthotopic steel deck. In some bridges, e.g. Zandhazenbrug and Vleutensespoorbrug 2 [7][8], the concrete deck works together with the main girders to transfer tension forces in the longitudinal direction. In this case, a relatively large amount of reinforcing steel is needed to take the forces. The steel-concrete composite structure is in the direction of the cross-girder loaded in compression by the load due to its own weight and vertical train loading. Concrete can be beneficial for sound emission due to its large weight. For the bridges in the Netherlands, a ballast bed is applied. This contributes to the reduction of sound emissions.

In the majority of the discussed bridges, a (rectangular) box main girder is used. This type of girder has more torsional resistance compared to I-profile girders [51]. In addition, this type of profile can be made airtight, to protect the inside against environmental influences. The height of the box girders varies between 1220 and 3040 [mm]. The alignment of the infrastructure can influence the maximum possible height of the main- and cross-girders. The thickness of the inner web of the box girders is between 15 and 50 [mm], for the considered bridges.

Inside the main girder, diaphragms (stiffeners) are placed to transfer shear forces from the main girder inner web plate to torsional forces, contributing to the stability of the girder. The diaphragm design and position can influence the rotational stiffness of the connection between the main girder and cross-girder, as will be further explained in Chapter 3. Both the diaphragm and the main- to cross-girder connection are typically prone to fatigue.

The number of tracks on the bridge influences both the span of the cross-girder and, consequently, the height of the cross-girder. In addition, the center-to-center (c-t-c) distance of the cross-girders can be

varied to meet requirements. The c-t-c distance could also affect the stresses at the main- to cross-girder connection. For cross-girders mainly I-profiles are used, with heights varying between 600 and 1090 millimeters at the location of the connection, for two tracks. Large forces should be introduced in the main girder at relatively low heights. The c-t-c distance between cross-girders varies between 1.5 and 3.8 meters.

Table 2.6: Overview characteristics from different bridge designs
Data Zandhazenbrug, Vleutenspoorbrug 2, and Theemswegtracé from [lv-Infra], data Bert Swartbrug from [43], and data Herentals and Kuringen from [Infrabel]

	Zandhazenbrug	Bert Swartbrug	Vleutenspoorbrug 2	Theemswegtracé	Herentals	Kuringen
Type of structure						
Span [m]	255	175.2	168	172.8	164.2	123
Hangers	Diagonal	Vertical	Vertical	Vertical	Diagonal	Diagonal
Type of deck	Steel-concrete	Steel-concrete	Steel-concrete	Steel-concrete	Steel-concrete, OSD	OSD
Ballast bed	Yes	Yes	Yes	Yes	No	No
Main girder						
Profile	Box	Box	Box	I-profile	Box	I-profile, no upper flange
Height inner web [mm]	3040	2930	2400	5500	1220	1221
t inner web [mm]	32		15	35	50	35
Cross-girder						
No. of tracks	2	1	2	2	2	2
Span [m]	11.5	5.5	9	18	9.4	10.29
C-t-c distance [m]	1.6	3.75	3.5	2.5	1.5	1.52
Profile	I-profile	Box	I-profile	I-profile	I-profile	I-profile
Height constant over width	No	No	No	No	Yes	Yes
Height at connection [mm]	638.4	300	600.25	1090	795	898
t upper flange [mm]	15		25	15	15	15
Diaphragm						
Aligned w. cross-girder	No		No	Yes		
C-t-c distance [m]	8		10.5	5		

2.6. Fatigue load models railway bridges

The Eurocode includes two fatigue assessment load models for railway bridges. A relatively simple factored Load Model 71 (LM71) [52] and a more realistic load model that consists of combinations of 12 standard trains described in Annex D of EN 1991-2 [53]. These load models will be discussed in Section 2.6.1 and Section 2.6.2.

In general, fatigue assessment includes vertical rail traffic actions including dynamic and centrifugal effects. Nosing and longitudinal traffic actions may be disregarded. For structures consisting of multiple tracks, the load should be applied on a maximum of two tracks at the most unfavorable positions [53].

EN 1991-2 [53] describes the possibility to distribute the forces from the load model in the longitudinal direction. A point force due to Load Model 71 or a wheel load of a Fatigue Train may be distributed over three rail support joints, see Figure 2.31. In addition, for the design of e.g. local floor elements, the point load may be distributed with the ratio 4:1 in the longitudinal direction due to the ballast and sleeper, see Figure 2.32.

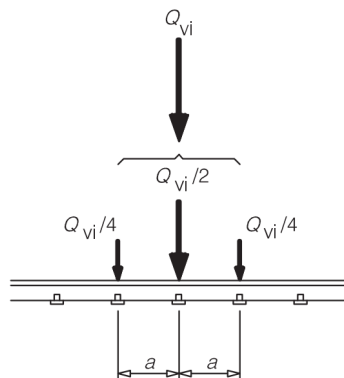


Figure 2.31: Longitudinal distribution by the rail [53]

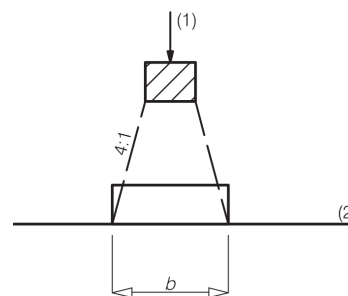


Figure 2.32: Longitudinal distribution by a sleeper and ballast [53]

where:

- Q_{vi} = the point force on each rail due to LM71 or a wheel load of a Fatigue Train
 a = the distance between rail support points
 (1) = the load on the sleeper
 (2) = the reference plane (the upper surface of the deck)

There are additional requirements for fatigue assessment if a dynamic analysis is required. Figure 2.33 shows a flowchart to determine if a dynamic analysis is necessary. The two fatigue load models will be discussed for the case when no dynamic analysis is required.

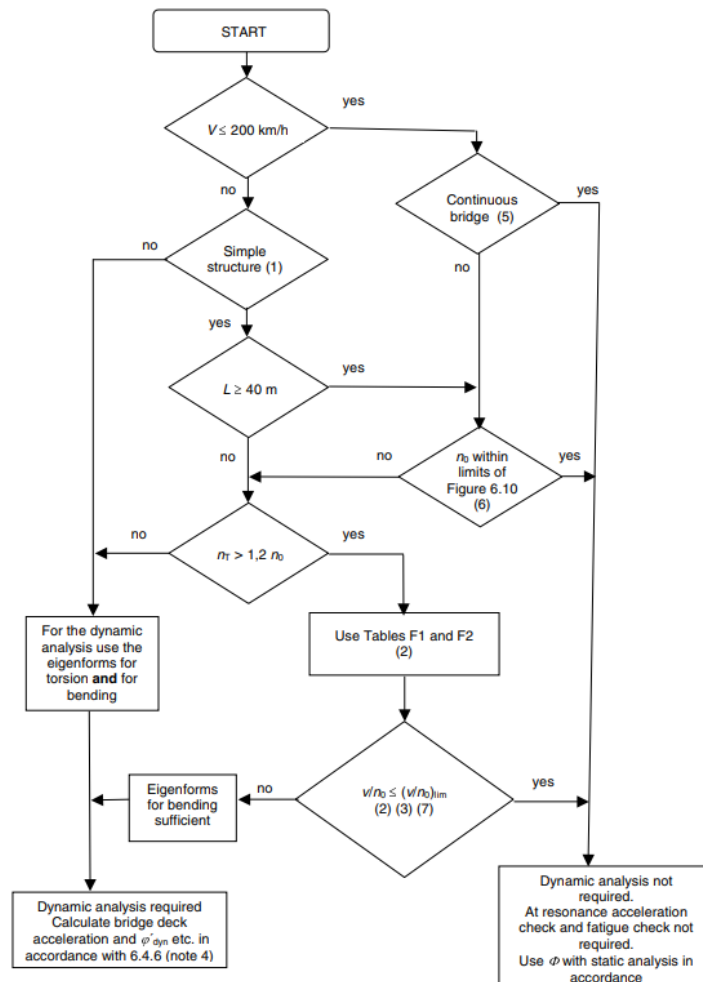


Figure 2.33: Flowchart to determine if a dynamic analysis is required according to NEN-EN1991-2 [53]

where:

- V = the maximum line speed at the site [km/h]
 L = the span length [m]
 n_0 = the first natural bending frequency of the bridge loaded by permanent actions [Hz]
 n_T = the first natural torsional frequency of the bridge loaded by permanent actions [Hz]
 v = the maximum nominal speed [m/s]
 $(v/n_0)_{lim}$ = given in NEN-EN 1991-2 Annex F

2.6.1. Load model 71

When the equivalent damage method is used, as described in NEN-EN 1993-2 [52], only one load model is considered. The load model is described in NEN-EN 1991-2 [53]. The load model is called Load Model 71 and represents the static effect of normal rail traffic, see Figure 2.34.

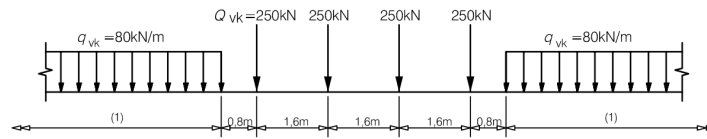


Figure 2.34: Load Model 71 and characteristic values for vertical loads [53]

Formula 2.9 is used to perform the fatigue check when the equivalent damage method is used.

$$\gamma_{Ff} \lambda \phi_2 \Delta \sigma_{71} \leq \frac{\Delta \sigma_C}{\gamma_{Mf}} \quad (2.9)$$

where:

- γ_{Ff} = the partial factor for equivalent constant amplitude stress ranges. The recommended value, according to NEN-EN1991-2/NB is $\gamma_{Ff} = 1.00$ [-] [54]
- λ = the damage equivalence factor for fatigue, defined in NEN-EN 1993-2 [52]
- ϕ_2 = the dynamic factor, defined in NEN-EN 1991-2 [53]
- $\Delta \sigma_{71}$ = the stress range caused by Load Model 71 without the α -factor and the load is placed on the most unfavorable position for the considered detail
- γ_{Mf} = the partial factor for fatigue strength $\Delta \sigma_C$ [9]. According to OVS300030-6 [11], $\gamma_{Mf} = 1.35$ [-] for all details

A damage equivalence factor λ should be applied to the stress range determined by LM71 for railway bridges with a span of up to 100 meters. If larger spans are considered, the λ -method will be conservative. The damage equivalence factor is calculated with Formula 2.10 [52]. To determine λ_1 , λ_2 , λ_3 , and λ_4 tables 9.3-9.7 from EN 1993-2 can be used.

$$\lambda = \lambda_1 \times \lambda_2 \times \lambda_3 \times \lambda_4 \leq \lambda_{max} \quad (2.10)$$

where:

- λ_1 = the factor for the damage effect of traffic and depends on the length of the influence line
- λ_2 = the factor for the traffic volume
- λ_3 = the factor for the design life of the bridge
- λ_4 = the factor for the structural element is loaded by more than one track
- λ_{max} = the maximum value taking account of the fatigue limit, $\lambda_{max} = 1.4$ [-] [52]

If no dynamic analysis is required, the dynamic factor ϕ_2 can be determined with Formula 2.11 [53].

$$\phi_2 = \frac{1.44}{\sqrt{L_\phi - 0.2}} + 0.82 \quad (2.11)$$

with:

$$1.00 \leq \phi_2 \leq 1.67$$

where:

L_ϕ = the determinant length [m], determined in accordance to NEN-EN1991-2 section 6.4.5.3

End cross-girder

For end cross-girders, other requirements are described by Eurocode. NEN-EN1991-2/NB [54] defines that ϕ_3 instead of ϕ_2 [53] must be used when fatigue assessment is performed for end cross-girders. This factor depends on the determinant length L_ϕ . For end cross-girders the determinant length is in most cases lower, compared to middle cross-girders. This results in a higher dynamic factor.

2.6.2. Annex D model

NEN-EN 1991-2 [53] Annex D describes another fatigue assessment load model for railway bridges. In total three different standard traffic scenarios are defined: the standard traffic mix, the heavy traffic mix, and the light traffic mix. The traffic scenarios are different combinations of 12 standard fatigue trains, see for example Figure 2.35. The traffic mix used should be in agreement with the type of traffic expected for the railway bridge. In the Netherlands, ProRail defined additions to Eurocode for railway structures [11]. In OVS00030-6 is defined that for fatigue assessment the heavy traffic mix with 25t (250kN) axles should be considered, see Table 2.7. In addition, if two railway tracks are considered, 12% of the train passages should be simultaneously on both tracks and both passing train types are identical [11].

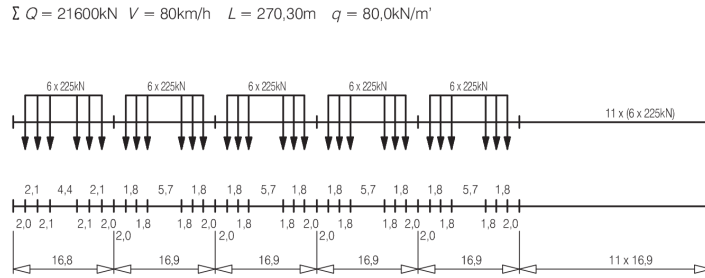


Figure 2.35: Train type 5: Locomotive-hauled freight train [53]

Table 2.7: Heavy traffic mix with 25t (250kN) axles [53]

Train type	Number of trains/day	Mass of train [t]	Traffic volume [10^6 t/year]
5	6	2160	4.73
6	13	1431	6.79
11	16	1135	6.63
12	16	1135	6.63
	51		24.78

If no dynamic analysis is required, the dynamic factor for fatigue analysis for each train can be determined with Formula 2.12. In this formula, it is accounted for the average effect of the structure over a reference time of 100 years. The formula can be used for a maximum permitted vehicle speed of 200 [km/h] [53].

$$\phi = 1 + \frac{1}{2} \cdot (\varphi' + \frac{1}{2}\varphi'') \tag{2.12}$$

where:

$$\varphi' = \frac{K}{1 - K + K^4}$$

with:

$$K = \begin{cases} \frac{v}{160} & \text{if } L_\phi \leq 20 \text{ [m]} \\ \frac{v}{47.16 \cdot L_\phi^{0.408}} & \text{if } L_\phi > 20 \text{ [m]} \end{cases}$$

and:

$$\varphi'' = 0.56e^{\frac{L_\phi^2}{100}}$$

where:

v = the maximum permitted vehicle speed [m/s]

2.7. Rotational stiffness

The rotational stiffness of a connection is the bending moment-to-angular rotation ratio. The rotational stiffness is necessary when performing an elastic global analysis of the structure. It influences both the internal forces in the members and in the connections of the structure. The stiffness depends on the connected sections and the components used. Eurocode 3 part 1-8 [55] classifies three types of rotational stiffness: pinned, semi-rigid, and rigid, see Figure 2.36. $S_{j,ini}$ is the initial rotational stiffness of the connection that can be determined by, for example, finite element modeling or the component based method according to EN1993-1-8. The boundary when a connection is "rigid" is given in Formula 2.13 and "pinned" in Formula 2.14.

A pinned connection has zero rotational stiffness and does not transmit any bending moments. It only transmits shear forces. A rigid connection has an infinite stiffness and transfers forces and bending moments with limited rotating. This kind of connection often requires thicker and more components. The properties of a semi-rigid connection are in between that of a pinned and rigid connection. This kind of connection transfers shear forces and some bending moments and has some degree of rotation ability. The design of the connection can be adapted to get an optimal distribution of bending moments in the beam [56].

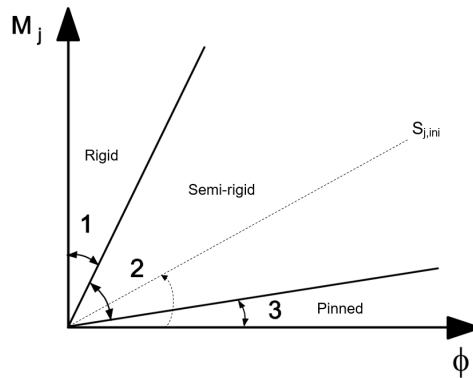


Figure 2.36: Classification of the connection by rotational stiffness, adapted from [55]

$$S_{j,ini} \geq \frac{k_b \cdot E \cdot I_b}{L_b} \quad (2.13)$$

$$S_{j,ini} \leq \frac{0.5 \cdot E \cdot I_b}{L_b} \quad (2.14)$$

with:

$k_b = 8$, for frames where the bracing system reduces the horizontal displacement by at least 80%

$k_b = 25$, for other frames, provided that in every storey $K_b/K_c > 0.1$

where:

E = the elastic modulus

I_b = the second moment of area of the beam

I_c = the second moment of area of the column

L_b = the span of the beam

L_c = the storey height of a column

K_b = the mean value of I_b/L_b for all beams at the top of that "storey"

K_c = the mean value of I_c/L_c for all columns in that "storey"

Relation to fatigue in railway bridges

The design of the main- to cross-girder connection is important in railway bridges. Train passages cause large stress ranges in the connection detail and in addition large dynamic factors should be accounted

for. Often, the total construction height of the railway bridge is restricted due to the space available between the traffic road and the railway bridge. As a consequence, high stress ranges should be transferred by a small beam height [7][8]. If a close-to-pinned connection can be achieved, the clamping moments in the connection can be limited. This could be beneficial for fatigue strength. However, when a close-to-pinned connection is used, higher bending moments are taken by the beam, so larger beam heights are needed [56]. This height is not always available.

The profile of the main girder does, for example, influence the flexibility of the connection. In design, rectangular closed profiles can be preferred because it is possible to fabricate the profile airtightly. This reduces conservation costs. In addition, closed profiles provide better torsional resistance compared to open shapes, for example, I-girders [51]. However, this makes it more difficult to create a flexible connection with the cross-girder.

3

Methodology for parametric study

A parametric analysis of the connection between the main- and cross-girders is conducted. This study aims to assess how different design considerations impact the fatigue behavior of this connection. In this chapter, the methodology for conducting the parametric study will be outlined. The starting point will be a reference model, which will serve as the basis for introducing variations in design parameters.

The reference model and the finite element model will be discussed in Section 3.1 and 3.2, respectively. Thereafter, the fatigue assessment method will be explained. In Section 3.4, the parameters that will be considered will be elaborated on. Lastly, the methodology to make an estimation of the costs associated with the parametric change will be explained.

3.1. Reference model configuration

The reference model is based on the design of the bridges of *project Oostertoegang*. Iv-Infra is one of the contributing parties responsible for designing five newly constructed railway bridges that will replace the existing bridges on the eastern side of Amsterdam Central Station. Each bridge consists of three separate static determinate spans. None of the total 15 (5x3) bridge spans are identical but most of them have similarities in design. Due to the diverse range of designs and for the sake of simplicity, a simplified reference model will be used as a basis for a parametric study. At the moment of determining the configuration for research, the project Oostertoegang was still ongoing. Hence, the reference model is not based on the final design.

The outer spans are approximately 28 meters in length, while the middle span is around 20 meters, for each bridge. The plan view varies for each span, with a cross-girder span of approximately 9 [m] at the abutments and 8 [m] at the intermediate support points. For the parametric study, the plan view is simplified into a rectangular bridge structure based on the length of the middle span and the largest cross-girder span, see Figure 3.1 and Figure 3.2. The shorter span is chosen to reduce calculation time. The structure will only be locally studied. The dimensions are rounded, to simplify for parametric study.

Moreover, for this study, alterations have been made to the location and design of the diaphragms compared to the original design of the bridges of *project Oostertoegang*. The original and adapted designs of the diaphragms are shown in Figure 3.3. In the original design, the diaphragms are aligned with the cross-girder webs, and in the adapted design the diaphragms are positioned between two cross-girder webs. The design of the adapted diaphragm is based on the design of Vleutensespoorbrug 2 (see Figure 1.5). The difference between the two design principles is the rotational stiffness that is created at the main- to cross-girder connection. The adapted design results in more flexibility at the connection compared to the original design. This requires a different approach to design the connection to meet the fatigue requirements. The influence of the different types of diaphragms and their placement on the fatigue damage of critical fatigue details (Section 3.3) is shown in Section 4.2.1.

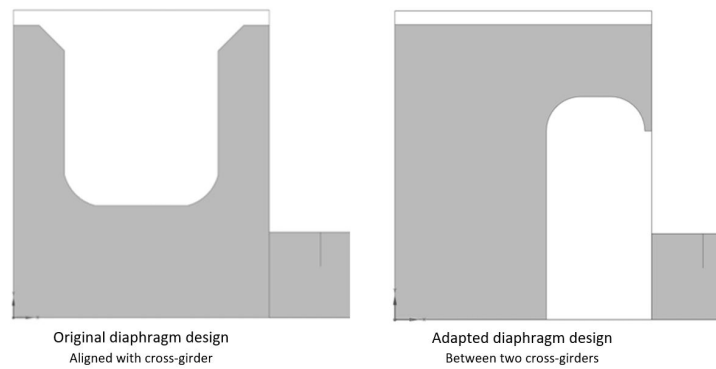


Figure 3.3: Diaphragm's original design and adapted design [3]

Figure 3.4 illustrates the dimensions and types of welds used. An OSD deck is used with a cross-girder spacing of 1900 [mm]. The bottom flange of the cross-girder is extended over the entire length of the bridge. Both the main girders and cross-girders are welded airtight. The choice of weld types is determined by this design decision to facilitate the fabrication process.

The design of the adapted diaphragm design has a gap at the location of the connection between the diaphragm and the inner web of the main girder to gain more flexibility. This could make the welds connecting the diaphragm with the internal web and the bottom flange of the main girder critical because the weld length is shortened. The length of the welds should be as long as possible to take the shear forces but as short as possible to ensure flexibility.

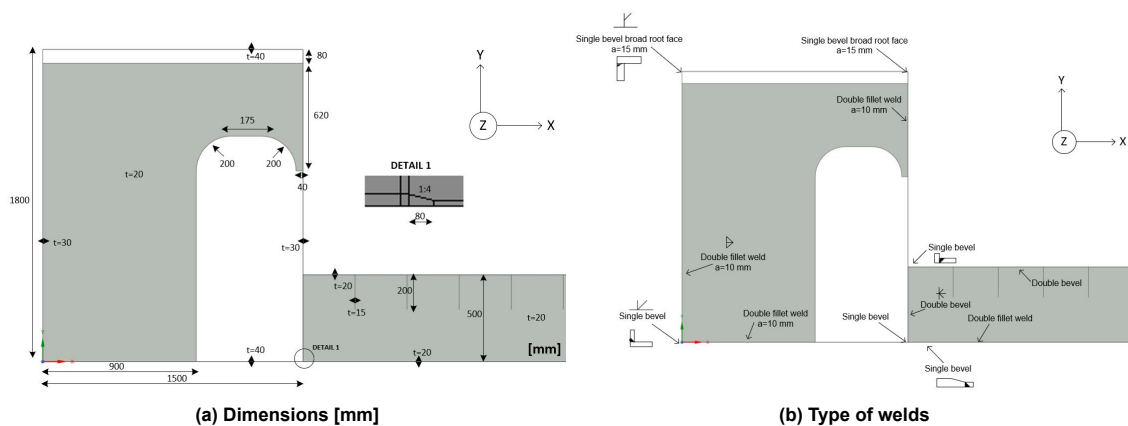


Figure 3.4: Considered configuration at the location of the connection between the main- and cross-girder [3]

3.2. Finite element model

A static structural analysis of the bridge is conducted using shell elements in the finite element software *Ansys® 2022 R2* [3]. A linear elastic model is considered, so it is assumed that the behavior of the material is linearly elastic and that the material is isotropic. The model calculates the effects of a moving unit load for two railway tracks. Subsequently, a Python code provided by Iv-Infra is used in conjunction with the Ansys model to compute the fatigue damage resulting from train loading. This section provides a description of the FE model. In section 3.3, the fatigue assessment will be further explained.

Material properties

The properties of steel grade S355 are considered for the entire structure. The modulus of elasticity is taken as $E = 210000$ [MPa], and Poisson's ratio as $\nu = 0.3$ [-].

Boundary conditions

The support of the bridge is statically determinate, as shown in Figure 3.5. In the out-of-plane direction (y-direction), all supports are constrained against movement. At supports 1 and 2 movements are free in the x-direction, and at supports 2 and 4 movements are free in the z-direction.

To mitigate singularities in the model, the support is modeled as a triangle with a high stiffness, see Figure 3.6. The isosceles triangle (45°) has a thickness of 500 [mm] and the boundary conditions are located at the tip.

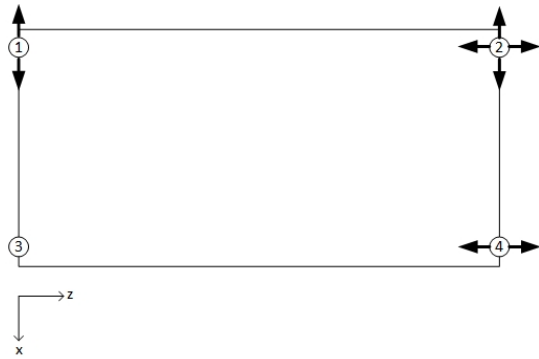


Figure 3.5: Boundary conditions

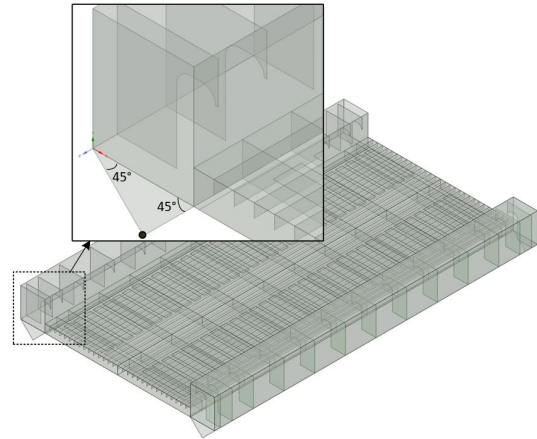


Figure 3.6: Modeling support [3]

Fatigue load

The fatigue loading considered is based on Eurocode [53] and OVS [11] guidelines. The load model described in Annex D from NEN-EN1991-2 [53], as described in Section 2.6.2, is considered for the analysis. This model requires a more time-consuming calculation but results in a more realistic solution [57].

It is assumed that dynamic analysis is not required, so a dynamic factor should be applied. This is based on the flowchart shown in Figure 2.33. The maximum speed of the train at the bridge is 80 [km/h], so $V \leq 200$ [km/h]. The bridge is supported on both ends, so is not continuous. If n_0 is within the limits of figure 6.10 from NEN-EN1991-2, no dynamic analysis is required. The natural frequency, n_0 , of a simply supported bridge subjected to bending only can be estimated with Formula 3.1 [53]. Iv-Infra estimated that the natural frequency lies within the limits, so no dynamic analysis is required.

$$n_0 \text{ [Hz]} = \frac{17.75}{\sqrt{\delta_0}} \quad (3.1)$$

δ_0 = the deflection at midspan due to permanent actions [mm]

A unit load of 100 [kN] is used to determine the influence line due to the loading at the location of the considered node. This influence line is used to determine the stresses induced by the fatigue trains at that location. The heavy traffic mix with 25t axles (Table 2.7) is considered to determine the total fatigue damage, applying the Palmgren-miner cumulative damage rule. The rainflow method is applied to count the load cycles.

Ansys Parametric Design Language (APDL) commands are used to define the moving unit load in Ansys Mechanical. APDL is a programming language that can interact with the Ansys Mechanical solver. For both railway tracks, in total 32 load steps are specified. The unit load of 100 [kN] can be distributed by the rail, sleeper, and ballast, as shown in Figure 2.31 and Figure 2.32. The distance between the rail supports is $a = 600$ [mm], as defined by OVS00030-6-V005 section 6.3.6.1 [11]. OVS00030-6 section 6.3.6.2 defines the type of sleeper and rail that should be considered: NS-90 and UIC-54, respectively. The surface of an NS-90 sleeper is 2520×260 [mm]. The ballast thickness considered in this study is

310 [mm], defined as the minimum thickness in the assumption report of the Oostertoegang and differs from OVS00056-5.1, where it is larger. The (unit) load will be distributed with a ratio of 1:2:1 over a surface area of $b \times d$:

- $b = 260 + \frac{310}{4} \cdot 2 = 415$ [mm]
- $d = 2520 + \frac{310}{4} \cdot 2 = 2675$ [mm]

The load distribution per load step is visualized in Figure 3.7. A distance of 600 [mm] is considered, representing the distance between the rail supports. The distance between the inner web of the main girder and the middle of the load path is considered 2075 [mm]. The load is positioned directly above the middle cross-girder of the reference model. The position of the load will remain the same in relation to the bridge length throughout the parametric study.

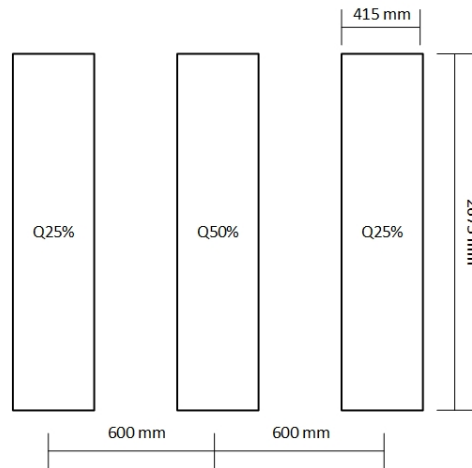


Figure 3.7: Fatigue load distribution

Weld modeling

As discussed in Section 2.4.1 there are different modeling possibilities to consider the stiffness of the weld in the shell element model. The fatigue assessment method used determines whether or not modeling the weld influences the results using FE modeling. For example, when the nominal stress method is considered, it is not needed to include welds in the model because the nominal stress is extracted at a distance x from the weld location where the stress remains undisturbed by the connection, see Figure 2.7. The hot spot stress, however, is determined by extrapolating the stresses from reference points to the weld toe. According to IIW [10], if the weld is not modeled, the hot spot stress should be extrapolated to the structural intersection point to not underestimate the stress. However, when the weld is modeled, the hot spot stress should be extrapolated to the location of the weld toe [10][4].

In this research, the hot spot stress method will be used to determine the fatigue resistance of specific critical details (see Section 3.3). The weld will be considered by increasing locally the thickness. Because of the different types of welds in the design and the clarity of use, the prTS 1993-1-901 (draft) [4] modeling technique will be used in the FE model for parametric study.

In Section 4.1.1, the influence of considering the weld using an increased thickness or not with shell element models will be compared with the results using a solid model. The solid model is used as a reference that gives a good estimation of reality. This comparison will be done for two simple cruciform joints with a longitudinal fillet weld and a transverse fillet weld. Pandit [13] conducted similar research, however, without considering the prTS 1993-1-901 modeling technique. To make verification of the modeling technique possible, the same conditions as in the research from Pandit will be considered.

In total three welds will be modeled at the location of interest (see Section 3.3). These include the weld connecting the diaphragm to the inner web of the main girder (*Weld 1*), the weld connecting the orthotropic steel deck to the inner web of the main girder (*Weld 2*), and the connection of the cross-girder

web to the main girder (*Weld 3*). See Figure 3.8 for an overview of the increased thickness approach at these locations.

Weld 1 is assumed to have a weld throat thickness of 10 [mm] in all cases, resulting in a weld leg length of $10\sqrt{2} \text{ [mm]}$. For welds 2 and 3, a weld toe angle of 45° is assumed and the weld is 3 [mm] non-flat. Thus, L_1 in these cases is $\frac{t_2}{2} + 3 \text{ [mm]}$.

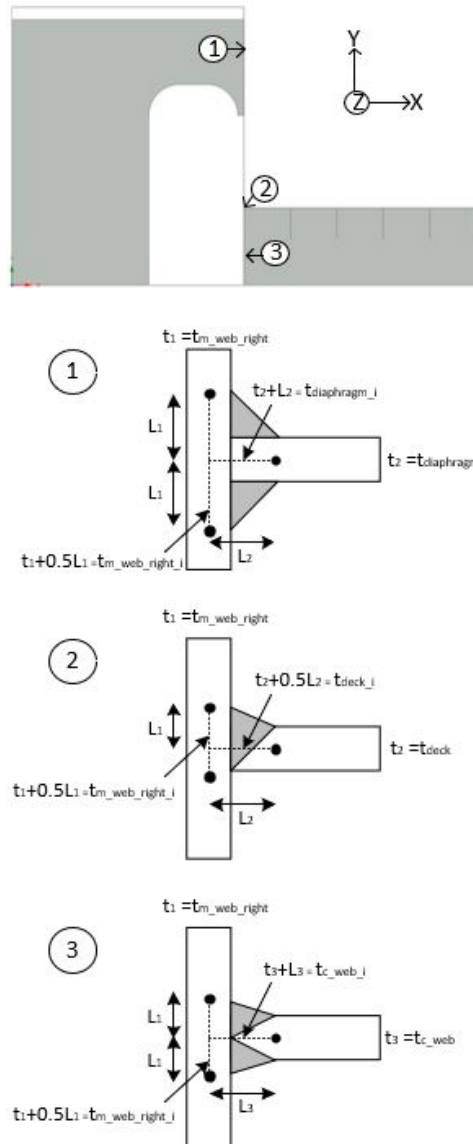


Figure 3.8: Thickness increase at the location of the weld

According to prTS 1993-1-901 (draft) [4], full penetration butt welds can be disregarded when modeling the welds. These are, for example, detail 1 and 2 of table B.1 of EN 1993-1-9 [9]. An exception is made for the case the misalignment is larger than described for those details. In the design of the bridge considered in this study, such a full penetration butt weld is used to attach the bottom flange of the cross-girder to the main girder.

Mesh size

The mesh size has an impact on the stresses obtained from the finite element software. Smaller element sizes lead to higher stresses at plate intersection locations. Also, the smaller the mesh size, the closer the unaveraged value matches the averaged value.

The IIW [18] provides guidelines for mesh sizing when the hot spot stress method is used with shell elements. For type a welds and fine FE models, the size of the elements should be smaller than or equal to $0.4t \cdot t$. Only type a welds are considered in this study. There are no specific guidelines for mesh sizing when the nominal stress method is used. The IIW [10] suggests that a simple and coarse element size can be used when determining the stress range with the nominal stress method.

The global mesh size of the model is $175 [mm]$. At the location of interest (see Section 3.3), the middle of the bridge, the mesh size is refined to $50 [mm]$ with a sphere of influence. The center of the sphere of influence is positioned at the point where the orthotropic steel deck is connected to the inner web of the main girder, at the location of the middle cross-girder web. The radius is twice the center-to-center distance between the cross-girders. At the location of the welds considered, a mesh refinement of $0.4t \cdot t$ is applied, in accordance with IIW (HSS) recommendations. This refinement may change if the parameters are modified. The growth rate of the mesh is 1.1. Figure 3.9 shows the mesh of the reference model.

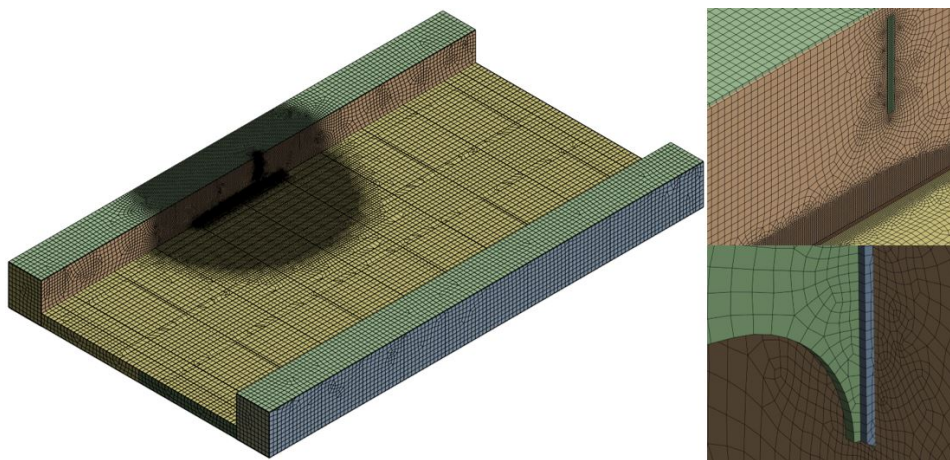


Figure 3.9: Global mesh and mesh at welded details [3]

Offset type

In a shell element model, the parts are typically modeled at the mid-plane of the structural component. However, it is also possible to assign the element a top, bottom, or self-defined offset. When an offset is applied differently than mid-plane in a shell element model, an eccentricity is introduced. This eccentricity can cause additional bending moments.

For the finite element model of this study, the offset type of each plate is chosen at mid-plane. This choice provides the closest approximation to reality, with the assumption that overlapping thicknesses in shell element models are negligible.

In the case of fatigue-prone details with an axial or angular misalignment, such as the connection between the bottom flange of the main girder and the bottom flange of the cross-girder in the considered bridge structure, Eurocode 3 part 1-9 [9] and IIW [18] define an additional stress concentration factor. For this example, the eccentricity resulting from the inclined thickness can induce secondary bending stresses in the plate when subjected to a normal force, as illustrated in Figure 3.10. Consequently, the actual stresses are different from those calculated with the FEM. The modified stress takes this into account. This detail, however, is not further considered in the study and does not influence the investigated welded details (see Section 3.3).

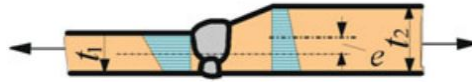


Figure 3.10: Eccentricity at the attachment of the cross-girder flange to the main girder [18]

3.3. Fatigue assessment method

In this section, the fatigue assessment method of the parametric study is explained. In this study, a selection is made of details that will be examined at a specific location of the bridge. Firstly, the location of interest will be discussed. Thereafter, the fatigue-prone details that will be investigated at this location are discussed. Finally, the methodology of the fatigue calculation that is performed in each iteration of the parametric study will be explained.

Location of interest

For the parametric study, only a specific location will be viewed for the fatigue calculation. The reason for this is the comparability of the results gathered. The location considered is between the three central cross-girders. So, when the assessed weld is in the longitudinal direction of the bridge, it will only be considered in the aforementioned zone. Fatigue-critical welds in other directions will only be considered at the middle of the bridge. In cases where the number of cross-girders is even, two "middle" cross-girders exist. Given this scenario, the lower one will be considered the middle one. However, due to symmetry, the results should be (approximately) equivalent. The same principle applies to the diaphragms.

By altering parameters, the stress distribution across the bridge will change. This can optimize the fatigue resistance of the details that are taken into account but it is possible that other, unconsidered details might deteriorate in terms of fatigue. This is not taken into account in this study. The focus of this research is on the most vulnerable fatigue details at the main- to cross-girder connection in the middle of the bridge. However, other fatigue-prone details should be examined during the actual design of a bridge.

Fatigue critical details

The fatigue assessment method used determines the way the fatigue critical details should be assessed. Relatively fast and commonly used fatigue assessment methods are the hot spot stress method and the (modified) nominal stress method. The effective notch method is used less in practice. For this reason, only the first two methods are considered in this study.

Appendix A shows the fatigue detail categories that can be considered for the nominal stress method and the hot spot stress method at the location of the main- to cross-girder connection, according to NEN-EN1993-1-9 [9]. The hot spot stress method will be used for the critical details where possible. If this is the case, the surface stresses are read at $0.4t$ and $1.0t$ from the weld toe location and extrapolated to the weld with: $\sigma_{hs} = 1.67 \cdot \sigma_{0.4t} - 0.67 \cdot \sigma_{1.0t}$ (fine mesh). The specific reading points will vary based on changes in the parameters. If it is not possible to use the hot spot method, the nominal stress method will be used. The reason for this is the doubtfulness of using the nominal stress method in combination with finite element modeling. Reading the stress at the location of the critical detail will overestimate the nominal stress because the nominal stress should only account for the macro geometrical effects due to the design. The other effects are incorporated in the detail category. In principle, the nominal stress can be calculated by hand. When FEM is used, the nominal stress can be read at a distance x away from the connection, where x is the point at which the stresses remain undisturbed by the connection and are uniform.

Based on the stresses in the reference model and the critical details of the design of "Vleutensespoorbrug 2", a selection is made of which fatigue details will be researched in the parametric study. These are shown in Figure 3.11. Determining the critical welded details is a comparison between the local stress range at the vicinity of the weld and the fatigue detail category that should be considered for the detail. For all these details, the hot spot stress method can be used to determine the fatigue damage. The three details will be further referred to in the report as M1.1, M1.2, and M2, where:

- $M1.1$ is the stress in the y-direction at the diaphragm end in the main girder inner web. The hot spot method is used, so the detail category is 100 (NEN-EN1993-1-9 table B.1 detail 5).
- $M1.2$ is the stress in the z-direction in the main girder inner web at the location where the diaphragm is welded to the inner web of the main girder. The hot spot method is used, so the detail category is 100 (NEN-EN1993-1-9 table B.1 detail 4).
- $M2$ is the stress in the x-direction in the deck plate where the bridge deck is welded to the main girder web. The hot spot method is used. The assumed detail category is 100 (NEN-EN1993-1-9 table B.1 detail 3). It should be noted that this detail category differs from the actual configuration. The detail category considers a cruciform joint and a double bevel weld, while this connection is a T-joint welded with a single bevel.

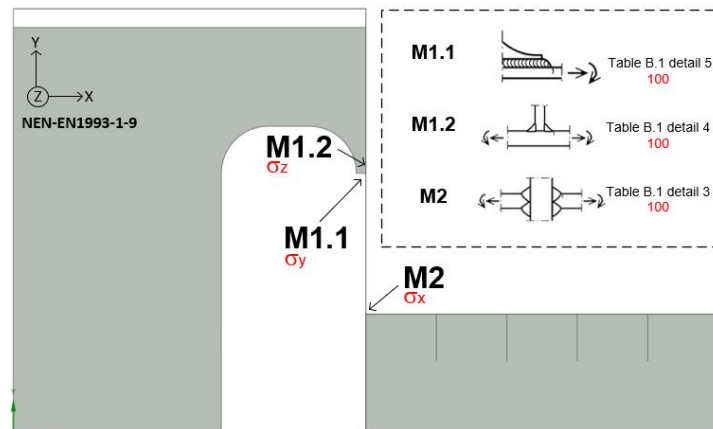


Figure 3.11: Fatigue detail categories at the location of the connection between the main- and cross-girder, considered in the parametric study [3][9]

The designated reading points for assessing the stress in detail M1.1 remain consistently positioned in relation to the diaphragm, namely at the diaphragm end tip. The critical location of details M1.2 and M2 could differ along the weld length. Nevertheless, it is assumed that for detail M1.2 the diaphragm end tip is the governing location and for detail M2 two potential critical points could emerge: one at the deck plate above the cross-girder web and the other aligned with the diaphragm. Only these locations will be considered during the parametric study.

Dynamic factor

The assumption is made that no dynamic analysis is required (see Section 3.2). Consequently, a dynamic factor should be applied that can be calculated with Formula 2.12. The dynamic factor is in generally based on a maximum permitted speed of 80 [km/h]. The determinant length, L_ϕ , is determined in accordance with NEN-EN1991-2 section 6.4.5.3 [53]. This value changes when changing parameters and is different for the considered fatigue details. The determinant lengths considered in the parametric study are given in Table 3.1.

Table 3.1: The determinant lengths, L_ϕ , corresponding with the considered fatigue details [53]

Fatigue detail	L_ϕ	Source
M1.1	The span in the main girder direction	EN1991-2 table 6.2, case 5.1
M1.2	The span in the main girder direction	EN1991-2 table 6.2, case 5.1
M2	Three times the cross-girder spacing	EN1991-2 table 6.2, case 1.1

Additional critical fatigue detail

In addition to the previous three mentioned fatigue details, fatigue detail M3 will be researched for the parameters, see Figure 3.12. Detail M3 is at the location where the deck plate is welded to the main girder. The stresses are determined in the y-direction in the main girder inner web plate. The assumed hot spot detail category is 100 (NEN-EN1993-1-9 table B.1 detail 4). It should be mentioned that this

detail category considers a fillet weld, instead of a single bevel weld.

This fatigue detail was not of influence for the fatigue design of Vleutensespoorbrug 2 and the original design of the bridges of project Oostertoegang. The reason for this is the steel-concrete deck used in the design of Vleutensespoorbrug 2 and the stiffeners placed in alignment with the cross-girder web in the original design of the bridges of Oostertoegang.

This detail will not be researched for all steps considered in the parametric study, see Section 3.4. The total damage value will be calculated for the reference model, and the smallest and largest value considered for the parameter. However, the same fatigue assessment methodology will be used. Similar to detail M2, only two possible critical locations are considered: in alignment with the cross-girder and diaphragm. The results are discussed in Section 4.3.

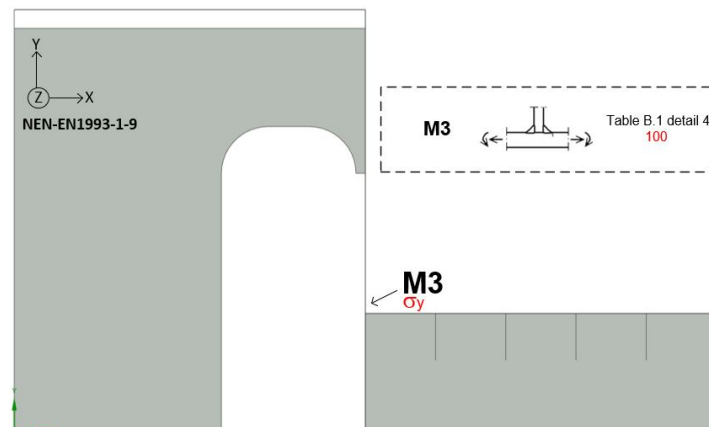


Figure 3.12: Fatigue detail category, M3 [3][9]

The determinant length for detail M3 considered in the parametric study is given in Table 3.2.

Table 3.2: The determinant length, L_ϕ , corresponding with fatigue detail M3 [53]

Fatigue detail	L_ϕ	Source
M3	The span in the main girder direction	EN1991-2 table 6.2, case 5.1

Iv-Tool fatigue calculation

Iv-Infra is working on the automatization of the fatigue calculation. A fatigue tool is being developed, which is designed to operate in combination with Ansys® 2022 R2 [3]. This tool is further referred to as *Iv-Tool*. This tool, in its current form, will be used to perform the damage calculation in the parametric study. This section will describe the Iv-Tool.

The Iv-Tool is an Ansys extension that can be linked to an Ansys structural model. The objective of the Iv-Tool is to determine the cumulative fatigue damage value of a detail, which should be smaller than 1 to fulfill requirements. This tool makes it possible to retrieve results from Ansys and automatically determine the damage value from the given input. Ansys is used to give the input for the calculation, Python to perform the calculation, and Microsoft Excel to present the output data.

The input for the tool is an Ansys shell element model, loaded by a moving unit load of 1 [kN]. Different railway tracks can be combined, by combining different static structural analyses in Ansys. If another unit load is implemented, a scaling factor can be used to scale to 1 [kN]. The selection of the location where the stress should be determined is done by selecting a node and its adjacent elements. This requires a generated mesh. The unit load is used to determine the influence line for the selected location for each railway track that is selected for research. Thereafter, an input menu in Ansys is used, to give input for the Python calculation. In this input menu, the following can be filled in to perform the calculation as desired:

- The stress direction: X, Y, or Z.
- The stress position: top or bottom.
- The influence length L_ϕ per railway track.
- The percentage of the same type of trains simultaneously over the railway tracks. If OVS guidelines [11] are followed, this is 12%.
- Train combination: train type(s) and number of trains per day. According to NEN-EN 1991-2 [53], there are 12 train types. If OVS [11] guidelines are used, the heavy traffic mix should be considered for fatigue calculation, see Table 2.7.
- The train velocity in [km/h].
- The lifetime of the bridge (100 years).
- Number of days in a year.
- In Ansys, each load step is implemented by hand and is set as a time step. To know the location of the load per time, this should be given as input. This should be specified to get the scaled influence line.
- The detail category and type of S-N curve (normal or shear), according to NEN-EN 1993-1-9.
- The partial factor. The partial safety factor is $\gamma_{Mf} = 1.35 [-]$, according to the Dutch national annex to Eurocode 3 part 1-9 [58] for safe life and high consequence of failure. This factor should be used according to OVS [11].
- Reduction factor due to geometry K_s . The standard is 1.

Firstly, the Iv-Tool generates an Excel where all stresses per load step at the selected location are categorized by stress type (normal/shear), direction (x/y/z), and position (top/bottom). Thereafter, the influence line that should be used according to the input menu is selected by Python and used to determine the stresses caused by the entered train types. The train "drives" over the influence line with a step size of $0.1 [m]$ to determine the stress plot per train type. In addition, the dynamic factor due to the influence length L_ϕ and the train velocity are determined, according to the Annex D model (see Section 2.6.2). However, in its current state, performing fatigue analysis with the hot spot method is not possible. To solve this issue, the influence lines at $0.4t$ and $1.0t$ will be determined and extrapolated in a separate sheet. This information will be entered into the Excel file generated by the Iv-Tool, which is utilized in the calculation of fatigue damage.

Next, rainflow counting is performed for one train per train type per railway track. Appendix B verifies the rainflow counting method of Python using a random stress plot. When two trains are simultaneously on the bridge, the maximum stress range determined with the rainflow counting method from track 1 is summed up with that of track 2. The maximum number of cycles of the two is selected. The same process is repeated for the second-highest stress range, the third-highest stress range, and so on, down to the lowest stress range. The stress ranges are then multiplied by the dynamic factor.

Subsequently, the Palmgren-Miner cumulative damage rule determines the damage value per track/track combination and train type. The allowed number of load cycles N_i is determined for each stress range determined with the rainflow counting method. This value depends on the detail category, which is reduced by the partial factor $\gamma_{Mf} : \frac{\Delta\sigma_c}{\gamma_{Mf}}$. The partial factor γ_{Ff} is equal to 1, so does not influence the results. The number of trains that cross the bridge during its lifetime n_i is determined for each track/track combination (simultaneity) and train type. The cumulative damage per track/track combination and train type is determined by: $D = \sum_{i=1}^n (\text{number of cycles})_i \cdot \frac{n_i}{N_i}$. Finally, all damage values are summed up to determine the total damage, which must be smaller than 1 to meet requirements.

In Section 4.1.2, the Iv-Tool calculation will be validated by comparing the results with a hand calculation. In this calculation, the reference model configuration and the critical fatigue details will be considered.

3.4. Parameters

Different design considerations, referred to as parameters, will be investigated in the parametric study. In this section, each parameter will be discussed. Each parameter will be modified individually within

the reference model to assess its impact on the fatigue results. The range within which the parameters are studied is based on Table 2.6. While the dimensions of the structural elements may not be realistic in all cases, they provide an impression of the influence on the stress range within the connection.

Figure 3.13 provides a visual representation of the six parameters that will be investigated. Also, the critical fatigue locations and stress orientations that will be researched are shown in blue (see Section 3.3). The parameters cover:

1. $c-t-c$: The center-to-center distance between the cross-girders
2. H_{cg} : The height of the cross-girder
3. H_{mg} : The height of the main girder
4. T_{mg} : The thickness of the inner web of the main girder
5. T_{dia} : The thickness of the diaphragm
6. T_{deck} : The thickness of the steel deck plate

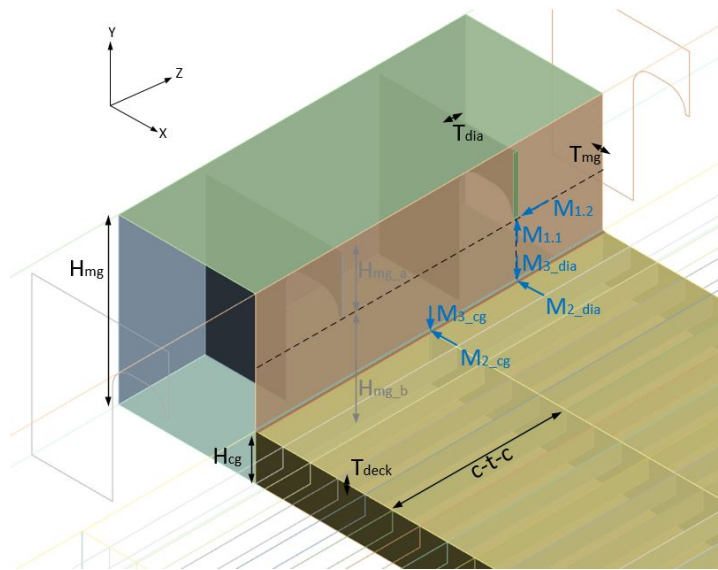


Figure 3.13: Visualization of the parameters for parametric study [3]

The parameters will be discussed below.

The center-to-center distance between the cross-girders

The center-to-center ($c-t-c$) distance between the cross-girders influences the bending stiffness of the orthotropic deck. When there are more cross-girders, the deck deforms less under the same loading conditions, resulting in less rotation required for the main girder. This may influence the stresses at fatigue details M1.1, M1.2, and M3. Also, the rotational stiffness of the main girder is affected by the center-to-center distance. Additional cross-girders reduce the rotation possibilities of the main girder, potentially influencing the stresses at M2. Moreover, the condition that one diaphragm is placed between two cross-girders is maintained. More diaphragms can increase the rotational stiffness of the main girder. This may have an effect on the stresses at detail M2.

In the parametric study, the length of the bridge remains constant and the $c-t-c$ distance between the end-cross-girders is not changed. The number of cross-girders in the reference model is 8 with a $c-t-c$ distance of 1900 [mm]. In the parametric study, the number of cross-girders varies between 4 and 10 cross-girders. This corresponds to a center-to-center distance between 1555 and 3420 [mm]. The diaphragms are consistently positioned between two cross-girders.

The height of the cross-girder

The cross-girder height influences the moment of inertia of the cross-girder. A higher cross-girder deforms less under the same loading conditions. As a consequence, the main girder has to rotate less to

react to the deformation of the cross-girders and deck plate. This could influence the stresses at details M1.1, M1.2, and M3. Furthermore, elevating the cross-girder height brings the deck plate closer to the diaphragm end tip. The connection of the deck plate to the main girder becomes stiffer at this location which may affect the stresses at detail M2. Also, the out-of-plane bending capability of the inner web of the main girder is changed, which has possibly an effect on the stresses at details M1.1, M1.2, and M3.

The height of the cross-girder in the reference model is 500 [mm]. In the parametric study, the height will be adjusted within the range of 300 to 1000 [mm] with increments of 100 [mm].

The height of the main girder

In the reference model, the height of the main girder is 1800 [mm]. Heights between 1600 and 2400 [mm] with a step size of 100 [mm] will be investigated in the parametric study. The height of the cross-girder remains constant. However, there are different ways of taking into account the size of the diaphragm. The design of the diaphragm will influence the stiffness of the main- to cross-girder connection.

It is assumed that the weld length of the connection between the diaphragm and the inner web of the main girder is the minimum length necessary. The shear force in the main girder web does not change if the height is adjusted, so the weld that connects the diaphragm should take the same shear force. Thus, when the height of the main girder is lower than the reference height, the connected diaphragm length does not change (see Figure 3.13: H_{mg_a}), while the available free space decreases (see Figure 3.13: H_{mg_b}). If the main girder height is increased, there are two options investigated:

- The free space increases with increasing height, so the welded length stays the same.
- The free space stays constant with increasing height, so the welded length increases.

The distinction between those two options is the influence of the gap size. Frequently, a minimum gap size is required for fabrication and maintenance considerations. The final design seeks a balance between the minimum weld length needed to handle the shear forces and the minimum gap size necessary to facilitate structural fabrication and maintenance.

The cross-girders, deck, and loading remain constant in the study, resulting in a consistent deformation of the cross-girders. When the gap size increases, it enhances the flexibility of the inner web of the main girder. This change may have an impact on the stresses at details M1.1, M1.2, M2, and M3. Conversely, if the main girder size is increased while maintaining a constant gap size, it results in an extended welded length, creating a more rigid connection between the diaphragm and the inner web of the main girder. This alteration could affect the fatigue critical details M1.1 and M1.2.

The thickness of the inner web of the main girder

The thickness of the inner web of the main girder can influence the rotational stiffness of the main- to cross-girder connection. A thinner web makes the connection more flexible. As discussed in Chapter 2, the rotational stiffness influences the stress distribution within the connection. The rotational stiffness at the connection between the deck plate and the main girder may influence the stresses at detail M2. If the inner web of the main girder is made thinner, the thickness of the outer web should increase to take the shear forces. A thinner web, however, has a lower moment of resistance which will increase the stress levels in the plate. This could influence the fatigue detail M1.1, M1.2, and M3.

In the reference model, the thickness of the inner web is 30 [mm]. For the parametric study, the thickness is varied within the range of 10 and 50 [mm], in increments of 5 [mm]. If an inner web thickness between 10 and 25 [mm] is applied, the thickness of the outer web of the main girder is increased such that the combined thickness of the inner and outer webs is at a minimum of 60 [mm].

The thickness of the diaphragm

The diaphragm serves the purpose of transferring the shear forces in the cross-girders through the inner web of the main girder to torsional forces and contributes to the main girder's overall stability. A thicker diaphragm increases the diaphragm's stiffness, and it also enhances the stiffness of the connection with the inner web of the main girder. When a load is moving over the bridge, the bending of

the inner web of the main girder at the connection between the diaphragm and the inner web may be restricted. This could impact the stresses at details M1.1 and M1.2.

In the reference model, the thickness of the diaphragm is equal to 20 [mm]. In the parametric study, a thickness between 10 and 30 [mm] is researched. The step size is taken as 5 [mm].

The thickness of the steel deck plate

The thickness of the steel deck plate could influence the stresses at the connection. A thicker deck offers higher rigidity and can better withstand applied forces. This could have an effect on detail M2. Due to the rigidity, the deck plate will deform less and the main girder has to rotate less. This could have an influence on details M1.1, M1.2, and M3.

In the reference model, the thickness of the deck plate is 20 [mm]. In the parametric study, a thickness between 10 and 40 [mm] will be investigated. The thickness of the total deck plate is varied but it might also be possible to change the thickness only at the critical fatigue location to have an effect on the fatigue damage at the main- to cross-girder connection. The step size used is 10 [mm].

3.5. Costs

Modifying a parameter within the bridge structure incurs associated costs. The results of the parametric study will be used to make an estimation of the costs to lower the total fatigue damage with 1 [-] for each considered parameter and fatigue critical detail. In this section, the methodology used to determine the costs to influence the damage value will be discussed.

The costs associated with the parametric change will be based on the material and welding costs. The costs will be computed for the total bridge. Assumed is a material cost of 1 euro per kilogram of steel, based on an assumption of Bouwen met Staal [59]. The density of steel is 7850 [kg/m³]. The welding costs represent mainly the labor costs. Based on Figure 3.14, it is assumed that the welding process occurs at an average speed of 50 [cm³/hour]. To include the time for assembly a factor of 2 is applied. The welding speed becomes 25 [cm³/hour]. It is assumed that a welder is paid 20 [€/hour] [59]. To include overhead costs a factor of 3 is applied to the salary of the welder. The welding costs become 2.40 [€/cm³]. Material and labor costs depend on various factors, such as the economy. For this reason, the assumed costs give only an indication. An overview of the assumed costs is shown below.

- Costs of steel: 1.00 [€/kg]
- Costs of welding: 2.40 [€/cm³]

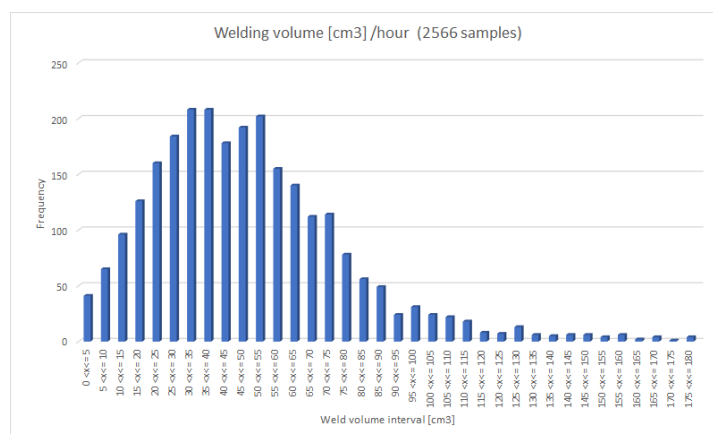


Figure 3.14: Measured welding speeds from a data set with 2566 samples by Oostingh ASK Romein [59]

In addition to determining the costs linked to altering the parameter, a correlation between the parameter adjustment and the resultant shift in damage should be established. The least squares method will

be applied to do so. This is a statistical procedure with which the (linear) line of best fit between the measured data points can be determined. The coefficient of determination, R^2 , is a statistical measure of how well the linear regression line fits the measured data points. The R^2 -value can be determined by dividing the sum squared regression (SSR) by the total sum of squares (SST) and subtracting this value from 1, see Formula 3.2. An R-squared value close to 1 means that the line fits the actual data well, and close to 0 is a bad fit. This can be used to predict the possible accuracy of future outcomes.

However, it should be noted that the relationship between changing a parameter and the total fatigue damage is not linear. The different characteristics and mechanisms of a structure are not linearly correlated with the fatigue stresses. Moreover, the fatigue calculation using a moving train load and the S-N curve is not linear. So, in this study, linear regression is used to make a prediction of the direction coefficient but cannot be used to exactly determine the fatigue damage.

$$R^2 = 1 - \frac{SSR}{SST} = 1 - \frac{\sum_i (y_i - \hat{y}_i)^2}{\sum_i (y_i - \bar{y})^2} \quad (3.2)$$

where:

R^2 = the coefficient of determination

y_i = the observed value of the dependent variable (y) for the i^{th} data point

\hat{y}_i = the predicted value of the dependent variable (y) for the i^{th} data point based on regression analysis

\bar{y} = the mean value of the dependent variable (y) of all the observed data points

4

Method validation and results

In this chapter, the results of the conducted research will be elaborated. In Section 4.1, the results of the verification of some aspects of the method for parametric study are given. Thereafter, in Section 4.2, the results of the parametric study will be discussed individually for each parameter. In Section 4.3, the results of an additional fatigue critical detail are discussed. Finally, with the results gathered, suggestions for the design of *project Oostertoegang* will be given.

4.1. Validation of the method for parametric study

In this section, two choices made in the methodology of the parametric study will be investigated and verified. These are the weld modeling technique according to prTS 1993-1-901 [4] guidelines and the Iv-Tool calculation.

4.1.1. Weld modeling technique

To validate the choice of the modeling technique of the weld at the location of the connection detail, different modeling possibilities are compared on a cruciform joint. In the FE model of this study, the weld is modeled according to prTS 1993-1-901 [4] guidelines. Other possible weld modeling techniques for shell elements are discussed in Section 2.4.1. The modeling techniques that are compared, are:

- Solid
- Shell without considering the weld
- Shell + weld IIW, see Figure 2.14
- Shell + weld Eriksson, see Figure 2.15
- Shell + weld IIW+Eriksson
- Shell + prTS 1993-1-901, see Figure 2.16

In Appendix C, the approach is worked out in detail and the results are presented. Both, a cruciform joint with a transverse fillet weld and one with a longitudinal fillet weld are considered, see Figure 4.1. The former is loaded under in-plane bending, in-plane torsion, and out-of-plane torsion. The latter is subjected to in-plane bending and in-plane torsion. The same conditions as in the research of Pandit [13] are taken into account to make verification of the results possible. In addition to Pandit's research, this study also considers the weld modeling technique outlined in prTS 1993-1-901 (draft) [4].

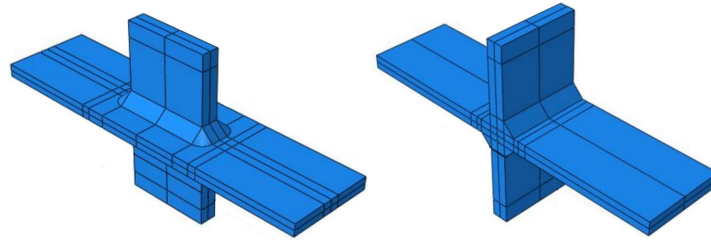


Figure 4.1: Geometry of cruciform joint, longitudinal (left) and transverse (right), adapted from [13]

Comparable results to those found in the research conducted by Pandit [13] are gathered. From the results, it can be concluded that the hot spot stress might be overestimated if the weld is not considered in the model and the IIW [10] recommendations are used. All modeling techniques considering an increased thickness demonstrate good agreement with the solid model. The solid model, in this case, provides the most accurate estimation of reality. This verification confirms that utilizing the prTS 1993-1-901 [4] modeling technique offers a reliable approximation when utilizing shell elements. However, it should be noted that the analysis is based on a cruciform joint with a limited number of load cases.

4.1.2. Hand calculation versus Iv-Tool

The results of the Iv-Tool are compared with those of a hand calculation to verify the outcome of the Iv-Tool. This comparison is conducted for the reference model configuration. The methodology used is the same (as outlined in Chapter 3), however, for the hand calculation, no detailed rainflow counting is performed and a reduced step size of 0.6 [m] is used to minimize calculation time. Fatigue details M1.1, M1.2, and M2 are considered.

The detailed calculation procedure is presented and explained in Appendix D. A summary of the results is provided in Table 4.1. It can be concluded that, for each critical fatigue detail, the order of magnitude of the total damage is the same. Therefore, the Iv-Tool determines the damage value well.

Table 4.1: Fatigue damage reference model, hand calculation versus Iv-Tool

Detail	Location detail	σ -direction	Fatigue method	Detail category [MPa]	Damage hand [-]	Damage Iv-Tool [-]
M1.1	Diaphragm to main girder inner web	Y	Hot spot	100	1.61	1.57
M1.2	Diaphragm to main girder inner web	Z	Hot spot	100	0.59	0.56
M2	Deck to main girder inner web	X	Hot spot	100	0.17	0.15

4.2. Results of the parametric study

In this section, the results of the parametric study will be discussed for each parameter. The methodology used to gather the results is explained in Chapter 3. Fatigue details M1.1, M1.2, and M2 are considered in this section. Section 4.3 discussed the results of detail M3.

4.2.1. The type and location of the diaphragm

In Section 3.1, two types of diaphragms are discussed: the original design of *project Oostertoegang* and an adapted diaphragm design based on *Vleutensespoorbrug 2* (see Figure 3.3). The original diaphragm design of the *Oostertoegang* results in a design with a certain rotational stiffness at the main-to-cross-girder connection. The adapted design creates more flexibility at the location of the connection. The location of the diaphragm with respect to the cross-girder web can also influence the stress distribution in the connection area. For example, the diaphragm can be located aligned or not aligned with the cross-girder web. The effect of both diaphragm designs and locations is determined for the reference model configuration. Figure 3.11 visualizes the critical fatigue locations that are considered. The weld throat thickness of the fillet weld connecting the diaphragm to the main girder is in all cases considered as 10 [mm]. The results are shown in Table 4.2.

Table 4.2: Damage, parameter: the type and location of the diaphragm

Type of diaphragm	Location of diaphragm	Damage M1.1 [-]	Damage M1.2 [-]	Damage M2 [-]	Location M2
Adapted	Not aligned w. cg	1.57	0.56	0.15	dia
Adapted	Aligned w. cg	2.59	0.63	0.91	cg
Oostertoegang	Not aligned w. cg			19.33	dia
Oostertoegang	Aligned w. cg			12.69	cg

Abbreviations: w. = with, cg = cross-girder, dia = diaphragm

Reference: the fatigue details correspond to those given in Figure 3.11 and Figure 3.13

Based on the results, it can be concluded that the diaphragm design primarily influences the critical fatigue location. The diaphragm design that increases the rotational stiffness at the connection results in a higher cumulative damage value in the deck plate (M2), while the design that induces flexibility results in governing fatigue damages at the connection between the diaphragm and the main girder inner web (M1.1 and M1.2). The more flexible main- to cross-girder connection attracts less force to the connection, leading to lower stress ranges. The maximum total damage of the original Oostertoegang diaphragm is higher compared to the adapted design. Nonetheless, it might still be preferable to choose the Oostertoegang design. The reason for this is the possibility of reducing the governing damage value. For example, when the critical fatigue location is at the connection between the deck plate and the main girder inner web (M2), extra plates with a certain thickness or cope holes can be applied at this location to reduce the stress ranges for fatigue design. However, it should be noted that more fatigue-prone details are created by adding more welded plates. This also increases fabrication costs. If the critical fatigue location is at the diaphragm (M1.1 and M1.2), it might be possible to satisfy fatigue requirements without adding extra plates. Which measures can positively influence the fatigue stresses for such a design, is determined with the other parameters in the parametric study.

Furthermore, the alignment of the diaphragm with the cross-girder web shows also an effect on the magnitude of the damage value and the critical fatigue location. In the case of the Oostertoegang diaphragm design, aligning the diaphragm with the cross-girder web results in a lower damage value in the top deck, with the critical location above the cross-girder. If the diaphragm is positioned between two cross-girder webs, the critical location of detail M2 changes to the location of the diaphragm. In addition, the total damage increases. This is probably caused by the squared angle connection of the plates. When considering the adapted diaphragm design (more flexibility), the case where the diaphragm is not aligned with the cross-girder is preferable for fatigue design.

The best placement of the diaphragm for the Oostertoegang design results in a maximum damage of 12.69, while the best placement of the adapted design results in a maximum damage of 1.57. This is an 88% reduction of the damage at the critical detail. The latter case will be further explored in the parametric study.

4.2.2. The center-to-center distance between the cross-girders

The first parameter checked for the adapted diaphragm design with the diaphragm located between two cross-girder webs is the center-to-center distance between the cross-girders. The reference model has 8 cross-girders and in the parametric study, the number of cross-girders varies between 4 and 10 cross-girders. The condition that between two cross-girder webs a diaphragm in the main girder is placed is maintained. The total fatigue damage for each case is determined at three critical fatigue locations: M1.1, M1.2, and M2. In Figure 3.13, the parameters and critical fatigue locations are visualized.

The numerical results are shown in Table 4.3. In this table, also, the percentage change in the total damage value is presented for each number of cross-girders considered, in comparison to the reference model.

In Figure 4.2, for each fatigue critical detail, the line of best fit for the measured data points is shown. The linear regression lines of all fatigue details are combined in Figure 4.3. While there is no linear ($y = m \cdot x + b$) relationship between the total damage value and the number of cross-girders, this will give a first indication of the slope coefficient when designing for fatigue. Here, m is the value by which the

total damage changes per extra added cross-girder (integers) if the linear regression line is considered. The coefficient of determination, R^2 , can be used to predict the possible accuracy of future outcomes. The m - and R^2 -value of the best linear fit for each fatigue detail is:

- M1.1: $m = -0.1896$ and $R^2 = 0.8737$
- M1.2: $m = -0.0989$ and $R^2 = 0.9356$
- M2: $m = -0.04$ and $R^2 = 0.5374$

For all details, it is visible that the damage value (slightly) decreases with an increasing number of cross-girders. In Appendix E Section E.1, the deformed shapes at the main- to cross-girder connection are shown for 4 and 10 cross-girders for a unit load of 100 [kN]. The shapes are shown when the load is at one of the ends of the bridge and in the middle of the bridge. As mentioned in Section 3.4, the number of cross-girders influences the deformation of the cross-girder and bridge deck. The results show that with more cross-girders, the main girder has to rotate less, and the stresses at details M1.1 and M1.2 decrease. The number of cross-girders has, however, almost no effect on the stresses at detail M2.

Table 4.3: Damage, parameter: the center-to-center distance between the cross-girders

No. of cg	c-t-c cg [mm]	Damage M1.1 [-]	M1.1 D \updownarrow	Damage M1.2 [-]	M1.2 D \updownarrow	Damage M2 [-]	M2 D \updownarrow	Location M2
4	3420	2.71	+73%	1.04	+86%	0.44	+193%	dia
5	2850	2.25	+43%	1.00	+79%	0.22	+47%	cg
6	2443	2.00	+27%	0.76	+36%	0.13	-13%	cg
7	2138	1.84	+17%	0.70	+25%	0.11	-27%	dia
8	1900	1.57	/	0.56	/	0.15	/	dia
9	1710	1.76	+12%	0.57	+2%	0.13	-13%	cg+dia
10	1555	1.41	-10%	0.47	-16%	0.12	-20%	cg

Abbreviations: no. = number, c-t-c= center-to-center, cg = cross-girder, dia = diaphragm, D \updownarrow = The difference in total damage with respect to the reference model

Elaboration: in bold = the results of the reference model

Reference: the fatigue details correspond to those given in Figure 3.11 and Figure 3.13

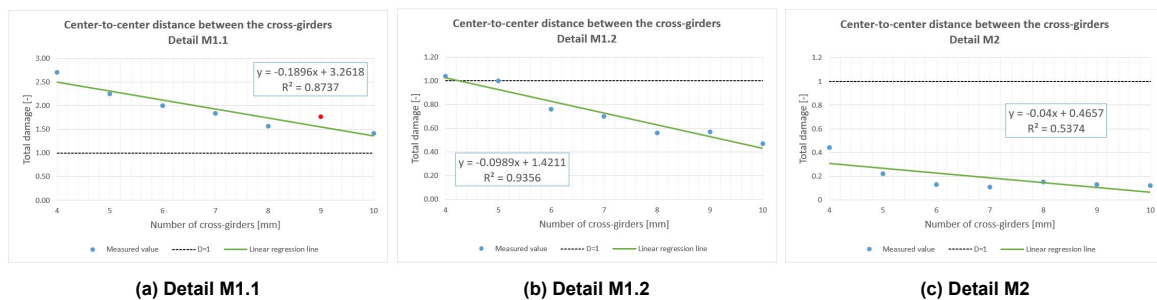


Figure 4.2: Linear regression using least squares method, parameter: the center-to-center distance between the cross-girders

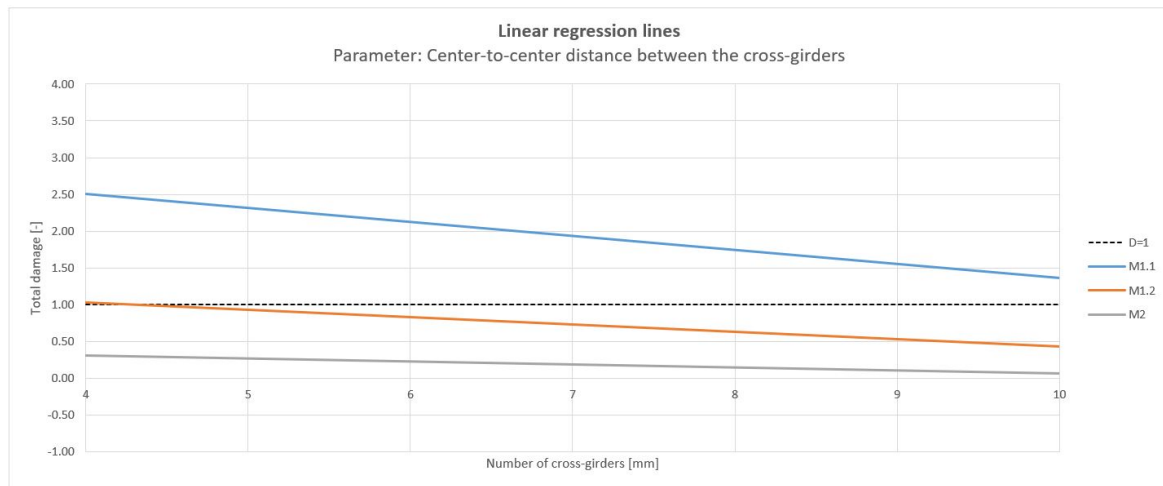


Figure 4.3: Linear regression lines for the parameter: the center-to-center distance between the cross-girders

The linear regression lines are used to determine the costs of changing the damage value with 1 [-]. An explanation of the methodology used to determine the costs is given in Section 3.5. The absolute value of the damage change linked to altering the number of cross-girders (m -value) is divided by the costs that come along with adding or removing this cross-girder. The costs of adding/ removing a cross-girder composed of:

- 1 steel cross-girder web plate
- 2 steel diaphragm plates
- The welds connecting the extra cross-girder plate to the main girders, the bottom flange, and the deck plate
- The welds connecting the diaphragms to the main girders

The costs for each fatigue detail are shown in Table 4.4. Increasing the number of cross-girders will increase the costs. For all fatigue details, the costs will increase when reducing the total damage value.

Adding an extra cross-girder will increase the weight of the steel bridge structure with 1279 tonnes. The steel industry holds the top position as the largest energy consumer worldwide within the industrial sector [60]. Energy consumption is related to environmental impact. Increasing the amount of steel increases carbon dioxide emissions.

Table 4.4: Costs to change the total damage value with 1, parameter: the center-to-center distance between the cross-girders

Fatigue detail	Damage [-] / cross-girder	Costs [€] / damage [-]	€ \updownarrow D \downarrow
M1.1	0.1896	6791435	+
M1.2	0.0989	13019778	+
M2	0.0400	32191400	+

Abbreviations: € \updownarrow D \downarrow = increase (+) or decrease (-) of the costs when reducing the damage value

Deviating values

A deviating trendline value for M1.1 can be visualized at 9 cross-girders. There are different factors that could influence the damage value. When the spacing between cross-girders changes, the coordinates to be read also change. However, the location of the unit load remains unchanged, resulting in a shift in the position of the load relative to the critical fatigue detail. In the case of 9 cross-girders, the load is positioned such that it is in line with the diaphragm. This results in the highest possible damage for detail M1.1. Adjusting the load position to the most favorable for this detail reduces the damage value from 1.76 to 1.67 [-].

Furthermore, with two middle diaphragms or cross-girders, the lower middle diaphragm/ cross-girder is considered. With an even number of cross-girders, the location of the middle diaphragm does not

change, and the location of the middle cross-girder changes (detail M2). Conversely, with an odd number of cross-girders, the location of the middle cross-girder does not change, and the position of the diaphragm changes (details M1.1 and M1.2). No difference in the damage value should occur if the upper diaphragm or cross-girder is considered instead of the lower one. This is checked for the case where 9 cross-girders (odd) and detail M1.1 are considered.

In Figure 4.4 is the position of the left (lower) diaphragm shown and in Figure 4.5 the right (upper) diaphragm. Figure 4.6 shows the influence lines for both diaphragm positions for detail M1.1. These influence lines suggest that, aside from the shift due to reading location, the magnitude of influence is the same (and thus the damage should be the same). However, if the influence lines are given as input in the Iv-Tool, the total damages computed are not equal. For the left and right diaphragms, the damage values are 1.76 and 1.65 [-], respectively. The difference is caused by the method of the Iv-Tool. When two trains are simultaneously on the bridge, the maximum stress range determined with the rainflow counting method from track 1 is summed up by the one from track 2, for a specific train type. The higher of the two cycle counts is taken. This process is repeated for subsequent stress ranges. However, in some cases, the number of cycles of the stress range from track 1 significantly differs from track 2. This is the case if there are small differences measured in stress ranges by Python. A random example of the three highest stress ranges with the corresponding number of cycles for a certain train type is given in Table 4.5. If the second and third highest stress ranges are considered, there are substantial discrepancies in the number of cycles of track 1 and track 2. As a consequence, if the stress ranges of tracks 1 and 2 are summed up to consider simultaneity on the bridge, more load cycles are in total considered than present. The total damage calculated increases, so becomes more conservative. This is a phenomenon that can occur in some cases due to the methodology used in the Iv-Tool calculation.

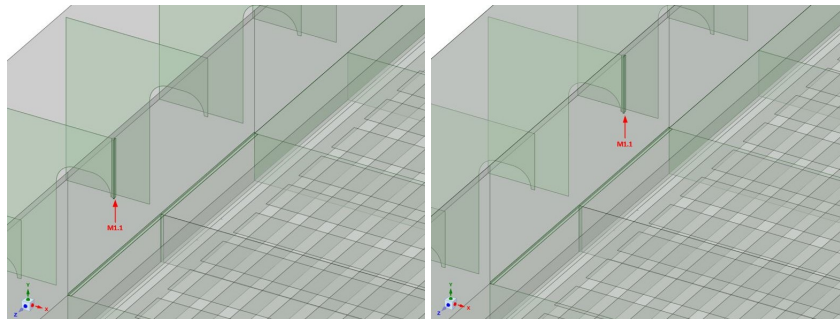


Figure 4.4: Middle diaphragm, left [3]

Figure 4.5: Middle diaphragm, right [3]

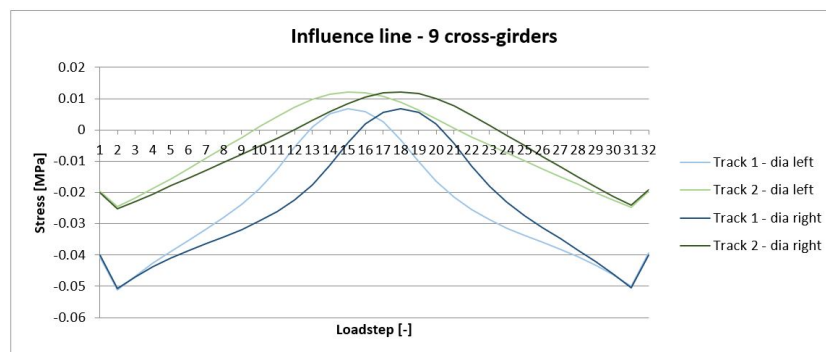


Figure 4.6: Influence lines for 9 cross-girders, position diaphragm left and right, detail M1.1

Table 4.5: Example deviated value due to Iv-Tool method

Track 1		Track 2		Track 1 + Track 2	
#Cycles	Stress range [MPa]	#Cycles	Stress range [MPa]	#Cycles	Stress range [MPa]
⋮	⋮	⋮	⋮	⋮	⋮
8	38	2	16	8	38 + 16
0.5	44.5	8	20	8	44.5 + 20
0.5	45	1	25	1	45 + 25

4.2.3. The height of the cross-girder

In this section, the results of the parameter the height of the cross-girder will be discussed. All dimensions are kept the same, but the height of the cross-girder changes. The height of the cross-girder in the reference model is 500 [mm] and is changed between 300 and 900 [mm]. In Figure 3.13, the parameters and critical fatigue locations M1.1, M1.2, and M2 are visualized.

The results of the parametric study are presented in Table 4.6. In Figure 4.7, a linear regression line ($y = m \cdot x + b$) is established using the least squares method for the three fatigue details considered. Those lines are combined in Figure 4.8. The R-squared value close to 1 means that the regression line fits the data well. Here, the variable m represents the change in total damage for every one-millimeter increase in the height of the cross-girder. The m - and R^2 -value of the best linear fit for each detail is:

- M1.1: $m = -0.0048$ and $R^2 = 0.9257$
- M1.2: $m = -0.0018$ and $R^2 = 0.8525$
- M2: $m = 0.0007$ and $R^2 = 0.5761$

From the results, it can be concluded that increasing the cross-girder height has a positive effect on fatigue details M1.1 and M1.2 and a negative influence on detail M2. In Section E.2 of Appendix E, the deformed plots of a cross-girder height of 300 and 1000 [mm] are shown. It is visible that there is less deformation of the cross-girder and rotation of the main girder with a cross-girder height of 1000 [mm] compared to a height of 300 [mm]. This reduced deformation has a beneficial effect on the fatigue stresses at details M1.1 and M1.2. However, from a height of 700 [mm] and higher the rotational stiffness of the connection between the main girder and deck plate increases. This is caused by the shorter distance between the deck plate connection and the diaphragm end tip. The stresses at M2 increase at the location of the diaphragm.

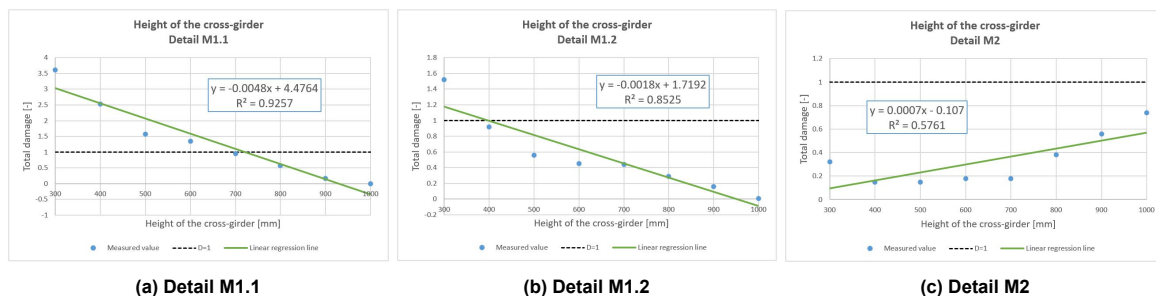
Table 4.6: Damage, parameter: the height of the cross-girder

Height of cg [mm]	Damage M1.1 [-]	M1.1 D↓	Damage M1.2 [-]	M1.2 D↓	Damage M2 [-]	M1.1 D↑	Location M2
300	3.61	+130%	1.52	+171%	0.32	+113%	cg
400	2.53	+61%	0.92	+64%	0.15	+0%	cg
500	1.57	/	0.56	/	0.15	/	dia
600	1.34	-15%	0.45	-20%	0.18	+20%	dia
700	0.96	-39%	0.44	-21%	0.18	+20%	dia
800	0.57	-64%	0.29	-48%	0.38	+153%	dia
900	0.16	-90%	0.16	-71%	0.56	+273%	dia
1000	0.00	-100%	0.01	-98%	0.74	+393%	dia

Abbreviations: cg = cross-girder, dia = diaphragm, D↓ = The difference in total damage with respect to the reference model

Elaboration: in bold = the results of the reference model

Reference: the fatigue details correspond to those given in Figure 3.11 and Figure 3.13



(a) Detail M1.1

(b) Detail M1.2

(c) Detail M2

Figure 4.7: Linear regression using least squares method, parameter: the height of the cross-girder

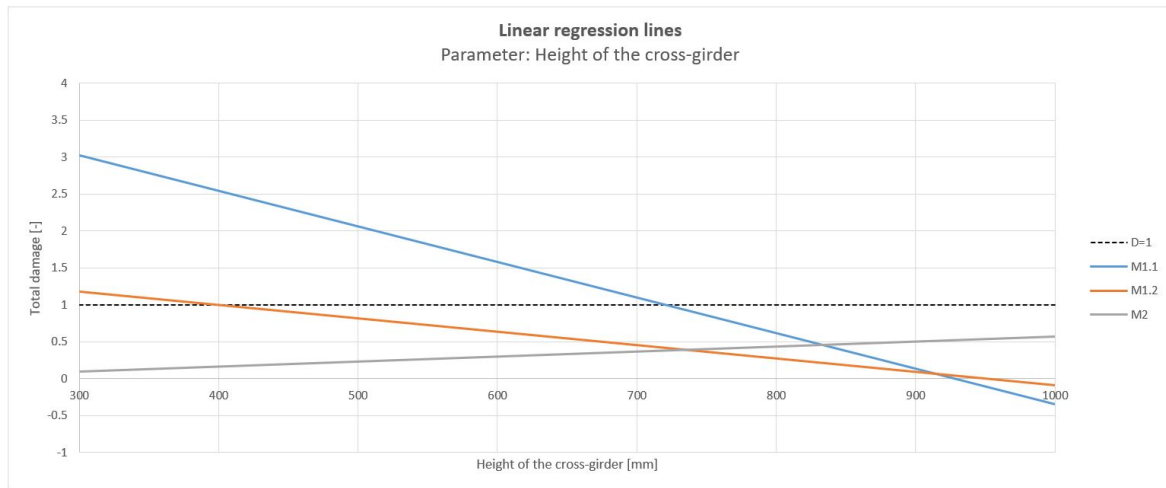


Figure 4.8: Linear regression lines for the parameter: the height of the cross-girder

In Table 4.7, the absolute costs that come along with changing the cross-girder height are shown per fatigue damage change. The linear regression lines of Figure 4.7 are used to determine the costs related to changing the damage value with 1 [-]. The costs of increasing/ decreasing the cross-girder height consists of:

- Extra steel to increase all cross-girders in height
- Extra welding length to weld the increased cross-girders to the main girder

Increasing the height will increase the costs and weight of the bridge structure. The weight increases by 2 [t] with every 100 [mm] increase in height. This reflects the pollution of the material [60].

Table 4.7: Costs to change the total damage value with 1, parameter: the height of the cross-girder

Fatigue detail	Damage [-] / 100 [mm]	Costs [€] / damage [-]	€↑ D↓
M1.1	0.4800	5941	+
M1.2	0.1800	15843	+
M2	0.0700	40740	-

Abbreviations: €↑ D↓ = increase (+) or decrease (-) of the costs when reducing the damage value

4.2.4. The height of the main girder

The parameter, the height of the main girder (H_{mg}), is investigated for two cases. The distinction lies in how the diaphragm moves along to the increase in the main girder height. The two cases are (see Figure 4.9):

1. The free space of the diaphragm increases with increasing height (H_{mg_b}), so the welded diaphragm length stays the same (H_{mg_a}).
2. The free space of the diaphragm stays constant with increasing height (H_{mg_b}), so the welded diaphragm length increases (H_{mg_a}).

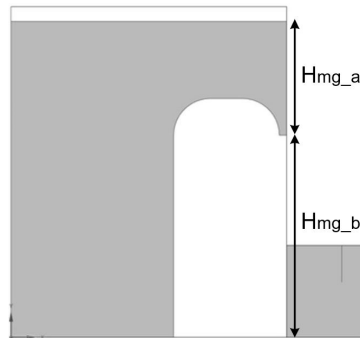


Figure 4.9: Definition of H_{mg_a} and H_{mg_b} [3]

The reference height of the main girder is 1800 [mm] and is changed between 1600 and 2400 [mm] when the gap size increases and between 1800 and 2400 [mm] when the gap size stays the same. The results of cases 1 and 2 are shown in Table 4.8 and Table 4.9, respectively.

Table 4.8: Damage, parameter: the height of the main girder - increasing gap size

Height main girder [mm]	Damage M1.1 [-]	M1.1 D↓	Damage M1.2 [-]	M1.2 D↓	Damage M2 [-]	M2 D↓	Location M2
1600	1.99	+27%	1.10	+96%	0.66	+340%	dia
1700	1.68	+7%	1.04	+86%	0.27	+80%	dia
1800	1.57	/	0.56	/	0.15	/	dia
1900	1.34	-15%	0.44	-21%	0.10	-33%	cg
2000	1.43	-9%	0.32	-43%	0.08	-47%	cg
2100	0.99	-37%	0.22	-61%	0.06	-60%	cg
2200	0.74	-53%	0.20	-64%	0.05	-67%	cg
2300	0.66	-58%	0.11	-80%	0.04	-73%	cg
2400	0.50	-68%	0.06	-89%	0.03	-80%	cg

Abbreviations: cg = cross-girder, dia = diaphragm, D↓ = The difference in total damage with respect to the reference model
 Elaboration: in bold = the results of the reference model

Reference: the fatigue details correspond to those given in Figure 3.11 and Figure 3.13

Table 4.9: Damage, parameter: the height of the main girder - same gap size

Height main girder [mm]	Damage M1.1 [-]	M1.1 D↓	Damage M1.2 [-]	M1.2 D↓	Damage M2 [-]	M2 D↓	Location M2
1800	1.57	/	0.56	/	0.15	/	dia
1900	1.67	+6%	0.69	+23%	0.16	+7%	dia
2000	1.77	+13%	0.81	+45%	0.12	-20%	dia
2100	1.78	+13%	0.83	+48%	0.12	-20%	dia
2200	1.74	+11%	0.91	+63%	0.12	-20%	dia
2300	1.71	+9%	0.90	+61%	0.13	-13%	dia
2400	1.71	+9%	0.94	+68%	0.13	-13%	dia

Abbreviations: cg = cross-girder, dia = diaphragm, D↓ = The difference in total damage with respect to the reference model
 Elaboration: in bold = the results of the reference model

Reference: the fatigue details correspond to those given in Figure 3.11 and Figure 3.13

In Figure 4.10, the lines of best fit for the case of the increased gap size are shown (case 1). The direction coefficient m shows the change of the total damage value per millimeter increased main girder height. The m - and R^2 -value of the linear regression lines are:

- M1.1 - increased gap size: $m = -0.0018$ and $R^2 = 0.9655$
- M1.2 - increased gap size: $m = -0.0013$ and $R^2 = 0.8772$
- M2 - increased gap size: $m = -0.0006$ and $R^2 = 0.6093$

For the case where the same gap size is considered (case 2), the linear regression lines are shown in Figure 4.11. The m - and R^2 -value of the best linear fit for each detail is:

- M1.1 - same gap size: $m = 0.0002$ and $R^2 = 0.2583$
- M1.2 - same gap size: $m = 0.0006$ and $R^2 = 0.8774$
- M2 - same gap size: $m = -0.00004$ and $R^2 = 0.3333$

Both results of applying the least squares method are shown in Figure 4.12.

The deformed shapes in Section E.3 and E.4 indicate that the flexibility of the inner web of the main girder influences the stresses at the considered details. While the deformation of the cross-girder is the same in all cases, the deformation of the main girder's inner web is different. When the connection between the deck plate is closer to the diaphragm end tip ($H_{mg} = 1600$ [mm] and $H_{mg} = 1700$ [mm]), higher stresses at M2 are measured, as is also concluded for the parameter, the height of the cross-girder. The reason for this is the increased rotational stiffness of this connection. Increasing the main girder height (both cases), however, does not have a large influence on the fatigue performance of detail M2. In all cases, the stresses at this detail fall within acceptable limits for fatigue. Only the critical location changes from the diaphragm to the cross-girder web with increasing gap size. At this location, the connection between the deck plate and the main girder is stiffer compared to the location of the diaphragm. Nevertheless, increasing the gap size has a beneficial effect on the determined fatigue damages of details M1.1 and M1.2. The increased flexibility of the inner web of the main girder reduces the stresses at M1.1 and M1.2. On the contrary, increasing the main girder height and keeping the same gap size slightly increases the fatigue damage at those details. The inner web is clamped over a longer length which makes it at the diaphragm end tip more rigid.

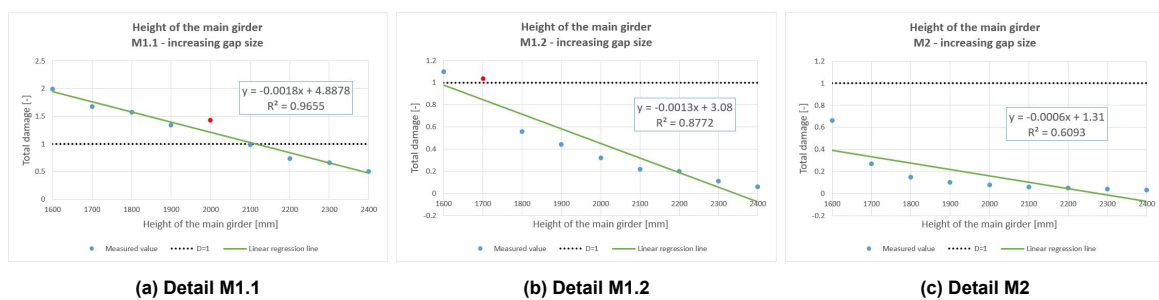


Figure 4.10: Linear regression using least squares method, parameter: the height of the main girder - increasing gap size

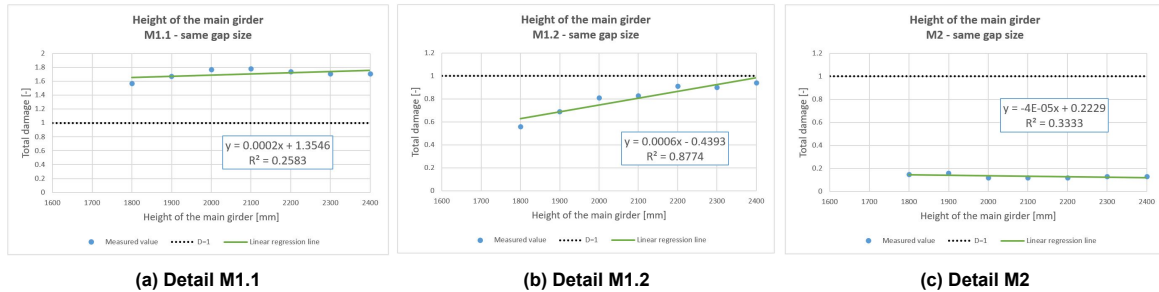


Figure 4.11: Linear regression using least squares method, parameter: the height of the main girder - same gap size

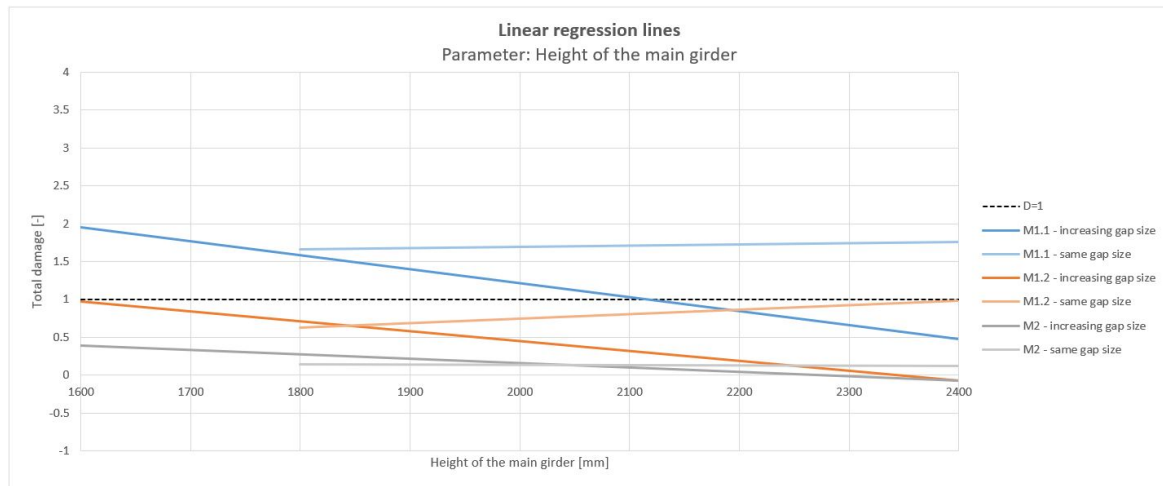


Figure 4.12: Linear regression lines for the parameter: the height of the main girder

The absolute costs that are linked to changing the main girder height (changing the gap size) and changing the damage values of all the details with 1 [-] are shown in Table 4.10. The costs of increasing the height include:

- The extra steel to increase the inner and outer web of the two main girders
- The extra steel to increase the height of all diaphragms and end stiffeners
- The additional welding of the connection between the heightened diaphragm/end stiffeners and the main girder's inner and outer web

Increasing the height increases the costs. In addition, the environmental impact is increased. The weight of the total structure is increased by 1404 [t] for every 100 [mm] increase.

Table 4.10: Costs to change the total damage value with 1, parameter: the height of the main girder - increasing gap size

Fatigue detail	Damage [-] / 100 [mm]	Costs [€] / damage [-]	€↑ D↓
M1.1	[0.1800]	[7806733]	+
M1.2	[0.1300]	[10809323]	+
M2	[0.0600]	[23420200]	+

Abbreviations: €↑ D↓ = increase (+) or decrease (-) of the costs when reducing the damage value

Deviating values

There are two main deviating values visible, namely the damage of detail M1.1 at a height of $H = 2000$ [mm] and of detail M1.2 at $H = 1700$ [mm] for the increased gap size case. Both deviations are the results of the methodology of the Iv-Tool, as explained in Section 4.2.2.

4.2.5. The thickness of the inner web of the main girder

The influence of the thickness of the inner web of the main girder on the fatigue response is determined. The thickness in the reference model is 30 [mm] and is changed between 10 and 50 [mm]. The results are shown in Table 4.11. Also, the linear best-fitted lines of the measured data for the three fatigue details are presented in Figure 4.13 and are combined in Figure 4.14. In this case, m represents the change in total damage per millimeter increase in inner web thickness. The m - and R^2 -value of the regression line for each detail is:

- M1.1: $m = -0.3107$ and $R^2 = 0.8738$
- M1.2: $m = -0.1451$ and $R^2 = 0.8262$
- M2: $m = 0.0481$ and $R^2 = 0.7779$

The results show that from a thickness of 30 [mm] and higher, the fatigue damage of detail M2 increases. A thicker main girder web makes the connection between the main girder and the cross-girder stiffer because less deformation of the inner web of the main girder is possible. This results in an increase

in stress in the deck plate at detail M2 with increasing inner web thickness. On the contrary, the increasing thickness results in notable lower fatigue damages of details M1.1 and M1.2. The stresses are reduced by the increased cross-sectional area of the plate. Moreover, in the case of a thin inner web, the rotational stiffness at the diaphragm is relatively higher compared to a thick web that is "stiff" over the total length of the bridge. The thinner web is restricted in its deformation capabilities at the diaphragm, causing peak stresses to occur. Increasing the web thickness reduces peak stresses at the diaphragm's end tip.

Table 4.11: Damage, parameter: the thickness of the inner web of the main girder

Thickness inner web [mm]	Damage M1.1 [-]	M1.1 D↓	Damage M1.2 [-]	M1.2 D↓	Damage M2 [-]	M2 D↓	Location M2
10	10.58	+574%	5.18	+825%	0.00	-100%	cg+dia
15	10.42	+564%	5.14	+818%	0.00	-100%	cg+dia
20	8.35	+432%	3.24	+479%	0.05	-67%	dia
25	4.21	+168%	1.35	+141%	0.10	-33%	dia
30	1.57	/	0.56	/	0.15	/	dia
35	0.87	-45%	0.23	-59%	0.37	+147%	cg
40	0.15	-90%	0.08	-86%	0.83	+453%	cg
45	0.04	-97%	0.02	-96%	1.39	+827%	cg
50	0.00	-100%	0.00	-100%	2.11	+1307%	cg

Abbreviations: cg = cross-girder, dia = diaphragm, D↓ = The difference in total damage with respect to the reference model

Elaboration: in bold = the results of the reference model

Reference: the fatigue details correspond to those given in Figure 3.11 and Figure 3.13

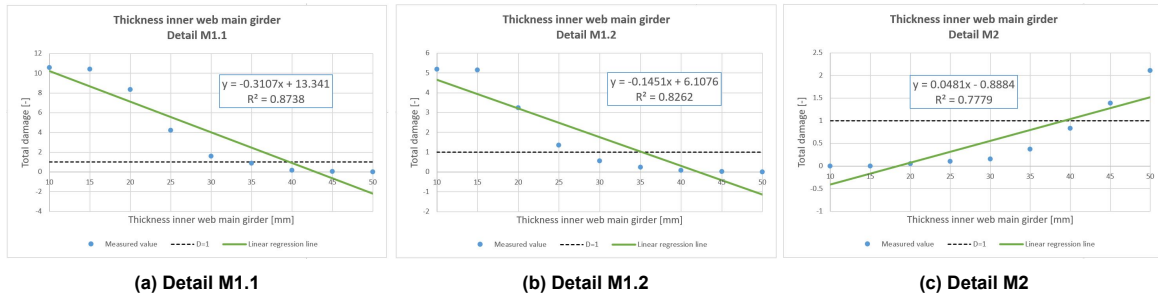


Figure 4.13: Linear regression using least squares method, parameter: the thickness of the inner web of the main girder

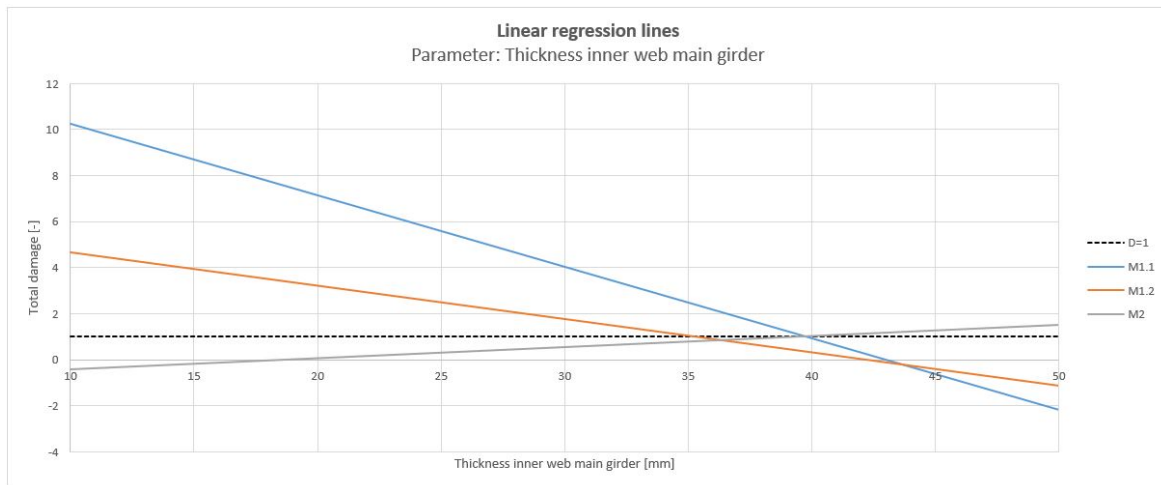


Figure 4.14: Linear regression lines for the parameter: the thickness of the inner web of the main girder

The costs that are related to changing the thickness of the inner web of the main girder and changing the damage value of all the details with 1 [-] are shown in Table 4.12. The costs include the extra steel needed to thicken the inner web of both main girders. Between a thickness of 10 and 30 [mm], no extra steel is considered in this study. There are no costs within this range due to the requirement that both

the inner and outer web thickness must be a minimum of 60 [mm]. The costs are calculated for an inner web thickness larger than 30 [mm].

Increasing the web thickness ($T_{mg} > 30$ [mm]) with 5 [mm] will increase the weight of the total structure with 2826 [t], contributing to the carbon footprint of the bridge [60].

Table 4.12: Costs to change the total damage value with 1, parameter: the thickness of the inner web of the main girder, $T_{mg} > 30$ [mm]

Fatigue detail	Damage [-] / 5 [mm]	Costs [€] / damage [-]	€ \updownarrow D \updownarrow
M1.1	1.5535	1819118	+
M1.2	0.7255	3895245	+
M2	0.2405	11750520	-

Abbreviations: € \updownarrow D \updownarrow = increase (+) or decrease (-) of the costs when reducing the damage value

4.2.6. The thickness of the diaphragm

The thickness of the diaphragm is altered in the parametric study. The thickness in the reference model is 20 [mm] and is changed between 10 and 30 [mm]. The consequence is determined for three fatigue critical details, see Figure 3.11. The results are shown in Table 4.13. In Figure 4.15 and Figure 4.16, the best-fitted linear lines for the measured values are shown for each fatigue detail. The slope m represents the change in total damage if the thickness of the diaphragm is increased by 1 [mm]. The m - and R^2 -value of the linear regression line for each detail is:

- M1.1: $m = 0.1218$ and $R^2 = 0.9875$
- M1.2: $m = 0.0454$ and $R^2 = 0.9919$
- M2: $m = 0.003$ and $R^2 = 0.3676$

A thicker diaphragm reacts more stiffly. The consequence is that all welded details close to the diaphragm experience higher peak stresses because the inner web of the main girder can deform less at this location under the same loading conditions. The influence of the diaphragm thickness is substantial. With a 5 [mm] reduction in thickness compared to the reference model, all details satisfy the fatigue requirements. However, further assessment is necessary to determine if this reduction is feasible in terms of the overall strength and stiffness of the entire structure.

Table 4.13: Damage, parameter: the thickness of the diaphragm

Thickness diaphragm [mm]	Damage M1.1 [-]	M1.1 D \updownarrow	Damage M1.2 [-]	M1.2 D \updownarrow	Damage M2 [-]	M2 D \updownarrow	Location M2
10	0.52	-67%	0.16	-71%	0.09	-40%	cg
15	0.87	-45%	0.35	-38%	0.12	-20%	cg
20	1.57	/	0.56	/	0.15	/	dia
25	2.16	+38%	0.78	+39%	0.09	-40%	dia
30	2.92	+86%	1.08	+93%	0.18	+20%	dia

Abbreviations: cg = cross-girder, dia = diaphragm, D \updownarrow = The difference in total damage with respect to the reference model

Elaboration: in bold = the results of the reference model

Reference: the fatigue details correspond to those given in Figure 3.11 and Figure 3.13

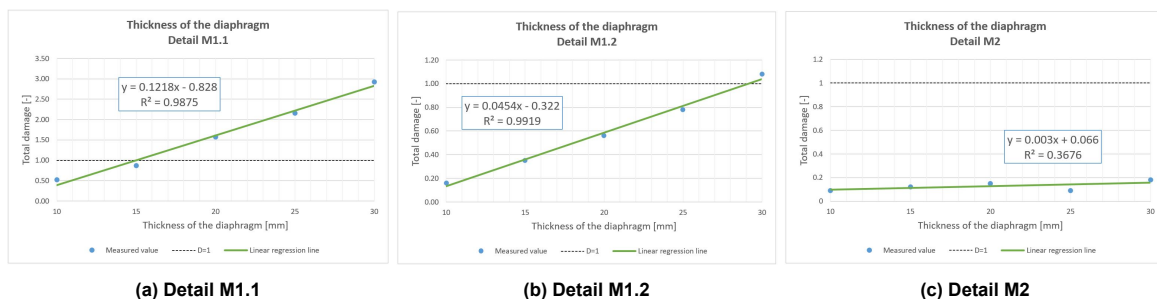


Figure 4.15: Linear regression using least squares method, parameter: the thickness of the diaphragm

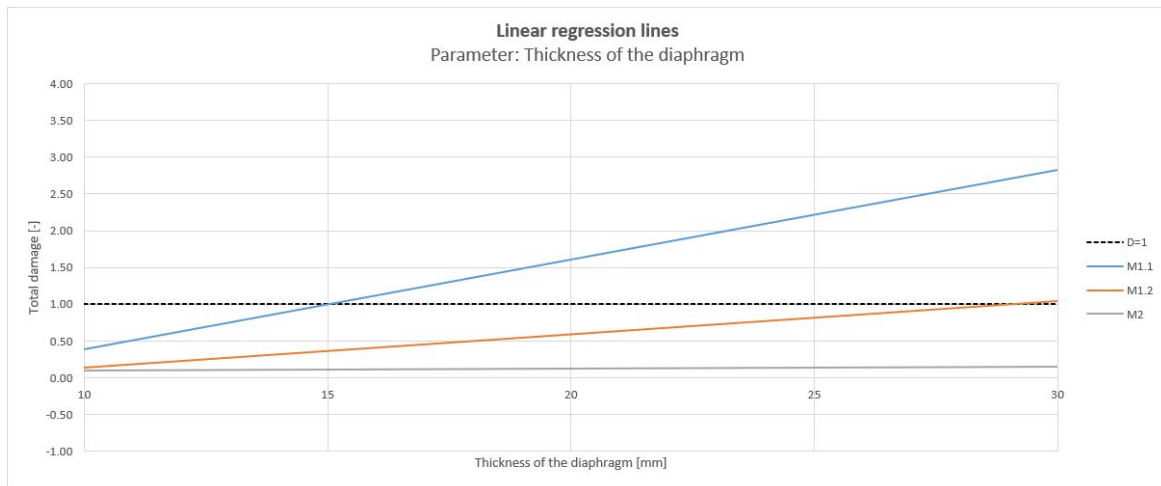


Figure 4.16: Linear regression lines for the parameter: the thickness of the diaphragm

The costs that are related to changing the thickness of the diaphragm and changing the damage value of all the details with 1 [-] are shown in Table 4.14. The cost consists of the extra steel needed to thicken the diaphragm. Decreasing the thickness, which is in this case the more beneficial option for fatigue design, will reduce the costs of the bridge. Moreover, reducing the thickness of 26 diaphragms with 5 [mm] decreases the weight of the total bridge structure by 1860 [t]. Less steel needs to be produced, which reduces CO_2 emissions [60].

Table 4.14: Costs to change the total damage value with 1, parameter: the thickness of the diaphragm

Fatigue detail	Damage [-] / 5 [mm]	Costs [€] / damage [-]	€ \updownarrow D \downarrow
M1.1	[0.6090]	[3053403]	-
M1.2	[0.2270]	[8191729]	-
M2	[0.0150]	[123968173]	-

Abbreviations: € \updownarrow D \downarrow = increase (+) or decrease (-) of the costs when reducing the damage value

4.2.7. The thickness of the steel deck plate

The results of the study of the thickness of the steel deck plate on the fatigue damage are shown in Table 4.15. The thickness of the deck plate in the reference model is 20 [mm] and is changed between 10 and 40 [mm]. In addition, Figure 4.17 and Figure 4.18 show the linear regression lines for each detail. Here, m represents the change in total damage per millimeter increase in the thickness of the steel deck plate. The m - and R^2 -value of the linear regression line for each detail is:

- M1.1: $m = -0.0341$ and $R^2 = 0.6699$
- M1.2: $m = -0.0182$ and $R^2 = 0.7778$
- M2: $m = -0.1468$ and $R^2 = 0.6248$

The results show minimum effect for all details. In Figure 3.11, the locations of the details are explained. In Section E.7 of Appendix E, the deformed shapes for a thickness of 10 [mm] and 40 [mm] are shown. It shows that the thicker deck plate deforms less. In addition, the main girder rotates less. As a result, the inner web of the main girder has to deform less, which lowers the stresses at details M1.1 and M1.2. A thicker deck plate is stiffer and attracts more force but the larger area of the plate lowers the stresses at detail M2. At a thickness of 10 [mm] a higher total damage value of detail M2 is observed than what would be expected as the trend line is followed. The explanation for this is the mesh size and the reading points. With a smaller thickness, the mesh size at the weld connecting the deck plate to the main girder is smaller because the mesh is equal to $0.4t \cdot t$. A smaller mesh size results in higher stresses. Moreover, the reading points to determine the HSS of detail M2 are closer to the connection due to the weld geometry. Because of the right-angle connection, higher stresses are measured closer to this location.

Table 4.15: Damage, parameter: the thickness of the steel deck plate

Thickness deck plate [mm]	Damage M1.1 [-]	M1.1 D↓	Damage M1.2 [-]	M1.2 D↓	Damage M2 [-]	M2 D↓	Location M2
10	2.46	+57%	1.01	+80%	4.85	+3133%	cg
20	1.57	/	0.56	/	0.15	/	dia
30	1.25	-20%	0.47	-16%	0.02	-87%	dia
40	1.43	-9%	0.43	-23%	0.00	-100%	cg+dia

Abbreviations: cg = cross-girder, dia = diaphragm, D↓ = The difference in total damage with respect to the reference model
 Elaboration: in bold = the results of the reference model
 Reference: the fatigue details correspond to those given in Figure 3.11 and Figure 3.13

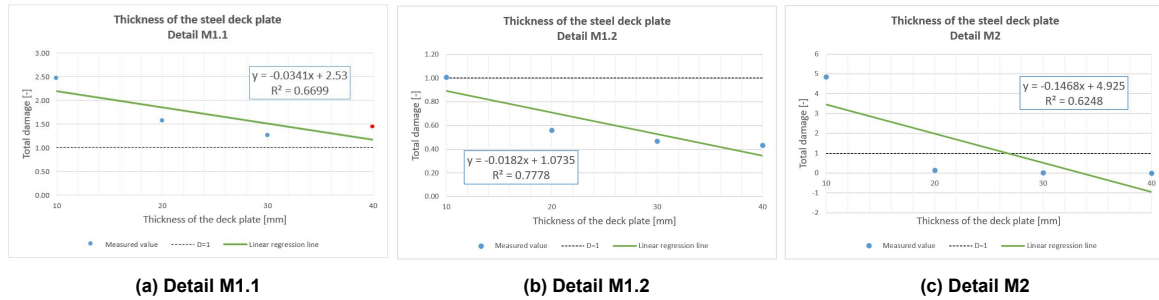


Figure 4.17: Linear regression using least squares method, parameter: the thickness of the steel deck plate

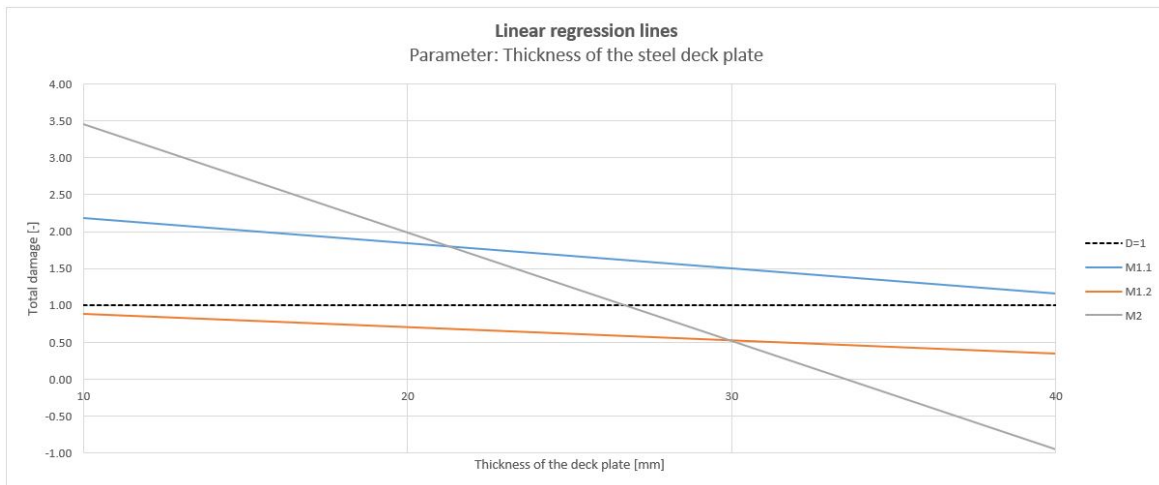


Figure 4.18: Linear regression lines for the parameter: the thickness of the steel deck plate

The costs that are related to changing the thickness of the steel deck plate and changing the damage value of all the details with 1 [-] are shown in Table 4.16. The cost consists of the extra steel needed to thicken the deck plate and the extra volume of the weld connecting the deck plate to both main girders. The latter is not linear, an assumption of an extra 125 [mm³] per 5 [mm] is made.

Increasing the thickness of the steel deck plate will result in elevated steel consumption. The manufacturing process of steel is associated with the release of carbon dioxide CO₂ emissions, and energy and water consumption [60]. In total, increasing the thickness of the deck plate with 5 [mm], increases the amount of steel with 7065 tonnes.

Table 4.16: Costs to change the total damage value with 1, parameter: the thickness of the steel deck plate

Fatigue detail	Damage [-] / 5 [mm]	Costs [€] / damage [-]	€↓ D↓
M1.1	0.1705	41468622	+
M1.2	0.0910	77696703	+
M2	0.7340	9632698	+

Abbreviations: €↓ D↓ = increase (+) or decrease (-) of the costs when reducing the damage value

Deviating values

A deviating value is visible at detail M1.1 at a thickness of 40 [mm]. The value is higher than expected, which is the result of the methodology of the Iv-Tool, as explained in Section 4.2.2.

4.3. Results of additional fatigue detail

In addition to fatigue details M1.1, M1.2, and M2, fatigue detail M3 is studied for the different parameters, see Figure 3.12. The results are shown in Appendix F. For each parameter, however, the total damage value is only measured for three values: the reference model and the two extreme considered values of the parameter. A linear line between these three points is created using the least squares method. The results of Section 4.2 show that in most cases a linear relationship gives a good approximation of the trend.

In general, it can be concluded that the total fatigue damage of detail M3 cannot be reduced to below 1 with the parameters considered within realistic sizes. The fatigue damage of this detail can be slightly reduced with the (global) parameters considered. This detail can probably fulfill the requirements by applying local measures such as adding an external plate or a cope hole to mitigate excessive concentrated stresses.

4.4. Design recommendations for bridges project Oostertoegang

On the basis of the results of the parametric study (Section 4.2) suggestions will be made for the fatigue design of the bridges of *project Oostertoegang* with the adapted diaphragm design. Recommendations to enhance the fatigue design of the reference model will be based on both cost-effectiveness and feasibility. Only the fatigue details discussed in the parametric study will be considered. In addition, the total bridge structure will not be verified on strength and stability.

From the results, it can be concluded that fatigue detail M3 will not satisfy fatigue criteria by changing the considered parameters. This detail requires a local approach. Probably adding an external plate or a cope can improve the fatigue performance of this detail. For the reference model (see Section 3.1), fatigue requirements are also not met for the fatigue-prone detail M1.1, which exhibits a fatigue damage of 1.57 [–]. Suggestions to improve the fatigue damage of this detail with the considered parameters will be given.

Parametric alterations incur costs. In Table 4.17, the costs involved with changing the damage value with 1 [–] are sorted by magnitude for each fatigue detail. These costs are determined in Section 4.2. The parameter offering the most cost-effective means of reducing damage by 1 unit will be most interesting to change when designing for fatigue. To reduce the damage value of the particular detail, less material and welding may be required for certain parameters. This will save costs. In this case, the parameter with the highest absolute costs per damage is preferable to change. Other parameters require costs to optimize the damage value of the fatigue detail. In this situation, the parameter with the lowest costs per damage is most interesting to change if feasible.

In Table 4.17, some values that require attention are shown in bold. For all fatigue-prone locations, the parameter T_{mg} requires attention because between an inner web thickness of 10 and 30 [mm] the costs do not change. This is because the thickness of the main girder's inner web is compensated by the outer web. For detail M2 and the parameter T_{deck} , the costs to change the damage look favorable. However, the linear regression line is not fully representative because of the sensitivity to an outlier.

Table 4.17: Sorted costs per damage, in bold: results that require attention

(a) Detail M1.1			(b) Detail M1.2			(c) Detail M2		
Par.	Costs [€] / damage	€↑ D↓	Par.	Costs [€] / damage	€↑ D↓	Par.	Costs [€] / damage	€↑ D↓
H_{cg}	5941	+	H_{cg}	15843	+	H_{cg}	40740	-
T_{mg}	 1819118 	+	T_{mg}	 3895245 	+	T_{deck}	 9632698 	+
T_{dia}	3053403	-	T_{dia}	8191729	-	T_{mg}	 11750520 	-
c-t-c	6791435	+	H_{mg}	10809323	+	H_{mg}	23420200	+
H_{mg}	7806733	+	c-t-c	13019778	+	c-t-c	32191400	+
T_{deck}	41468622	+	T_{deck}	77696703	+	T_{dia}	123968173	-

Abbreviations: par. = parameter, €↑ D↓ = increase (+) or decrease (-) of the costs when reducing the damage value

To satisfy the fatigue requirements of detail M1.1, the thickness of the diaphragm could be decreased with 5 [mm] to a thickness of 15 [mm]. Less steel would reduce the costs of the bridge structure. This would be the most cost-effective option to design for these three fatigue details in the middle of the bridge. However, this alteration would affect the main girder's overall stability. For this reason, this optimization is probably not feasible.

Then, increasing the height of the cross-girder is shown to be a cost-effective solution to improve the fatigue stresses at M1.1 to a level that conforms to the standards. Increasing the height with 200 [mm] to 700 [mm] solves the fatigue issue for this detail. However, due to road and rail alignment requirements, this solution is not realistic for this case.

The third cost-effective solution that follows from the parametric study is increasing the thickness of the inner web of the main girder. Increasing the thickness with 5 [mm] to 35 [mm] would result in a damage value below 1 [-] for details M1.1, M1.2, and M2. It is a more expensive solution but does probably not have a large influence on the structural performance of the bridge. For this reason, it is the most feasible solution.

Other more costly solutions are increasing the number of cross-girders, increasing the height of the main girder, and increasing the thickness of the deck plate. With only increasing the number of cross-girders, fatigue requirements will not be met. The height of the cross-girder should be increased by at least 300 [mm] to meet the criteria, for which space might not be available. Increasing the deck plate thickness is a very costly procedure with low effect. These measures could be used as an addition to others, as a combination of parameters could also reduce the damage value to below 1 [-]. On the other hand, if it is possible to reduce these parameters, costs can be saved and the fatigue details will not be influenced that much. However, it should be noted that the potential for achieving these reductions is limited.

5

Conclusion and recommendations

In this chapter, the conclusions are presented. In addition, recommendations for further research will be put forth.

5.1. Conclusion

The purpose of this report is to determine how certain parameters affect the fatigue strength of the main- to cross-girder connection, and what parameter changes do this in the most cost-effective way. The goal is to minimize the necessity of welding additional plates to the connection while still meeting fatigue requirements. The main research question is: *How can the design of the connection between the main girder and cross-girder of a railway bridge be optimized for fatigue?*

To answer the research question a literature and parametric study is performed. The influence of several parameters on the fatigue performance of the connection is researched. The designs of the bridges of *project Oostertoegang* are the basis of the parametric study. A finite element model in *Ansys® 2022 R2* [3] is created to determine the stress ranges due to moving train loads at fatigue-prone details. Below the conclusions of this research are listed:

- The follow-up research to Pandit [13], modeling the weld with increased thickness of the shell elements, in accordance with the guidelines outlined in prTS 1993-1-901 [4], yielded hot spot stress results comparable to those of a solid model (see Section 4.1.1).
- Designing a diaphragm that increases the flexibility at the main- to cross-girder connection can reduce the maximum fatigue damage at the most critical location by 88% compared to a design with a certain rotational stiffness (see Section 4.2.1).
- Reducing the center-to-center distance between the cross-girders reduces the fatigue stresses at all considered hot spot locations (see Figure 3.11). However, this solution is relatively expensive, considering its minimal impact on fatigue and the costs associated with adjusting the parameter. The fatigue damage of detail M1.1 can be reduced by 17% when increasing the number of cross-girders from 7 to 8 (see Section 4.2.2).
- Increasing the height of the cross-girder reduces the stresses at details M1.1 and M1.2 and increases the stresses at detail M2. This parameter is one of the most cost-effective solutions out of the considered parameters to reduce the damage of detail M1.1. Increasing the height from 500 to 600 [mm] and from 500 to 700 [mm] reduces the damage value with 15% and 39%, respectively (see Section 4.2.3).
- Increasing the height of the main girder, thereby increasing the gap size (H_{mg_b}), reduces the fatigue damage of all details. Changing the height from 1800 to 1900 [mm] reduces the fatigue damage of detail M1.1 with 15% (see Section 4.2.4). However, the costs are high in relation to the advantage achieved.

- Increasing the thickness of the inner web of the main girder reduces the fatigue stresses at details M1.1 and M1.2 but increases those at detail M2. Increasing the thickness from 30 to 35 [mm] has a noticeable effect on the fatigue damage at detail M1.1 with a decrease of 45% (see Section 4.2.5). Also, the estimation is that this is a relatively cost-effective approach.
- Increasing the thickness of the diaphragm increases the fatigue damage at details M1.1 and M1.2 and has almost no influence on detail M2. Decreasing the thickness has a significant influence on the fatigue damage of detail M1.1. A thickness decrease from 20 to 15 [mm], reduces the damage with 45% (see Section 4.2.6). Moreover, decreasing the thickness would save costs and for this reason, is an attractive solution if feasible.
- Increasing the thickness of the deck plate decreases the damage values of the considered details. Increasing the thickness from 20 to 30 [mm] reduces, in this case, the damage of detail M1.1 with 20% (see Section 4.2.7). Increasing the deck plate thickness over the entire bridge is, however, a costly procedure.
- Detail M3 cannot meet fatigue requirements with the analyzed parameters (see Section 4.3). Implementing localized measures could enhance the fatigue life of this specific detail.
- Increasing the thickness of the inner web of the main girder is the most feasible and relatively cost-effective solution to fulfill the fatigue requirements of details M1.1, M1.2, and M2 for this bridge structure (see Section 4.4).

5.2. Recommendations for further research

Based on the results gathered in this report, certain subjects arise that require further detailed investigation. Recommendations for further research are listed below.

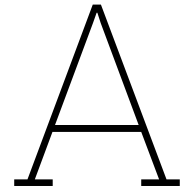
- Additional research is necessary to ascertain the suitability of the hot spot detail categories applied to fatigue detail M2 and M3. NEN-EN1993-1-9 table B.1 detail 3 depicts a cruciform joint featuring a full penetration K-butt weld, whereas detail M2 is a T-joint with a single bevel butt weld. Furthermore, NEN-EN1993-1-9 table B.1 detail 4 addresses a non-load carrying fillet weld, while detail M3 is a single bevel weld.
- Satisfying the fatigue requirements of detail M3 within the considered parameters is unfeasible. Further research is required to identify cost-effective local measures that could enhance the performance of this specific fatigue detail.
- The results of the weld modeling technique for shell elements according to prTS1993-1-901 [4] show good agreement with a solid model considering a welded cruciform joint. In order to check whether this is also the case for a T-joint and other load cases, further research needs to be performed.
- Optimizing the weld modeling technique could help minimize the disparity between the outcomes obtained using shell elements and those derived from solid elements. The computational time with shell elements is significantly lower compared to solid elements, so this would be beneficial.
- Many large steel railway bridges are constructed with either an arch or truss structure. This research only considers a beam railway bridge based on the bridge designs for *project Oostertoegang*. The inclusion of an arch or truss structure impacts the structural stiffness, thereby potentially affecting stress distribution within the structural elements. Further research is needed to understand how this may influence the fatigue performance of the connection between the main- and cross-girder.
- Steel-concrete decks are commonly seen in railway bridge structures. The weight of the bridge deck serves as a beneficial factor for mitigating sound emissions and managing tension forces within the hangers of an arch structure. This study only considers a steel deck. The influence of the steel-concrete deck on the fatigue strength of the main- to cross-girder connection can be further investigated.
- The impact of different cross-sectional shapes of the main girder (open or closed profiles) could be researched to determine the influence on the fatigue stresses at the connection with the cross-girder.

References

- [1] Dura Vermeer. (2022, July 27). *Project oostertoegang amsterdam definitief gegund aan dura vermeer*. <https://www.duravermeer.nl/nieuws/project-oostertoegang-amsterdam-definitief-gegund-aan-dura-vermeer/>
- [2] Pipinato, A. & Patton, R. (2015). *Innovative bridge design handbook: Chapter 19: Railway bridges* (1st ed.). Butterworth-Heinemann.
- [3] ANSYS, Inc. (2022). *Ansys workbench* (Version 2022 R2).
- [4] prTS 1993-1-901. (2021). *CEN/TC 250/TS 1993-1-901: Fatigue design of orthotropic bridge decks with the hot spot stress method (final draft)*. Brussels: European Standard.
- [5] ASM International Handbook Committee. (1996). *Asm handbook, volume 19, fatigue and fracture*. ASM International.
- [6] Haghani, R., Al-Emrani, M., & Hesmati, M. (2012). Fatigue-prone details in steel bridges. *Buildings*, 2(4), 456–476. <https://doi.org/10.3390/buildings2040456>
- [7] Van Lierop, P.J.C. & Langedijk, W.P.J. (2017). Geboorte van een boogbrug: Spoorbrug zandhazenbrug, muiderberg. *Bouwen met Staal*, (258), 14–21.
- [8] Langedijk, W.P.J., Van der Toll, Th.P.M., & Van der Poel, D.P. (2017). Brug in het nauw: Spoorbrug utark, utrecht. *Bouwen met Staal*, (260), 12–19.
- [9] NEN-EN 1993-1-9. (2012). *Eurocode 3: Design of steel structures - part 1-9: Fatigue*. Brussels: European Standard.
- [10] Hobbacher, A.F. (2016). *Recommendations for Fatigue Design of Welded Joints and Components: IIW document IIW-2259-15 ex XIII-2460-13/XV-1440-13* (2nd ed.). International Institute of Welding (IIW). Springer Nature Switzerland AG. <https://doi.org/https://doi.org/10.1007/978-3-319-23757-2>
- [11] OVS00030-6. (2018). *Ontwerpvoorschrift: Kunstwerken - deel 6 - Aanvullingen en wijzigingen op NEN-EN normen*. ProRail.
- [12] Richtlijn Ontwerp Kunstwerken 2.0. (2021-12). *Rijkswaterstaat Technisch Document: RTD 1001 Richtlijn Ontwerp Kunstwerken*. Rijkswaterstaat.
- [13] Pandit, S. (2020). *Finite element modelling of open longitudinal stiffener to crossbeam connection in osd bridges for hot-spot stress determination*. <http://repository.tudelft.nl/>
- [14] Schijve, J. (2009). *Fatigue of structures and materials*. Springer. <https://doi.org/https://doi.org/10.1007/978-1-4020-6808-9>
- [15] Al-emrani, M. & Mustafa, A. (2014). *Fatigue design of steel and composite bridges*.
- [16] Fustar, B., Lukacevic, I., & Dujmovic, D. (2018). Review of fatigue assessment methods for welded steel structures. *Hindawi*. <https://doi.org/https://doi.org/10.1155/2018/3597356>
- [17] Nussbaumer, A., Borges, L., & Davaine, L. (2011). *Fatigue design of steel and composite structures: Eurocode 3: Design of steel structures, part 1–9 fatigue; eurocode 4: Design of composite steel and concrete structures*. ECCS – European Convention for Constructional Steelwork. <https://doi.org/https://doi.org/10.1002/9783433608791>
- [18] Niemi, E., Fricke, W., & Maddox, S.J. (2018). *Structural Hot-Spot Stress Approach to Fatigue Analysis of Welded Components: Designer's Guide* (2nd ed.). International Institute of Welding (IIW). Springer. <https://doi.org/https://doi.org/10.1007/978-981-10-5568-3>
- [19] Downing, S.D. & Socie, D.F. (1982). Simple rainflow counting algorithms. *International Journal of Fatigue*, 4(1), 31–40. [https://doi.org/10.1016/0142-1123\(82\)90018-4](https://doi.org/10.1016/0142-1123(82)90018-4)
- [20] American Society for Testing and Materials. (1997). *Standard Practices for Cycle Counting in Fatigue Analysis* (E1049-85).
- [21] Matsuishi, M. & Endo, T. (1968). *Fatigue of metals subjected to varying stress*. Presented to the Japan Society of Mechanical Engineers, Fukuoka, Japan.
- [22] Rychlik, I. (1987). A new definition of the rainflow cycle counting method. *International Journal of Fatigue*, 9(2), 119–121. [https://doi.org/10.1016/0142-1123\(87\)90054-5](https://doi.org/10.1016/0142-1123(87)90054-5)
- [23] Lee, Y. & Tjhong, T. (2012). *Metal fatigue analysis handbook: Chapter 3 - rainflow cycle counting techniques*. Elsevier Inc. <https://doi.org/https://doi.org/10.1016/B978-0-12-385204-5.00003-3>

- [24] Pedersen, M.M. (2018, November). *Introduction to metal fatigue: Concepts and engineering approaches* (Technical report ME-TR-11). Aarhus University.
- [25] Aygül, M. (2012). *Fatigue analysis of welded structures using the finite element method*. Chalmers University of Technology.
- [26] Lee, J., Seo, J., Kim, M., Shin, S., Han, M., Park, J., & Mahendran, M. (2010). Comparison of hot spot stress evaluation methods for welded structures. *International Journal of Naval Architecture and Ocean Engineering*, 2(4), 200–210. <https://doi.org/https://doi.org/10.2478/IJNAOE-2013-0037>
- [27] Park, W. & Miki, C. (2008). Fatigue assessment of large-size welded joints based on the effective notch stress approach. *International Journal of Fatigue*, 30(9), 1556–1568. <https://doi.org/https://doi.org/10.1016/j.ijfatigue.2007.11.012>
- [28] Fricke, W. (2001). Recommended hot spot analysis procedure for structural details of FPSOs and ships based on round-robin FE analyses. *International Journal of Offshore and Polar Engineering*, 12(1), 1–8.
- [29] Storsul, R., Landet, E., & Lotsberg, I. (2004). *Convergence analysis for welded details in ship shaped structures* (OMAE-FPSO'04-0016. Int. Conf. Houston 2004).
- [30] Al-Emrani, M. & Aygul, M. (2014). *Fatigue design of steel and composite bridges*. Chalmers University of Technology.
- [31] Xiao, Z. & Yamada, K. (2004). A method of determining geometric stress for fatigue strength evaluation of steel welded joints. *International Journal of Fatigue*, 26(12), 1277–1293. <https://doi.org/https://doi.org/10.1016/j.ijfatigue.2004.05.001>
- [32] Dong, P. (2001). A structural stress definition and numerical implementation for fatigue analysis of welded joints. *International Journal of Fatigue*, 23(10), 865–876. [https://doi.org/https://doi.org/10.1016/S0142-1123\(01\)00055-X](https://doi.org/https://doi.org/10.1016/S0142-1123(01)00055-X)
- [33] Logan, D.L. (2007). *A first course in the finite element method* (4th ed.). Thomson.
- [34] Muelaner, J. (2020, September 30). *Shell or solid elements for thin walled parts?* <https://www.3dcadworld.com/shell-or-solid-elements-for-thin-walled-parts/>
- [35] Eriksson, Å., Olsson, C., & Spennare, H. (2003). *Weld evaluation using fem: A guide to fatigue-loaded structures*. Industrilitteratur.
- [36] Nikraftar, N. (2020). *Fatigue assessment of cross girder to main girder welded joints in steel bridges using solid and shell elements*. <https://research.tue.nl/en/studentTheses/fatigue-assessment-of-cross-girder-to-main-girder-welded-joints-i>
- [37] Niemi, E. (1995). *Stress determination for fatigue analysis of welded components: A volume in woodhead publishing series in welding and other joining technologies*. Woodhead Publishing.
- [38] Fayard, F.L., Bignonnet, A., & Dang Van, K. (1996). Fatigue design criterion for welded structures. *Fatigue Fracture of Engineering Materials Structures (FFEMS)*, 19(6), 723–729. <https://doi.org/https://doi.org/10.1111/j.1460-2695.1996.tb01317.x>
- [39] Romeijn, A. (2002). Evolutie van de verschijningsvorm van vaste bruggen vanaf 1940. *Bruggen*, 10(4), 14–23.
- [40] Romeijn, A. (2003). Evolutie van de verschijningsvorm van vaste bruggen vanaf 1940. *Bruggen*, 11(2), 4–15.
- [41] Berggren, H. (2021). *The use of higher steel grades in building elements*.
- [42] ZJA. (n.d.). *De zandhazenbrug, spoorbrug, muiderberg*. <https://www.zja.nl/nl/Zandhazenbrug-spoorbrug-Muiderberg>
- [43] Bouwen met Staal. (2022). *Spoorbrug zuidhorn: Noordhorn*. <https://www.nationalestaalprijs.nl/project/spoorbrug-zuidhorn>
- [44] Langejan, W. (2018). *Het is gelukt: Eerste treinen rijden over nieuwe spoorbrug*. <https://www.ad.nl/utrecht/het-is-gelukt-eerste-treinen-rijden-over-nieuwe-spoorbrug~a1c756e9/>
- [45] ProRail. (2020). *Kijk mee: Spoorbrug theemswegtracé gaat op z'n plek*. <https://www.prorail.nl/nieuws/kijk-mee-spoorbrug-theemswegtracé-gaat-op-z-n-plek>
- [46] Theemswegtracé, Rotterdam | Even een stukje havenspoorlijn verleggen. (2020). *Stedenbouw*. <https://www.stedenbouw.nl/artikel/theemswegtracé-rotterdam-even-een-stukje-havenspoorlijn-verleggen/>
- [47] De Vlaamse Waterweg. (2018a). *Spoorbrug herentals*. <https://www.vlaamsewaterweg.be/spoorbrug-herentals>

- [48] Gezelle, H. (2023). Spoorbrug herentals : Op definitieve plek op zondag 20/8. <https://nieuws.be/artikel/spoorbrug-herentals-op-definitieve-plek-op-zondag-208>
- [49] De Vlaamse Waterweg. (2018b). *Spoorbrug kuringen*. <https://www.vlaamsewaterweg.be/spoorbrug-kuringen>
- [50] Infrabel. (2020). *Eerste vernieuwde spoor tussen hasselt en kiewit/zonhoven bijna klaar*. <https://infrabel.be/nl/article/eerste-vernieuwde-spoor-tussen-hasselt-en-kiewitzonhoven-bijna-klaar>
- [51] Seaburg, P.A. & Carter, C.J. (2003). *Torsional analysis of structural steel members*. American Institute of Steel Construction.
- [52] NEN-EN 1993-2. (2011). *Eurocode 3: Design of steel structures - part 2: Steel bridges*. Brussels: European Standard.
- [53] NEN-EN 1991-2. (2011). *Eurocode 1: Actions on structures – part 2: Traffic loads on bridges*. Brussels: European Standard.
- [54] NEN-EN 1991-2/NB. (2011). *Dutch National Annex to Eurocode 1: Actions on structures – part 2: Traffic loads on bridges*. Brussels: European Standard (in Dutch).
- [55] NEN-EN 1993-1-8. (2011). *Eurocode 3: Design of steel structures - part 1-8: Design of joints*. Brussels: European Standard.
- [56] Bayo, E., Cabrero, J.M., & Gil, B. (2006). An effective component-based method to model semi-rigid connections for the global analysis of steel and composite structures. *Engineering Structures*, 28(1), 97–108. <https://doi.org/https://doi.org/10.1016/j.engstruct.2005.08.001>
- [57] Verkdenius, S., Hengevekd, S., & Maljaars, M. (2023). New fatigue load models for assessing railway bridges in europe. *Elsevier*, 284. <https://doi.org/10.1016/j.engstruct.2023.115914>
- [58] NEN-EN 1993-1-9/NB. (2011). *Dutch National Annex to Eurocode 3: Design of steel structures - part 1-9: Fatigue*. Brussels: European Standard (in Dutch).
- [59] Bouwen met Staal. (n.d.). *Cost components: What methods exist to estimate the costs of steel structures and how can these methods be used to make a cost optimization analysis?* <https://www.bouwenmetstaal.nl/themas/parametrisch-ontwerpen/smartconnection/cost-components>
- [60] Conejo, A.N., Birat, J., & Dutta, A. (2020). A review of the current environmental challenges of the steel industry and its value chain. *Journal of Environmental Management*, 259. <https://doi.org/10.1016/j.jenvman.2019.109782>



Fatigue detail categories

Figure A.1 and Figure A.2 show relevant fatigue detail categories at the location of the main- to cross-girder connection. Figure A.1 considers the detail categories for the nominal stress method and Figure A.2 for the hot spot stress method.

In Table A.1 and Table A.2 the fatigue detail categories are shown. The source of the detail categories is NEN-EN1993-1-9 [9]. Table A.1 includes detail categories for the nominal stress method and Table A.2 for the hot spot stress method. For each fatigue detail, the table number in Eurocode 3 part 1-9 and the detail number are shown.

Nominal stress method

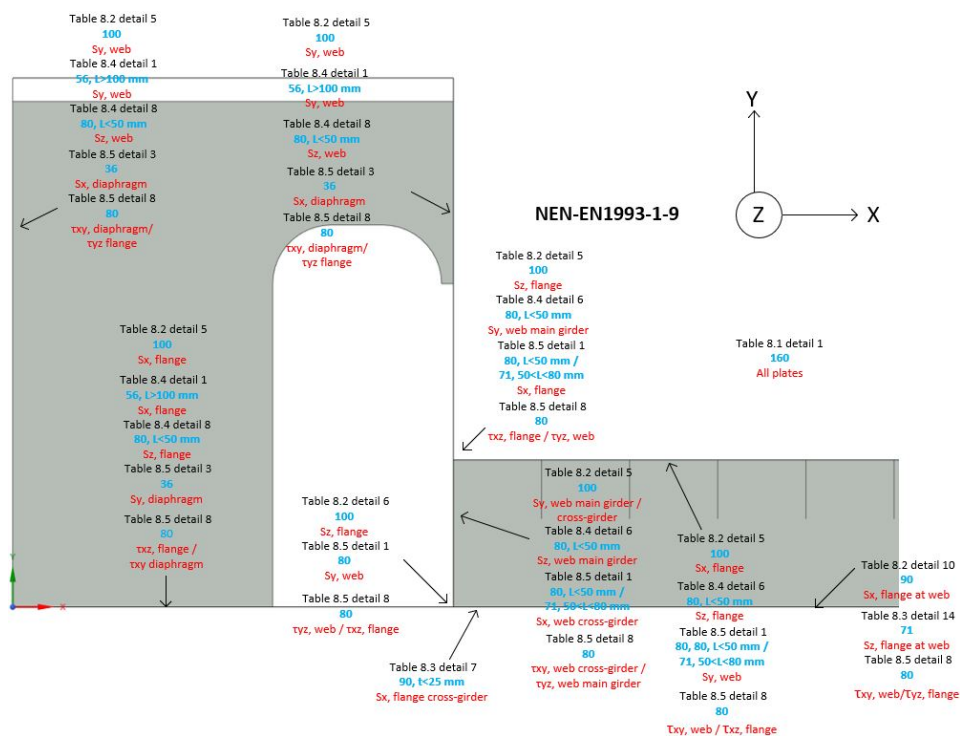
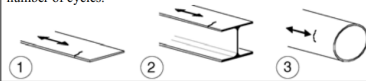
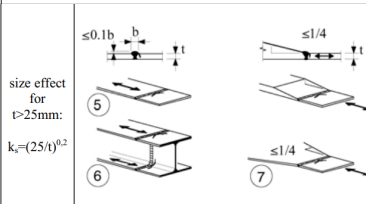
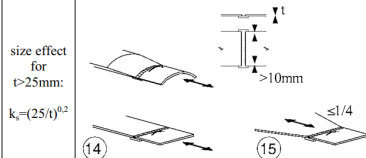
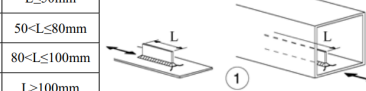
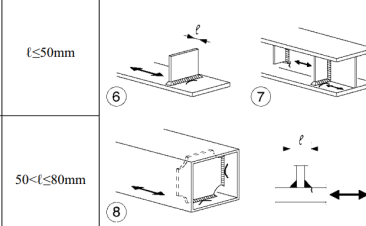
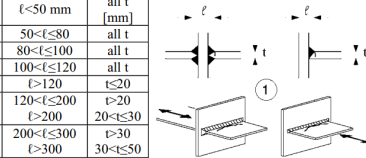
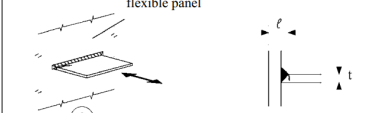
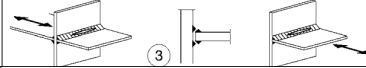
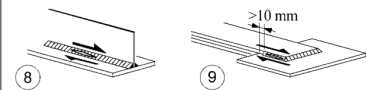


Figure A.1: Fatigue detail categories at the location of the connection between the main- and cross-girder for nominal stress method [3][9]

Table A.1: Fatigue detail categories EN1993-1-9, nominal stress method [9]

Table	Detail	Explanation																															
8.1	1	160	<p>NOTE The fatigue strength curve associated with category 160 is the highest. No detail can reach a better fatigue strength at any number of cycles.</p>  <p>Rolled and extruded products:</p> <ol style="list-style-type: none"> 1) Plates and flats; 2) Rolled sections; 3) Seamless hollow sections, either rectangular or circular. <p>Details 1) to 3):</p> <p>Sharp edges, surface and rolling flaws to be improved by grinding until removed and smooth transition achieved.</p>																														
8.2	5+6	100	 <p>5) Manual fillet or butt weld.</p> <p>6) Manual or automatic butt welds carried out from one side only, particularly for box girders</p> <p>5), 6) A very good fit between the flange and web plates is essential. The web edge to be prepared such that the root face is adequate for the achievement of regular root penetration without break-out.</p>																														
8.2	10	125 112 90	 <p>10) Longitudinal butt weld, both sides ground flush parallel to load direction. 100% NDT</p> <p>10) No grinding and no start/stop</p> <p>10) with start/stop positions</p> <p>5) Transverse splices in plates or flats.</p> <p>6) Full cross-section butt welds of rolled sections without cope holes.</p> <p>7) Transverse splices in plates or flats tapered in width or in thickness with a slope $\leq 1/4$. Translation of welds to be machined notch free.</p> <p>- The height of the weld convexity to be not greater than 10% of the weld width, with smooth transition to the plate surface.</p> <p>- Weld run-on and run-off pieces to be used and subsequently removed, plate edges to be ground flush in direction of stress.</p> <p>- Welded from both sides; checked by NDT.</p> <p>Details 5 and 7:</p> <p>Welds made in flat position.</p>																														
8.3	7	90	<p>size effect for $t > 25\text{mm}$: $k_s = (25/t)^{0.2}$</p>  <p>5) $\leq 0.1b$</p> <p>6) $\leq 1/4$</p> <p>7) $\leq 1/4$</p> <p>Details 5 and 7:</p> <p>Welds made in flat position.</p> <p>Details 14) and 15):</p> <p>Fillet welds attaching the backing strip to terminate ≥ 10 mm from the edges of the stressed plate. Tack welds inside the shape of butt welds.</p>																														
8.3	14	71	<p>size effect for $t > 25\text{mm}$: $k_s = (25/t)^{0.2}$</p>  <p>14) Transverse splice.</p> <p>15) Transverse butt weld tapered in width or thickness with a slope $\leq 1/4$. Also valid for curved plates.</p>																														
8.4	1	80 71 63 56	<p>$L \leq 50\text{mm}$</p> <p>$50 < L \leq 80\text{mm}$</p> <p>$80 < L \leq 100\text{mm}$</p> <p>$L > 100\text{mm}$</p>  <p>Longitudinal attachments:</p> <p>1) The detail category varies according to the length of the attachment L.</p>																														
8.4	6+8	80 71	<p>$t \leq 50\text{mm}$</p> <p>$50 < t \leq 80\text{mm}$</p>  <p>6) Welded to plate.</p> <p>7) Vertical stiffeners welded to a beam or plate girder.</p> <p>8) Diaphragm of box girders welded to the flange or the web. May not be possible for small hollow sections.</p> <p>The values are also valid for ring stiffeners.</p> <p>Details 6) and 7):</p> <p>Ends of welds to be carefully ground to remove any undercut that may be present.</p> <p>7) $\Delta\sigma$ to be calculated using principal stresses if the stiffener terminates in the web, see left side.</p>																														
8.5	1+3	80 71 63 56 50 45 40	<table border="1"> <tr> <td>80</td> <td>$t < 50$ mm</td> <td>all t [mm]</td> </tr> <tr> <td>71</td> <td>$50 < t \leq 80$</td> <td>all t</td> </tr> <tr> <td>63</td> <td>$80 < t \leq 100$</td> <td>all t</td> </tr> <tr> <td>56</td> <td>$100 < t \leq 120$</td> <td>all t</td> </tr> <tr> <td>56</td> <td>$t > 120$</td> <td>$t \leq 20$</td> </tr> <tr> <td>50</td> <td>$120 < t \leq 200$</td> <td>$t > 20$</td> </tr> <tr> <td>50</td> <td>$t > 200$</td> <td>$20 < t \leq 30$</td> </tr> <tr> <td>45</td> <td>$200 < t \leq 300$</td> <td>$t > 30$</td> </tr> <tr> <td>45</td> <td>$t > 300$</td> <td>$30 < t \leq 50$</td> </tr> <tr> <td>40</td> <td>$t > 300$</td> <td>$t > 50$</td> </tr> </table>  <p>Cruciform and Tee joints:</p> <p>1) Toe failure in full penetration butt welds and all partial penetration joints.</p> <p>2) For computing $\Delta\sigma$, use modified nominal stress.</p> <p>3) In partial penetration joints two fatigue assessments are required. Firstly, root cracking evaluated according to stresses defined in section 5, using category 36* for $\Delta\sigma_w$ and category 80 for $\Delta\sigma_w$. Secondly, toe cracking is evaluated by determining $\Delta\sigma$ in the load-carrying plate.</p> <p>Details 1) to 3):</p> <p>The misalignment of the load-carrying plates should not exceed 15 % of the thickness of the intermediate plate.</p>	80	$t < 50$ mm	all t [mm]	71	$50 < t \leq 80$	all t	63	$80 < t \leq 100$	all t	56	$100 < t \leq 120$	all t	56	$t > 120$	$t \leq 20$	50	$120 < t \leq 200$	$t > 20$	50	$t > 200$	$20 < t \leq 30$	45	$200 < t \leq 300$	$t > 30$	45	$t > 300$	$30 < t \leq 50$	40	$t > 300$	$t > 50$
80	$t < 50$ mm	all t [mm]																															
71	$50 < t \leq 80$	all t																															
63	$80 < t \leq 100$	all t																															
56	$100 < t \leq 120$	all t																															
56	$t > 120$	$t \leq 20$																															
50	$120 < t \leq 200$	$t > 20$																															
50	$t > 200$	$20 < t \leq 30$																															
45	$200 < t \leq 300$	$t > 30$																															
45	$t > 300$	$30 < t \leq 50$																															
40	$t > 300$	$t > 50$																															
		As detail 1 in Table 8.5	<p>flexible panel</p>  <p>2) Toe failure from edge of attachment to plate, with stress peaks at weld ends due to local plate deformations.</p>																														
		36*	 <p>3) Root failure in partial penetration Tee-butt joints or fillet welded joint and effective full penetration in Tee-butt joint.</p>																														
8.5	8	80 m=5	 <p>8) Continuous fillet welds transmitting a shear flow, such as web to flange welds in plate girders.</p> <p>9) Fillet welded lap joint.</p> <p>8) $\Delta\tau$ to be calculated from the weld throat area.</p> <p>9) $\Delta\tau$ to be calculated from the weld throat area considering the total length of the weld. Weld terminations more than 10 mm from the plate edge, see also 4) and 5) above.</p>																														

Hot spot stress method

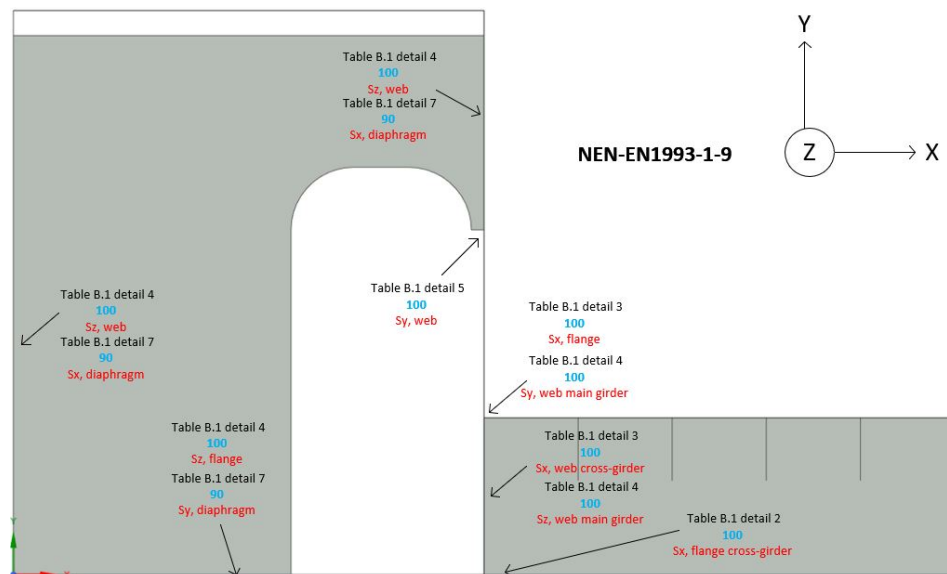
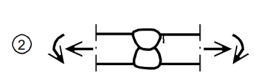
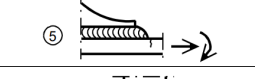


Figure A.2: Fatigue detail categories at the location of the connection between the main- and cross-girder for hot spot stress method [3][9]

Table A.2: Fatigue detail categories EN1993-1-9, hot spot stress method [9]

Table	Detail	Explanation
B.1	2	100  2) Full penetration butt joint. 2) - Weld not ground flush - Weld run-on and run-off pieces to be used and subsequently removed, plate edges to be ground flush in direction of stress. - Welded from both sides. - For misalignment see NOTE 1.
B.1	3	100  3) Cruciform joint with full penetration K-butt welds. 3) - Weld toe angle $\leq 60^\circ$. - For misalignment see NOTE 1.
B.1	4	100  4) Non load-carrying fillet welds. 4) - Weld toe angle $\leq 60^\circ$. - See also NOTE 2.
B.1	5	100  5) Bracket ends, ends of longitudinal stiffeners. 5) - Weld toe angle $\leq 60^\circ$. - See also NOTE 2.
B.1	7	90  7) Cruciform joints with load-carrying fillet welds. 7) - Weld toe angle $\leq 60^\circ$. - For misalignment see NOTE 1. - See also NOTE 2.
B.1	Note 1	Table B.1 does not cover effects of misalignment. They have to be considered explicitly in determination of stress.
B.1	Note 2	Table B.1 does not cover fatigue initiation from the root followed by propagation through the throat.

B

Rainflow counting Iv-Tool

Figure B.1 shows a stress plot due to train type 11 for a random influence line. Table B.1 shows the output of the rainflow counting performed by Python (Iv-Tool). In Figure B.2 the rainflow output is visualized in the stress plot. The load history is rotated 90 degrees clockwise to do the rainflow counting.

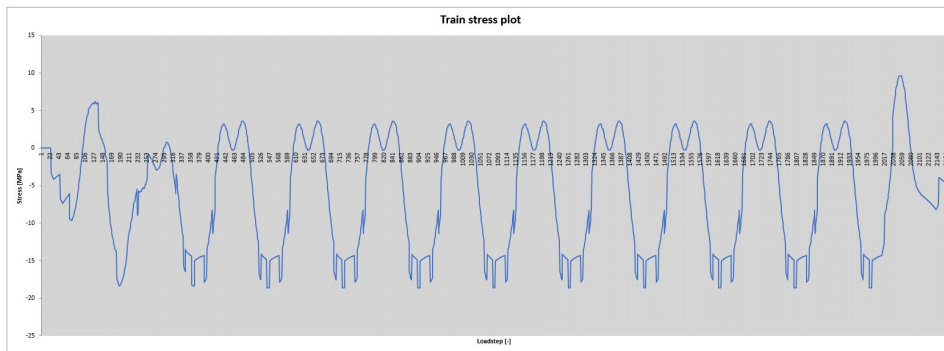


Figure B.1: Stress plot due to train type 11, random influence line

Table B.1: Rainflow counting output Python

Stress range [Mpa]	Average stress [Mpa]	Number of cycles	Start index	End index
0.7	-3.8	1	27	42
1.2	-6.7	1	49	84
9.7	-4.8	0.5	0	70
0.1	6	1	121	123
0.2	6	1	130	132
15.8	-1.7	0.5	70	127
0	-11.4	1	206	207
0	-5.8	1	234	235
0.2	-5.8	1	229	232
3.5	-7.2	1	226	227
0.2	-5.3	1	240	242
0	-0.9	1	251	254
2	-1.9	1	255	273
2.6	-4.8	1	319	320
3	-15	1	341	342
19.2	-8.8	1	184	297
3.6	-16.1	1	386	387
3.1	-9.8	1	406	407
3.5	1.5	1	434	455
3.4	-15.8	1	522	523
2.2	-7.4	1	362	477
3.6	-16.1	1	566	567
3.1	-9.8	1	586	587
3.5	1.5	1	614	635
3.4	-15.8	1	702	703
22.2	-7.5	1	542	657
3.6	-16.1	1	746	747
3.1	-9.8	1	766	767
3.5	1.5	1	794	815
3.4	-15.8	1	882	883
22.2	-7.5	1	122	837
3.6	-16.1	1	926	927
3.1	-9.8	1	946	947
3.5	1.5	1	974	995
3.4	-15.8	1	1062	1063
22.2	-7.5	1	902	1017
3.6	-16.1	1	1106	1107
3.1	-9.8	1	1126	1127
3.5	1.5	1	1154	1175
3.4	-15.8	1	1242	1243
22.2	-7.5	1	1082	1197
3.6	-16.1	1	1286	1287
3.1	-9.8	1	1306	1307
3.5	1.5	1	1334	1355
3.4	-15.8	1	1422	1423
22.2	-7.5	1	1262	1377
3.6	-16.1	1	1466	1467
3.1	-9.8	1	1486	1487
3.5	1.5	1	1514	1535
3.4	-15.8	1	1602	1603
22.2	-7.5	1	1442	1557
3.6	-16.1	1	1646	1647
3.1	-9.8	1	1666	1667
3.5	1.5	1	1694	1715
3.4	-15.8	1	1782	1783
22.2	-7.5	1	1622	1737
3.6	-16.1	1	1826	1827
3.1	-9.8	1	1846	1847
3.5	1.5	1	1874	1895
3.4	-15.8	1	1962	1963
22.2	-7.5	1	1802	1917
24.8	-6.3	0.5	127	1982
0	9.6	1	2050	2051
0.6	-4.2	1	2143	2156
28.2	-4.5	0.5	1982	2052
17.8	0.7	0.5	2052	2136
4.6	-5.9	0.5	2136	2162

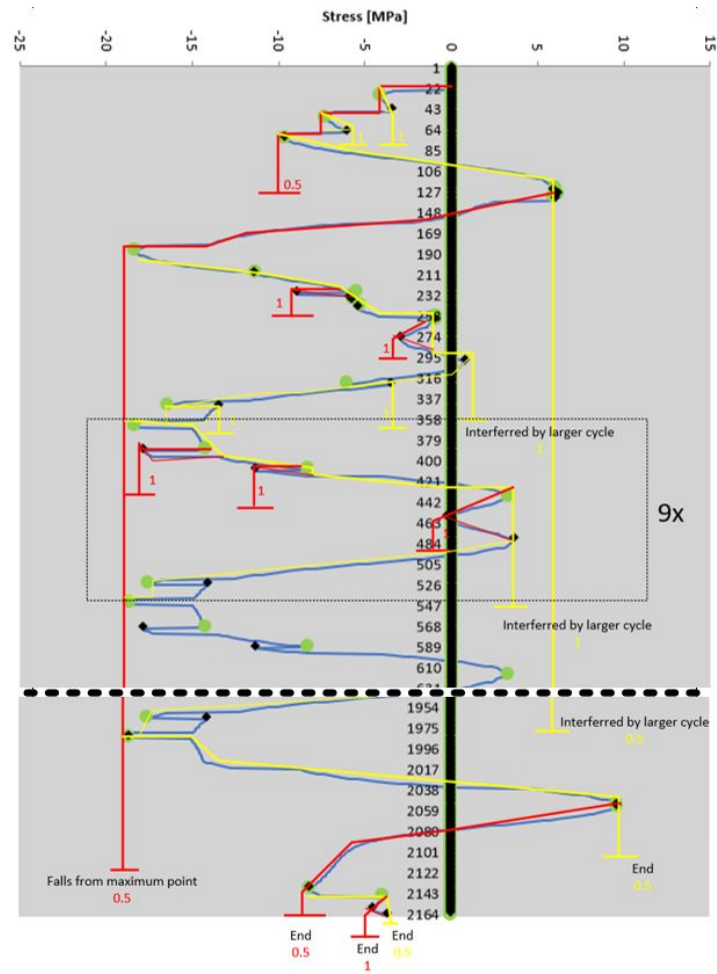
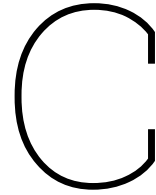


Figure B.2: Rainflow counting visualized (clipped stress plot), green dots are starting indexes and black dots are ending indexes determined by Python



Verification modeling technique

This section compares and verifies different weld modeling techniques using a reference model. As discussed in Section 2.4.1, if shell elements are used the weld can be modeled by increasing locally the thickness. This is especially important when the results are affected by local bending. Pandit [13] showed that a solid model gives a good estimation of reality, so the results of this model are used as a reference. The following modeling techniques are researched:

- Solid
- Shell without considering the weld
- Shell + weld IIW [18]
- Shell + weld Eriksson [35]
- Shell + weld IIW+Eriksson
- Shell + prTS 1993-1-901 [4]

The modeling techniques are compared on two cruciform joints with a longitudinal fillet weld and a transverse fillet weld, respectively. The geometry and dimensions are taken the same as in the research of Pandit [13], see Figure C.1 and Table C.1. The shell and solid models are modeled such that they are the same size. The shell model is modeled with mid-planes and the total height of the top/bottom plate is $H + \frac{t_b}{2}$. By comparing the results with the research of Pandit, the way of modeling is verified.

The stresses are determined between 0 [mm] and 50 [mm] perpendicular to the weld toe location, to the hot spot location. The hot spot location for the solid model is at the weld toe location. For the shell element model, the origin for stress extrapolation is at the intersection point between two adjacent plates. If the weld is modeled in the shell model, the hot spot location is taken at the weld toe location. This is in accordance with IIW [10].

The mesh size of all models is 1 [mm]. The mesh size of the model from Pandit is not known, so this can cause differences in the results. This report uses the FEM software Ansys® 2022 R2, while Pandit uses ABAQUS.

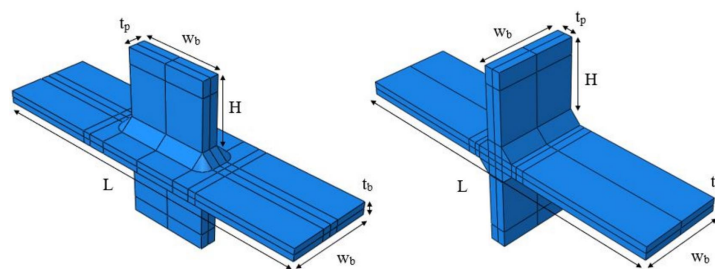


Figure C.1: Dimensions and geometry of cruciform joint, longitudinal (left) and transverse (right) [13]

Table C.1: Dimensions of cruciform joint, reference model [13]

Component	Abbreviation	Dimension [mm]
Length of the base plate	L	200
Height of the top and bottom plates	H	50
Thickness of the base plate	t_b	8
Thickness of the top and bottom plates	t_p	10
Width of the base plate	w_b	50
Width of the top and bottom plate	w_b	50
Throat thickness of the weld	a	5

C.1. Transverse fillet weld

In this research, four modeling techniques are used which are relevant for the transverse fillet weld: solid, shell, shell + weld Eriksson, and shell + weld prTS. The first three are based on the research of Pandit [13]. The same coordinate system, load cases, boundary conditions, and reading paths are considered as in the research of Pandit to make verification possible. Figure C.2 shows the numerical models of Pandit and Figure C.3 shows the numerical models for this research. The models are comparable.

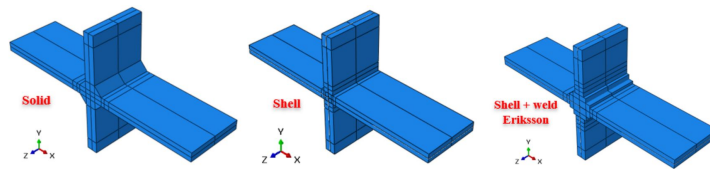
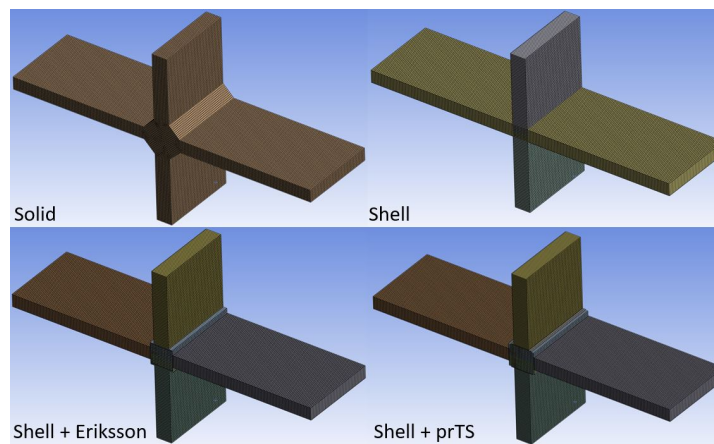
**Figure C.2:** Numerical models of the cruciform joint for different modeling techniques, transverse weld, reference [13]**Figure C.3:** Numerical models of the cruciform joint for different modeling techniques, transverse weld [3]

Figure C.4 shows the load cases and reading paths considered in the research of the cruciform joint with a transverse fillet weld. The load cases considered are:

- in-plane bending
- in-plane torsion
- out-of-plane torsion

The face and edge for the torsion load cases are taken 10 [mm] from the end of the top/bottom plates. The boundary conditions are placed at the mid-plane of the base plate. On one side is the displacement restricted in all directions and on the other side is the displacement free in x-direction.

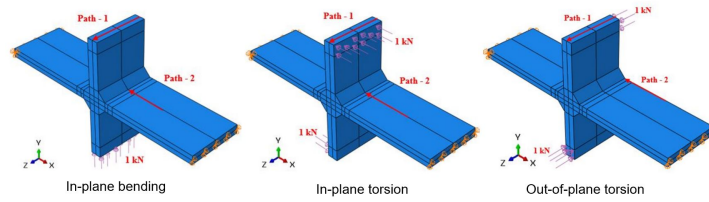


Figure C.4: Three load cases, transverse weld, reference model [13]

Figure C.28 to Figure C.8 shows the results for the load case in-plane bending. The results show the same order of magnitude as the research of Pandit. It can be concluded that all shell models where the weld is included show a good estimation of the behavior when compared to the solid model. However, the shell model without weld shows an overestimation of the stress, also at a distance x from the hot spot location.

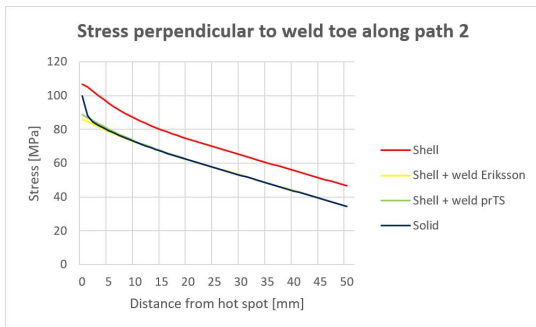


Figure C.5: Transverse fillet weld, in-plane bending stress

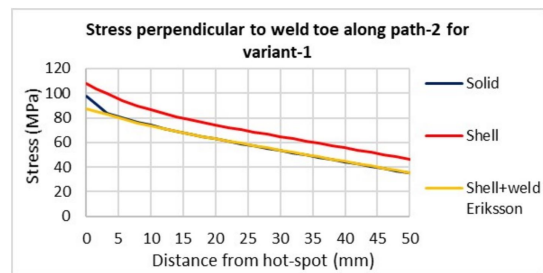


Figure C.6: Transverse fillet weld, in-plane bending stress, reference model [13]



Figure C.7: Transverse fillet weld, in-plane bending deformation

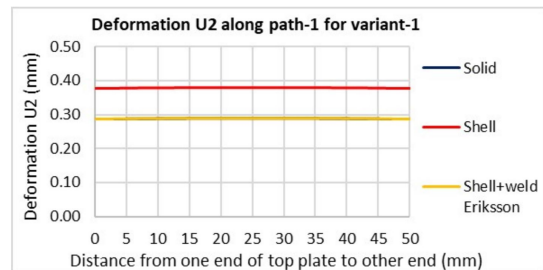


Figure C.8: Transverse fillet weld, in-plane bending deformation, reference model [13]

Figure C.30 to Figure C.12 shows the results for the load case in-plane torsion. Also, for this load case, the shell element model shows an overestimation of the stresses. All shell element models where the weld is included show good comparison with the solid model. The results have the same order of magnitude as the research of Pandit.

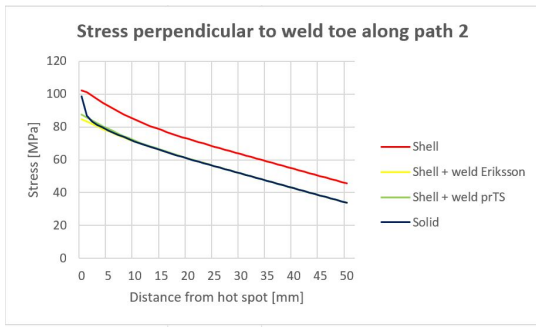


Figure C.9: Transverse fillet weld, in-plane torsion stress

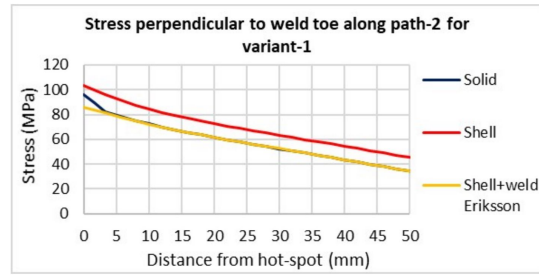


Figure C.10: Transverse fillet weld, in-plane torsion stress, reference model [13]



Figure C.11: Transverse fillet weld, in-plane torsion deformation

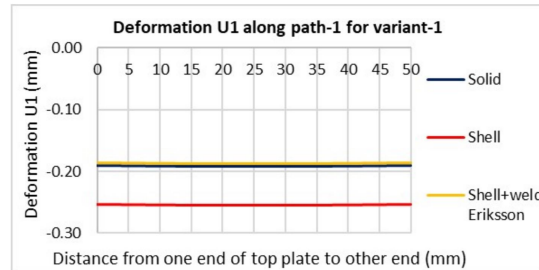


Figure C.12: Transverse fillet weld, in-plane torsion deformation, reference model [13]

Figure C.13 to Figure C.20 shows the results for the load case out-of-plane torsion. The results are comparable with the results of Pandit. It can be concluded that for this load case, the shell element model without the weld shows an overestimation of the stress. When the weld is modeled according to prTS1993-1-901 it also shows a small overestimation compared to the solid model.

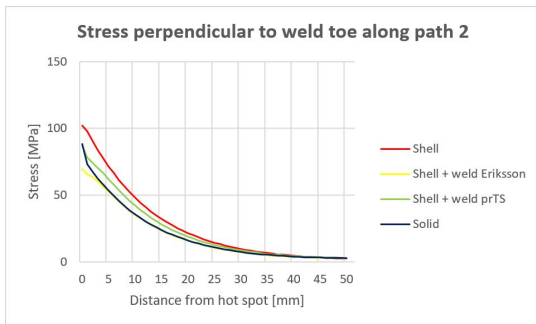


Figure C.13: Transverse fillet weld, out-of-plane torsion stress

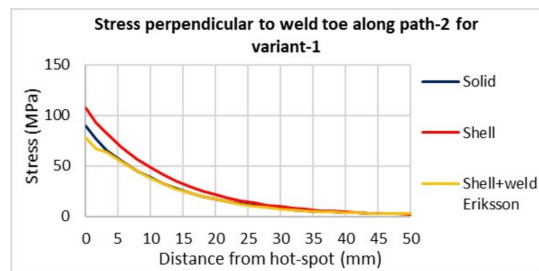


Figure C.14: Transverse fillet weld, out-of-plane torsion stress, reference model [13]



Figure C.15: Transverse fillet weld, out-of-plane torsion deformation X

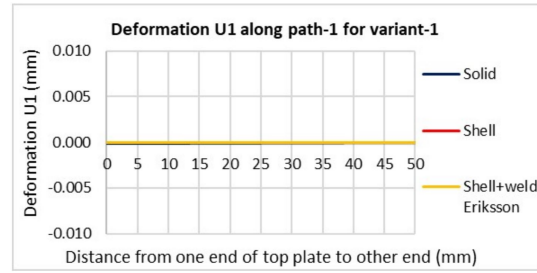


Figure C.16: Transverse fillet weld, out-of-plane torsion deformation X, reference model [13]

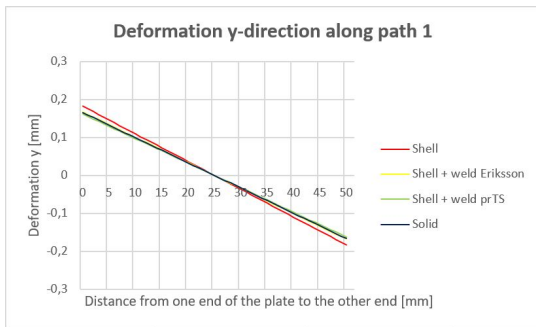


Figure C.17: Transverse fillet weld, out-of-plane torsion deformation Y

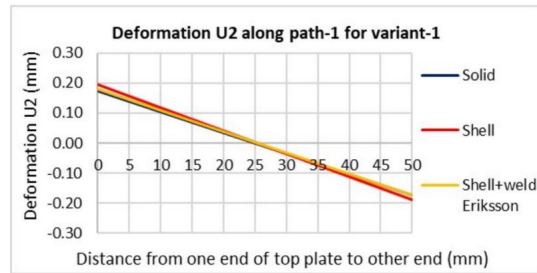


Figure C.18: Transverse fillet weld, out-of-plane torsion deformation Y, reference model [13]



Figure C.19: Transverse fillet weld, out-of-plane torsion deformation Z

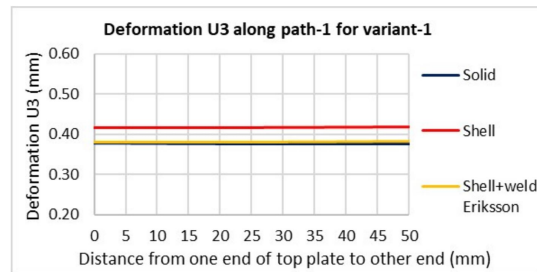


Figure C.20: Transverse fillet weld, out-of-plane torsion deformation Z, reference model [13]

Transverse double bevel weld

The same is done for a double bevel weld, see Figure C.23 for the geometry. Figure C.24 to Figure C.24 show the results for the same load cases used for the transverse fillet weld.

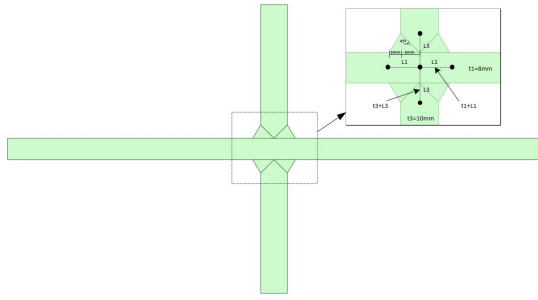


Figure C.21: Geometry double bevel weld

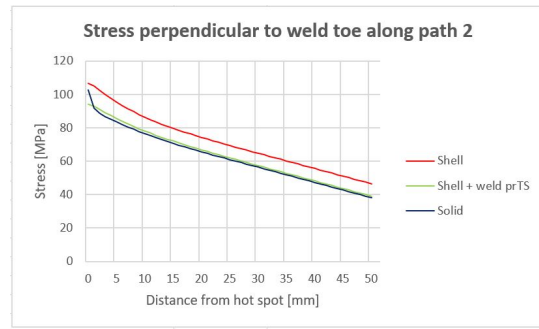


Figure C.22: Double bevel, in-plane bending stress

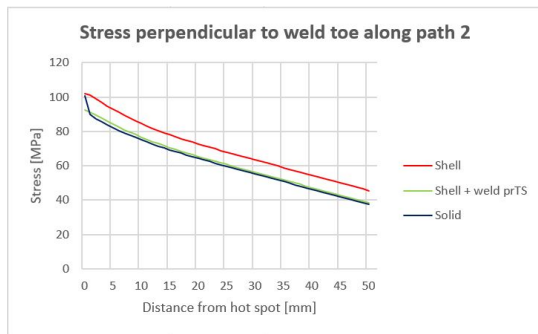


Figure C.23: Double bevel, in-plane torsion stress

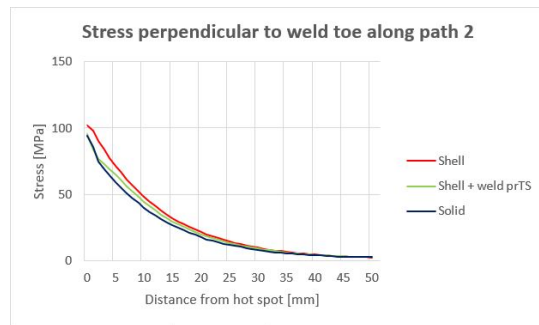


Figure C.24: Double bevel, out-of-plane bending stress

C.2. Longitudinal fillet weld

In this research, six modeling techniques are considered which are relevant for the longitudinal fillet weld: solid, shell, shell + weld IIW, shell + weld Eriksson, shell + weld IIW+Eriksson, and shell + weld prTS. The first five are based on the research of Pandit [13]. The same coordinate system, load cases, boundary conditions, and reading paths are considered as in the research of Pandit to make verification possible. Figure C.25 shows the numerical models of Pandit and Figure C.26 shows the numerical models for this research. The models are comparable.

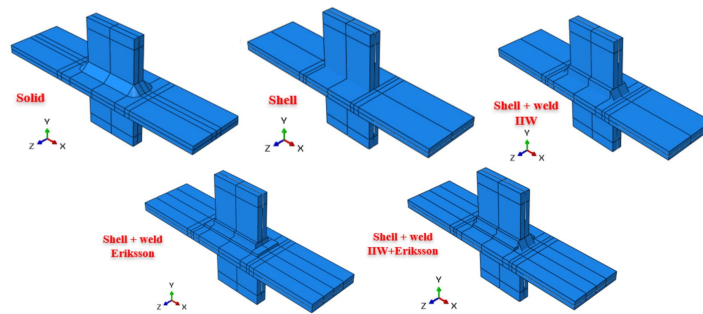


Figure C.25: Numerical models of the cruciform joint for different modeling techniques, longitudinal weld, reference [13]

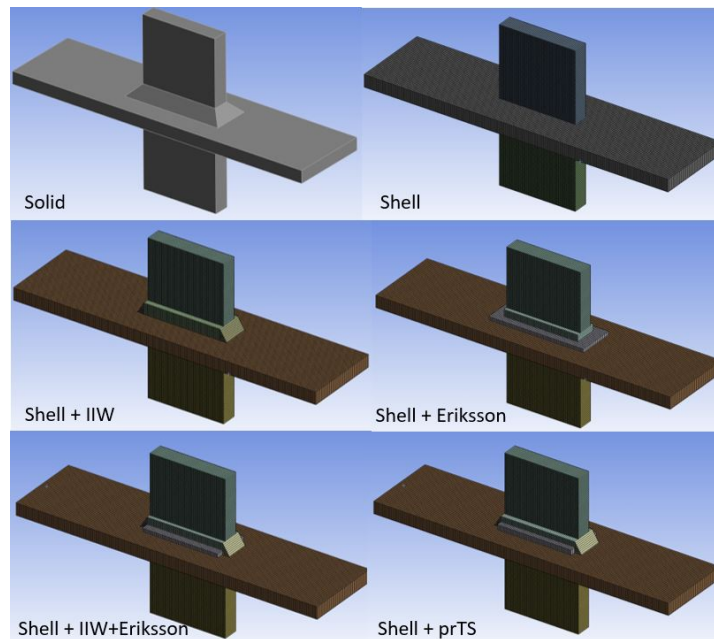


Figure C.26: Numerical models of the cruciform joint for different modeling techniques, longitudinal weld [3]

Figure C.27 shows the load cases and reading paths considered in the research of the cruciform joint with a longitudinal fillet weld. The load cases considered are:

- in-plane bending
- in-plane torsion

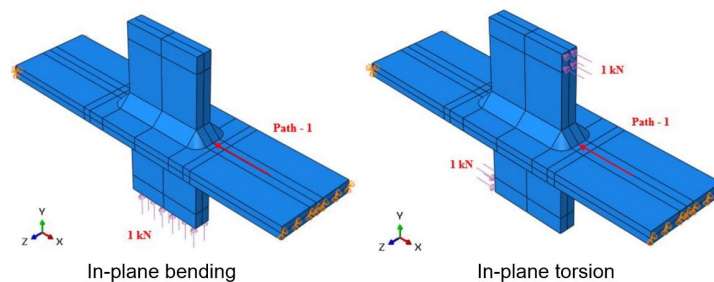


Figure C.27: Three load cases, longitudinal weld, reference model [13]

Figure C.28 shows the result for the load case in-plane bending. The results show the same order of magnitude as the research of Pandit, see Figure C.29. All modeling techniques where the weld is included in the shell element model show good comparison with the solid model. The shell element model without weld does overestimate the results.

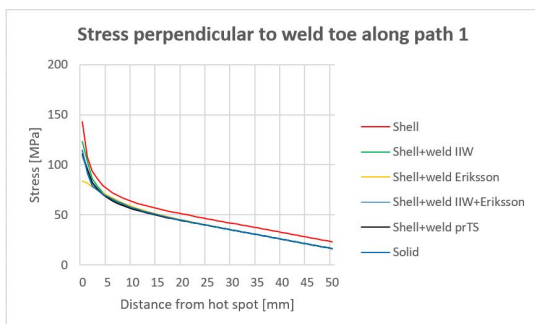


Figure C.28: Longitudinal fillet weld, in-plane bending

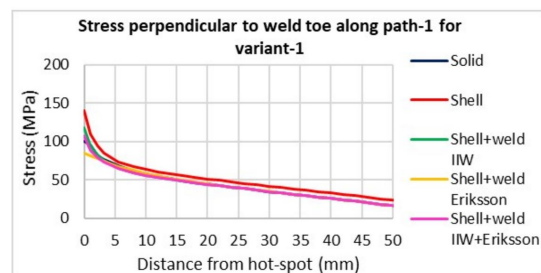


Figure C.29: Longitudinal fillet weld, in-plane bending stress, reference model [13]

Figure C.30 shows the result for the load case in-plane torsion. The results show the same order of magnitude as the research of Pandit, see Figure C.31. The shell element model shows a small overestimation of the results.

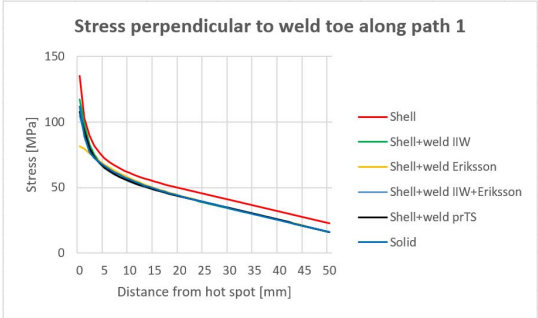


Figure C.30: Longitudinal fillet weld, in-plane torsion stress

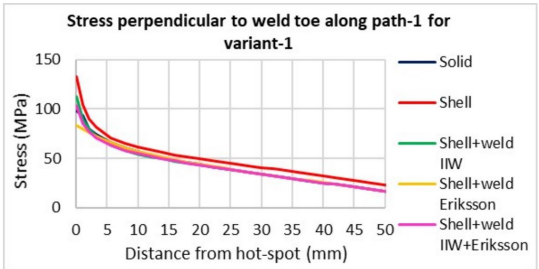


Figure C.31: Longitudinal fillet weld, in-plane bending, reference model [13]

D

Hand calculation versus Iv-Tool

The total damage of the three fatigue critical details (M1.1, M1.2 & M2) is calculated for the reference model configuration. The general methodology is described in Chapter 3. The calculation will be performed with the described Iv-Tool and compared with a hand calculation using Microsoft Excel.

The plate thickness in the shell element model is increased at the viewed location, according to prTS 1993-1-901 [4] guidelines, to consider the stiffness of the weld. This is at the location of the middle diaphragm (weld 1), between the three middle cross-girders (weld 2), and the middle cross-girder (weld 3). The increased thickness considered for the reference model is shown in Figure D.1.

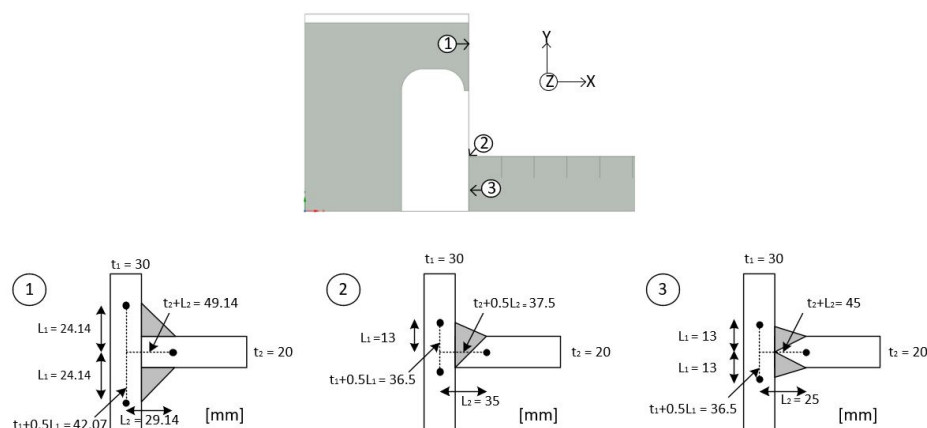


Figure D.1: Thickness increase at the location of the weld [mm]

The global mesh size is 175 [mm]. The mesh at the viewed location is refined to 50 [mm] with a sphere of influence with a radius of 2×1900 [mm]. At the location of the fatigue details the mesh is further refined to $0.4t$. The mesh refinement along weld 1 is 12 [mm] and weld 2 & 3 is 8 [mm]. The growth rate of the mesh is 1.1. So, the mesh size increases by 1.1 times the previous size each time as it moves further away from the defined location.

The fatigue damage is determined for in total three fatigue details, see Section 3.3. The detail category of all details is 100, if the hot spot method is used [9]. The stresses for detail M1.1 are always determined at the stiffener end in the y-direction, see Figure D.2. The stress for detail M1.2 is determined along weld 1 where the stress range is the highest. It is measured that this is always, for all parameters, the case at the stiffener end. The normal stress is determined in the z-direction. The hot spot method is used, so the stresses due to the unit load are read out at $0.4t = 12$ [mm] and $1.0t = 30$ [mm] from the weld toe location. The normal stress of M2 is read out in the x-direction at the top position of the

deck plate, see Figure D.3. Also, the hot spot method is applied to this detail and the reading points are: $0.4t = 8 [mm]$ and $1.0t = 20 [mm]$. However, the critical location along the weld can differ. There are two locations that can become governing for fatigue, namely at the location of the cross-girder web or at the location of the diaphragm. The location at the diaphragm is governing when the reference model is considered.

Ansys® 2022 R2 [3] determines the stress in the asked location per load step. There are in total 32 load steps, as described in Section 3.2 fatigue load. To determine the influence line for the different details, the unit load of $100 [kN]$ is scaled to a moving load of $1 [kN]$. The stress is determined at $0.4t$ and $1.0t$ from the weld toe per load step and per railway track. The HSS (influence line) is determined as: $\sigma_{h.s} = 1.67 \cdot \sigma_{0.4t} - 0.67 \cdot \sigma_{1.0t}$. Track 1 is considered on the side closest to the detail and track 2 is on the other side. In Figure D.4 and Figure D.5, the influence line due to the extrapolated hot spot stress per track is shown for detail M1.1 and M1.2, respectively. The influence lines for detail M2 are shown in Figure D.6.

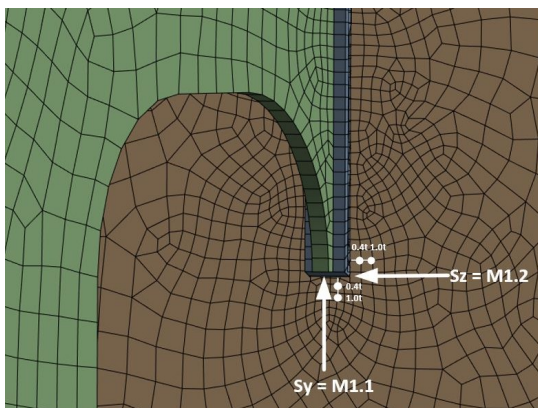


Figure D.2: Stress direction and reading points, detail M1.1 and M1.2 [3]

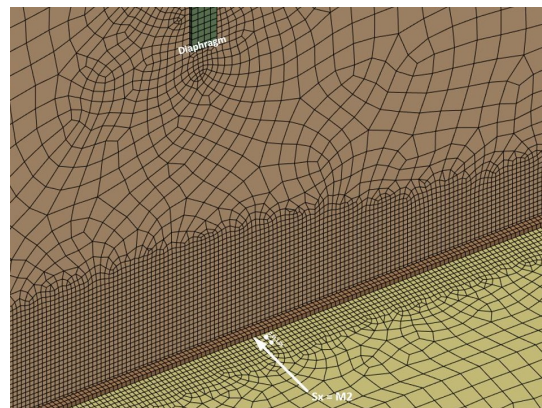


Figure D.3: Stress direction and reading points, detail M2 [3]

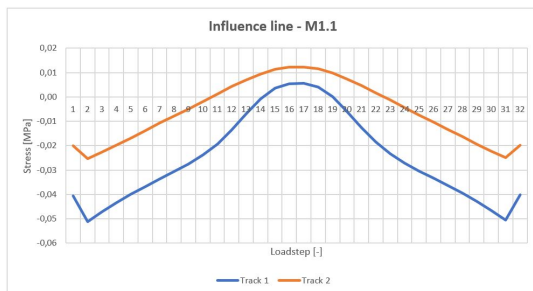


Figure D.4: Influence line M1.1

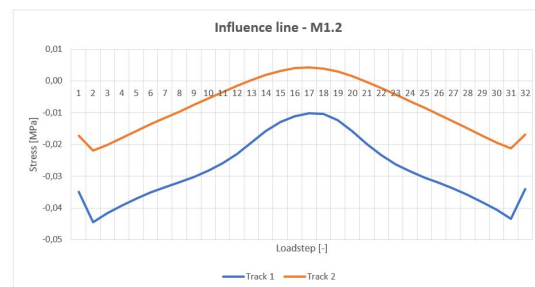


Figure D.5: Influence line M1.2

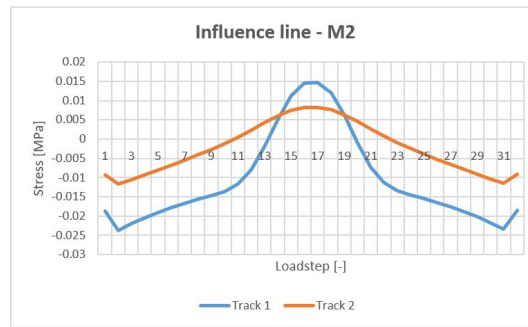


Figure D.6: Influence line M2

The dynamic factor that should be considered for each detail for the reference model is shown in Table D.1.

Table D.1: The dynamic factors for the reference model

Fatigue detail	L_ϕ [m]	K [-]	φ' [-]	φ'' [-]	$\phi = 1 + \frac{1}{2} \cdot (\varphi' + \frac{1}{2}\varphi'')$ [-]
M1.1	20	0.14	0.16	0.01	1.08
M1.2	20	0.14	0.16	0.01	1.08
M2	5.7	0.14	0.16	0.40	1.18

The same detail category, influence line, and dynamic factor that are determined in the hand calculation are used as input in the Iv-Tool. For hand calculation, Microsoft Excel macros are used. The four trains, from the heavy traffic mix, are "driven" over the influence line to determine the stress plots caused by the train loading. The step size with which the train drives over the influence line is chosen 0.6 [m] for the hand calculation and 0.1 [m] for the Iv-Tool. The Excel calculations take more time if the step size is taken smaller. Moreover, the hand calculation is less precise and a step size of 0.6 [m] will give a good estimation of the stress plot. With the hand calculation, an estimation of the stress ranges is made, while with the Iv-Tool the rainflow counting is executed precisely. The summation of two simultaneous trains on the bridge is done in the same way. The damage calculation of detail M1.1 will be worked out and compared for the hand calculation and Iv-Tool. The damage values of the other details are determined in the same manner.

Figure D.7 to Figure D.14 show the stress plots due to the trains from the traffic mix for detail M1.1 of the reference model. On the left, the stress plot due to hand calculation is shown, and on the right from Iv-Tool. It can be concluded that the stress plots are (almost) similar.



Figure D.7: Train 5, stress plot hand calculation

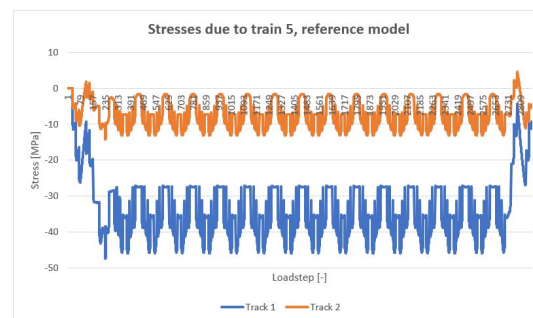


Figure D.8: Train 5, stress plot Iv-Tool

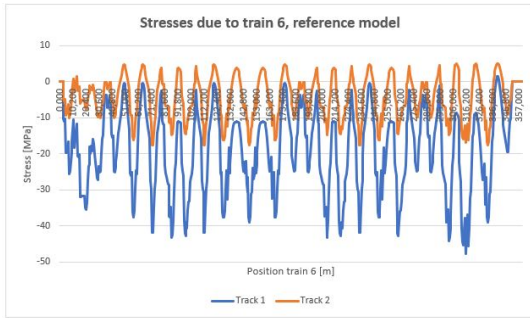


Figure D.9: Train 6, stress plot hand calculation

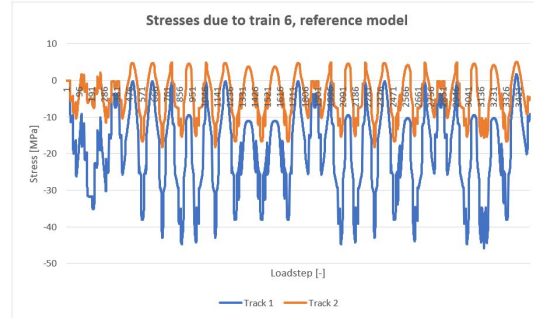


Figure D.10: Train 6, stress plot Iv-Tool

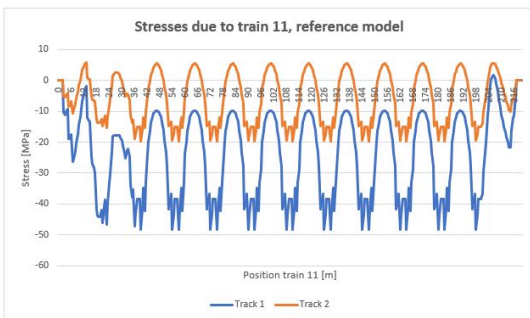


Figure D.11: Train 11, stress plot hand calculation

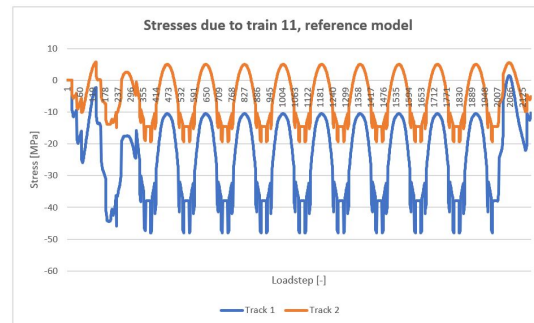


Figure D.12: Train 11, stress plot Iv-Tool

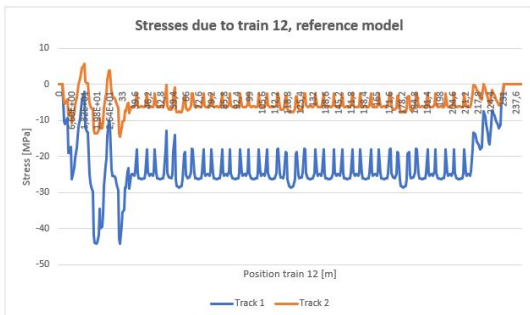


Figure D.13: Train 12, stress plot hand calculation

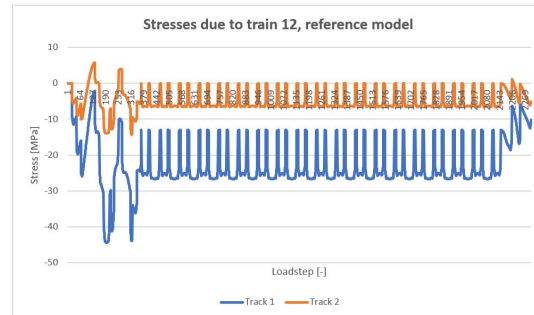


Figure D.14: Train 12, stress plot Iv-Tool

The hand calculation is shown in Table D.2. The assumption is made that for each train stress plot the maximum stress range is the maximum value minus the minimum value. One cycle of this value is accounted for in all cases. If there are (obviously) more cycles with a stress range that causes damage, these should also be accounted for. An estimation is made in this case. For detail M1.1 this is the case for train type 6 and train type 11. The estimation of the stress ranges is shown in Figure D.15 and Figure D.16. For train type 6, an extra 12 times a stress range of 41 [MPa] (track 1) and 20 [MPa] (track 2) is accounted for. These are also summed up in the case of simultaneity. For train 11, an extra 10 times a stress range of 40 [MPa] (track 1) and 25 [MPa] (track 2) is taken into account. The design number of load cases until failure (N_i) is determined with Formula 2.3. The 3 and 5 in N_3 and N_5 refer to the slope in the S-N curve that corresponds to the design stress range. The total damage for detail M1.1 becomes 1.61 [-].

Table D.2: Hand calculation reference model detail M1.1

Number of days per year	365 [days]								
Lifespan	100 [years]								
yMf	1.35 [-]								
Percentage of trains simultaneously	12 [%]								
Dyn. Factor	1.08 [-]								
ΔσC	100 [Mpa]								
ΔσC / yMf	74.07 [Mpa]	NC		2000000 [-]					
ΔσD	54.58 [Mpa]	ND		5000000 [-]					
ΔσL	29.98 [Mpa]	NL		100000000 [-]					

Train and track	Mass [tons]	Number of trains / day	Mass [tons] / year	Number of trains / lifespan	Δσ x dyn. Factor [Mpa]	N3 [-]	D3 [-]	N5 [-]	D5 [-]
Train 5 (track 1)	2160	5.28	4162752	192720	53.14			5715601	0.03
Train 5 (track 2)	2160	5.28	4162752	192720	19.46				
Train 5 (track 1+2)	4320	0.72	1135296	26280	72.60	2124317	0.01		
Train 6 (track 1)	1431	11.44	5975283.6	417560	53.30			5627776	0.07
Train 6 (track 2)	1431	11.44	5975283.6	417560	24.60				
Train 6 (track 1+2)	2862	1.56	1629622.8	56940	77.90	1719472	0.03		
Train 6 (track 1)	1431	11.44	5975283.6	417560	44.41			14017042	0.36
Train 6 (track 2)	1431	11.44	5975283.6	417560	21.66				
Train 6 (track 1+2)	2862	1.56	1629622.8	56940	66.07	2818019	0.24		
Train 11 (track 1)	1135	14.08	5832992	513920	54.12			5216440	0.10
Train 11 (track 2)	1135	14.08	5832992	513920	27.59				
Train 11 (track 1+2)	2270	1.92	1590816	70080	81.71	1489976	0.05		
Train 11 (track 1)	1135	14.08	5832992	513920	43.33			15858996	0.32
Train 11 (track 2)	1135	14.08	5832992	513920	27.08				
Train 11 (track 1+2)	2270	1.92	1590816	70080	70.41	2329128	0.30		
Train 12 (track 1)	1135	14.08	5832992	513920	47.88			9627151	0.05
Train 12 (track 2)	1135	14.08	5832992	513920	22.06				
Train 12 (track 1+2)	2270	1.92	1590816	70080	69.93	2376687	0.03		
								0.67	0.94
									1.61 [-]

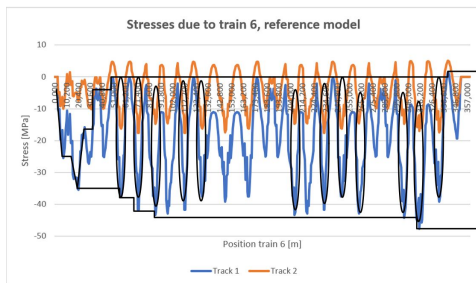


Figure D.15: Train 6, stress ranges hand calculation detail M1.1

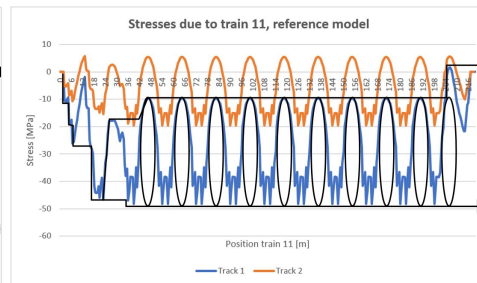


Figure D.16: Train 11, stress ranges hand calculation detail M1.1

The results of the Iv-Tool are shown in Table D.3. The total damage is equal to 1.57 [-]. This is almost equal to the cumulative damage of the hand calculation. The hand calculation is slightly higher because a rough estimation is made of the stress ranges. However, the difference is negligible for a fatigue damage calculation because the damage value changes fast if a value used in the calculation changes.

Table D.3: Iv-Tool calculation reference model detail M1.1

Track	Train type	Number of trains / day	Number of trains / lifespan	Cummulative damage [-]
Track 1	5	6	192720	0.02
Track 2	5	6	192720	0.00
Track 1+2	5	6	26280	0.02
Track 1	6	13	417560	0.40
Track 2	6	13	417560	0.00
Track 1+2	6	13	56940	0.40
Track 1	11	16	513920	0.31
Track 2	11	16	513920	0.00
Track 1+2	11	16	70080	0.30
Track 1	12	16	513920	0.06
Track 2	12	16	513920	0.00
Track 1+2	12	16	70080	0.05
				1.57 [-]

For the other details, the same approach is used. The results are shown in Table 4.1.

E

Deformed shapes

Figure E.1 and Figure E.2 show the total deformation of the reference model used for the parametric study for a unit load of 100 [kN] at load step 2 ($t = 2$ [s]) and load step 17 ($t = 17$ [s]), respectively. At load step 2, the unit load is at the beginning/end of the bridge, and at load step 17, the unit load is positioned at the middle of the bridge structure. The unit load is distributed by the rail, sleeper, and ballast, as described in Section 3.2). Only the railway track closest to the location of interest is considered (see Section 3.3). The results have been extracted from Ansys 2022 R2 [3].

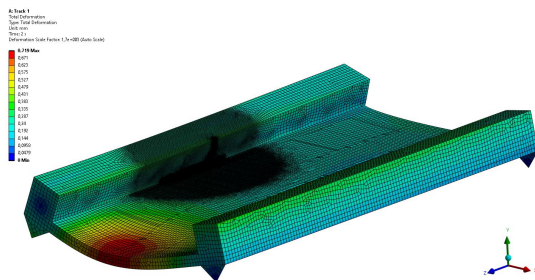


Figure E.1: Total deformation of total bridge structure at $t = 2$ [s] [3]

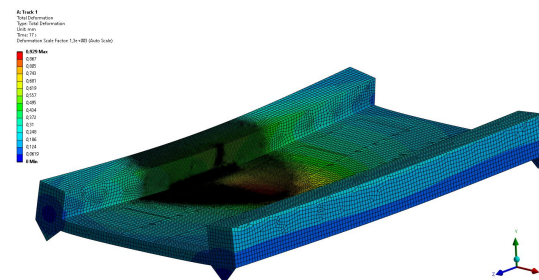


Figure E.2: Total deformation of total bridge structure at $t = 17$ [s] [3]

In Sections E.1 to Section E.7, for each parameter the deformed shapes of the cross-section are shown for the two extreme values considered in the parametric study. The cross-sectional deformation aligned with the middle diaphragm at $t = 2$ [s] and $t = 17$ [s] is considered. In this area, there is no cross-girder web, which allows for the deformation of the deck plate to be visible. These figures also include the equivalent stresses (Von Mises). In addition, the normal stress in the y-direction at the location of detail M1.1 (see Figure 3.11) is shown for load step 2. This load step results in the most significant (negative) stress value at this location when the load is moving over the length of the bridge. This is also the case when the load is at the end of the bridge.

E.1. The center-to-center distance between the cross-girders

In this section, the plots of the parameter, the center-to-center distance between the cross-girders, are shown. The figures show the deformed shape and Von Mises stresses for the cases where there are 4 and 10 cross-girders present. Also, the normal stresses in the y-direction at the location of fatigue detail M1.1 are shown at $t = 2$ [s].

$t = 2$ [s]

At $t = 2$ [s] a deformation scale factor of 1000 is applied.

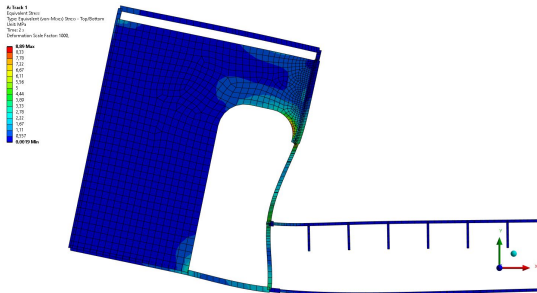


Figure E.3: Equivalent stress and deformed shape, No. of cg = 4 and $t = 2$ [s] [3]

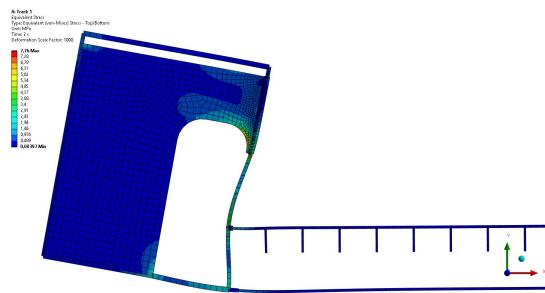


Figure E.4: Equivalent stress and deformed shape, No. of cg = 10 and $t = 2$ [s] [3]

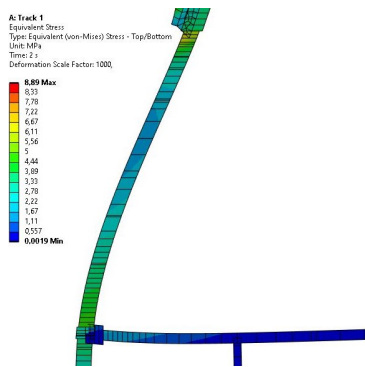


Figure E.5: Zoomed in, equivalent stress and deformed shape, No. of cg = 4 and $t = 2$ [s] [3]

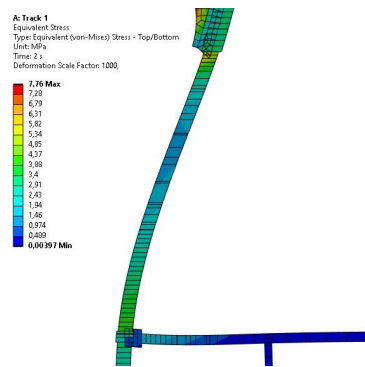


Figure E.6: Zoomed in, equivalent stress and deformed shape, No. of cg = 10 and $t = 2$ [s] [3]

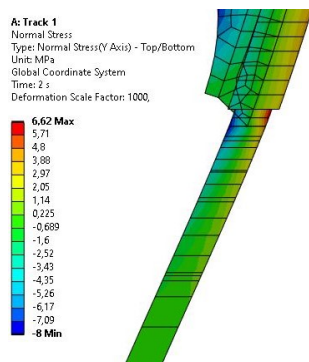


Figure E.7: Zoomed in at detail M1.1, normal stress in y-direction and deformed shape, No. of cg = 4 and $t = 2$ [s] [3]

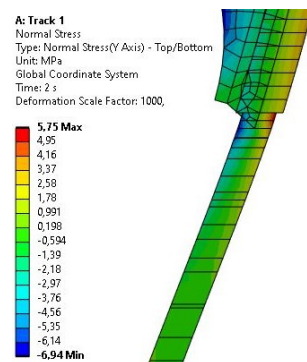


Figure E.8: Zoomed in at detail M1.1, normal stress in y-direction and deformed shape, No. of cg = 10 and $t = 2$ [s] [3]

$t = 17 [s]$

At $t = 17 [s]$ a deformation scale factor of 500 is applied.

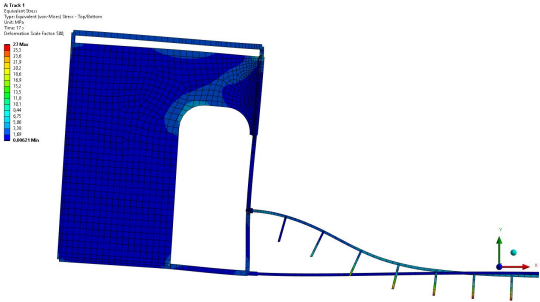


Figure E.9: Equivalent stress and deformed shape, No. of cg = 4 and $t = 17 [s]$ [3]

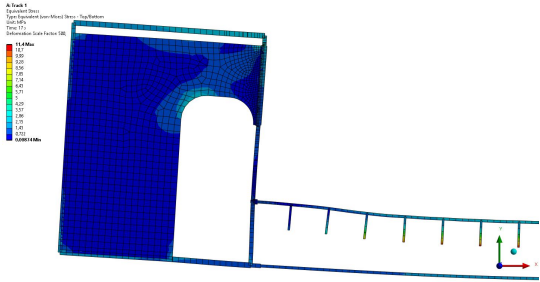


Figure E.10: Equivalent stress and deformed shape, No. of cg = 4 and $t = 17 [s]$ [3]

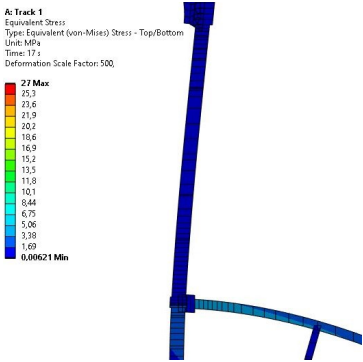


Figure E.11: Zoomed in, equivalent stress and deformed shape, No. of cg = 4 and $t = 17 [s]$ [3]

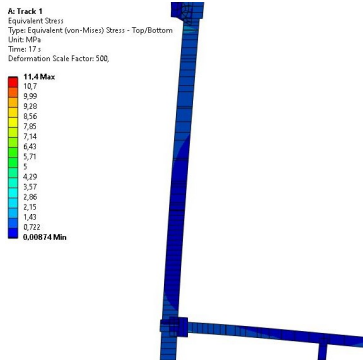


Figure E.12: Zoomed in, equivalent stress and deformed shape, No. of cg = 10 and $t = 17 [s]$ [3]

E.2. The height of the cross-girder

In this section, the plots of the parameter, the height of the cross-girder, are shown. The figures show the deformed shape and Von Mises stresses for a cross-girder height of 300 [mm], and 1000 [mm]. Also, the normal stresses in the y-direction at the location of fatigue detail M1.1 are shown at $t = 2$ [s].

$$t = 2 \text{ [s]}$$

At $t = 2$ [s] a deformation scale factor of 1000 is applied.

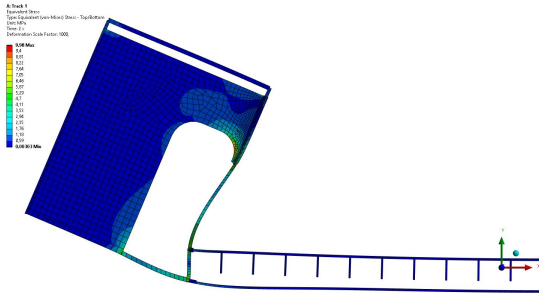


Figure E.13: Equivalent stress and deformed shape, $H_{cg} = 300$ [mm] and $t = 2$ [s] [3]

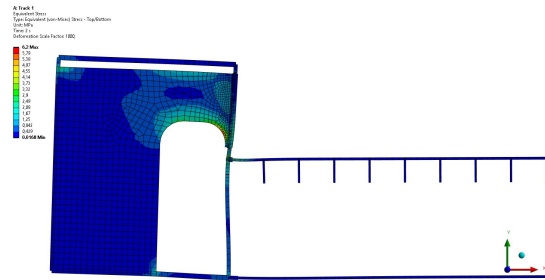


Figure E.14: Equivalent stress and deformed shape, $H_{cg} = 1000$ [mm] and $t = 2$ [s] [3]

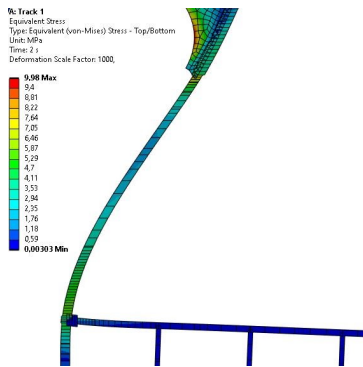


Figure E.15: Zoomed in, equivalent stress and deformed shape, $H_{cg} = 300$ [mm] and $t = 2$ [s] [3]

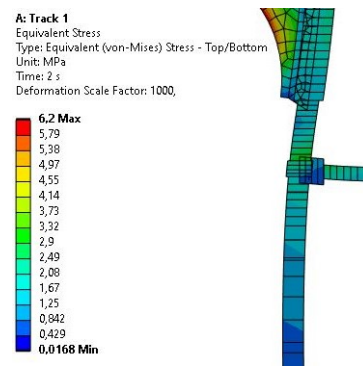


Figure E.16: Zoomed in, equivalent stress and deformed shape, $H_{cg} = 1000$ [mm] and $t = 2$ [s] [3]

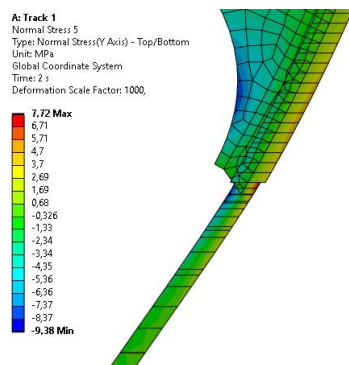


Figure E.17: Zoomed in at detail M1.1, normal stress in y-direction and deformed shape, $H_{cg} = 300$ [mm] and $t = 2$ [s] [3]

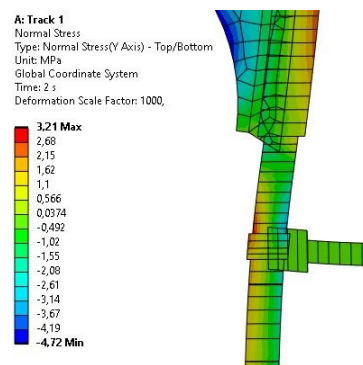


Figure E.18: Zoomed in at detail M1.1, normal stress in y-direction and deformed shape, $H_{cg} = 1000$ [mm] and $t = 2$ [s] [3]

$t = 17 [s]$

At $t = 17 [s]$ a deformation scale factor of 500 is applied.

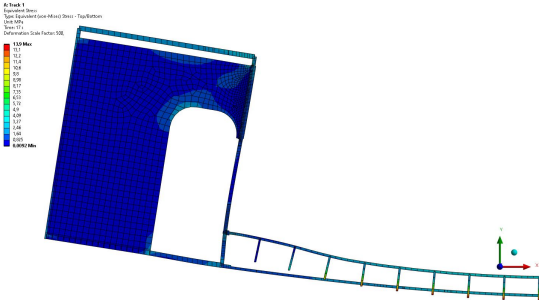


Figure E.19: Equivalent stress and deformed shape, $H_{cg} = 300 [mm]$ and $t = 17 [s]$ [3]

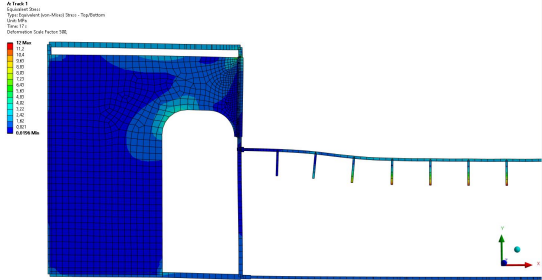


Figure E.20: Equivalent stress and deformed shape, $H_{cg} = 1000 [mm]$ and $t = 17 [s]$ [3]

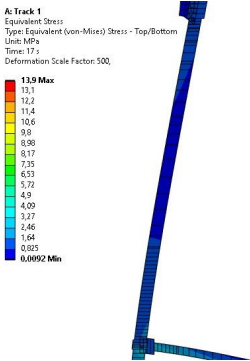


Figure E.21: Zoomed in, equivalent stress and deformed shape, $H_{cg} = 300 [mm]$ and $t = 17 [s]$ [3]

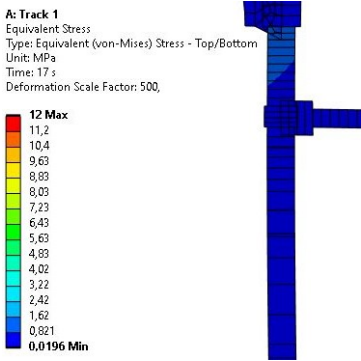


Figure E.22: Zoomed in, equivalent stress and deformed shape, $H_{cg} = 1000 [mm]$ and $t = 17 [s]$ [3]

E.3. The height of the main girder - increasing gap size

In this section, the plots of the parameter, the height of the main girder (increasing gap size), are shown. The figures show the deformed shape and Von Mises stresses for a main girder height of 1600 [mm], and 2400 [mm]. Also, the normal stresses in the y-direction at the location of fatigue detail M1.1 are shown at $t = 2$ [s].

$$t = 2 \text{ [s]}$$

At $t = 2$ [s] a deformation scale factor of 1500 is applied.

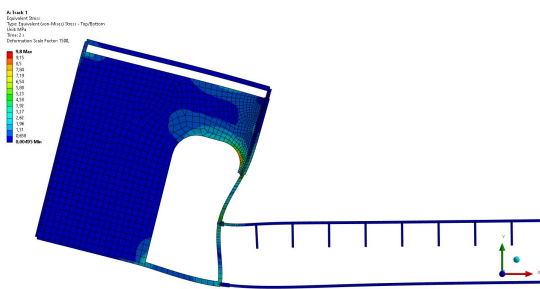


Figure E.23: Equivalent stress and deformed shape, $H_{mg} = 1600$ [mm] and $t = 2$ [s] [3]

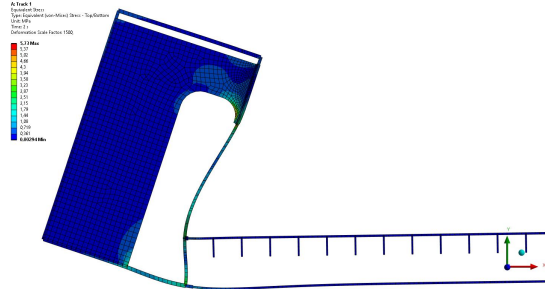


Figure E.24: Equivalent stress and deformed shape, $H_{mg} = 2400$ [mm] and $t = 2$ [s] [3]

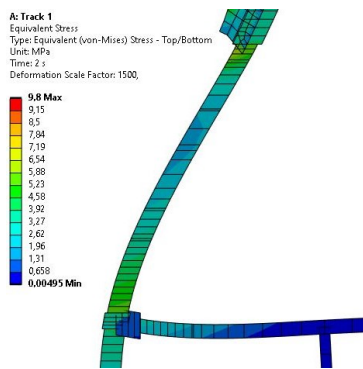


Figure E.25: Zoomed in, equivalent stress and deformed shape, $H_{mg} = 1600$ [mm] and $t = 2$ [s] [3]

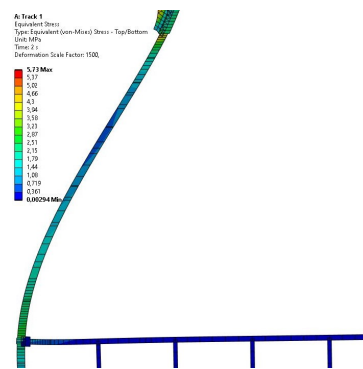


Figure E.26: Zoomed in, equivalent stress and deformed shape, $H_{mg} = 2400$ [mm] and $t = 2$ [s] [3]

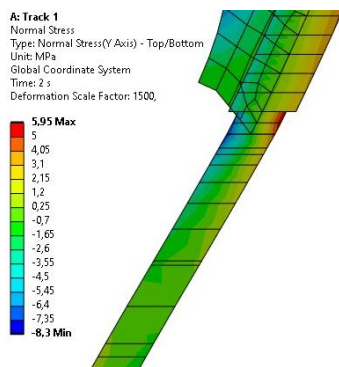


Figure E.27: Zoomed in at detail M1.1, normal stress in y-direction and deformed shape, $H_{mg} = 1600$ [mm] and $t = 2$ [s] [3]

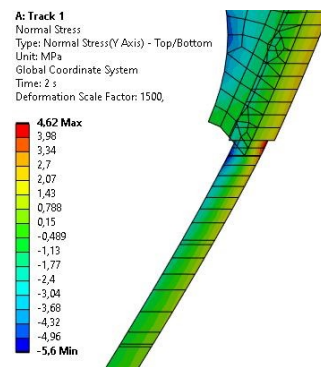


Figure E.28: Zoomed in at detail M1.1, normal stress in y-direction and deformed shape, $H_{mg} = 2400$ [mm] and $t = 2$ [s] [3]

$$t = 17 \text{ [s]}$$

At $t = 17 \text{ [s]}$ a deformation scale factor of 1700 is applied.

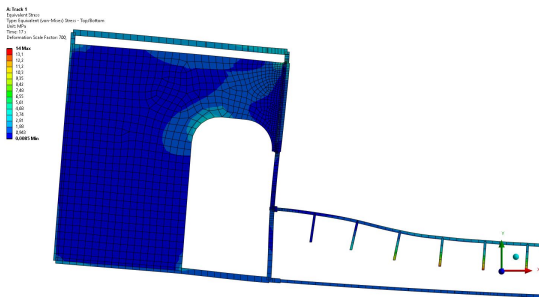


Figure E.29: Equivalent stress and deformed shape, $H_{mg} = 1600 \text{ [mm]}$ and $t = 17 \text{ [s]}$ [3]

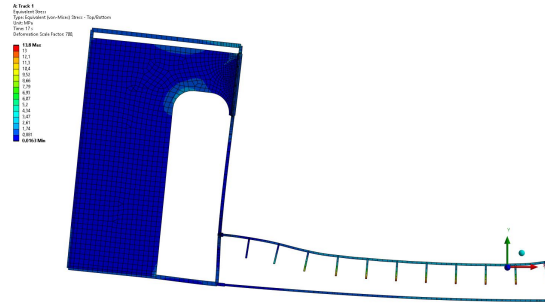


Figure E.30: Equivalent stress and deformed shape, $H_{mg} = 2400 \text{ [mm]}$ and $t = 17 \text{ [s]}$ [3]

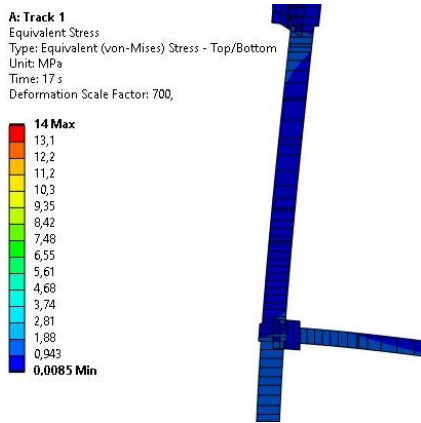


Figure E.31: Zoomed in, equivalent stress and deformed shape, $H_{mg} = 1600 \text{ [mm]}$ and $t = 17 \text{ [s]}$ [3]

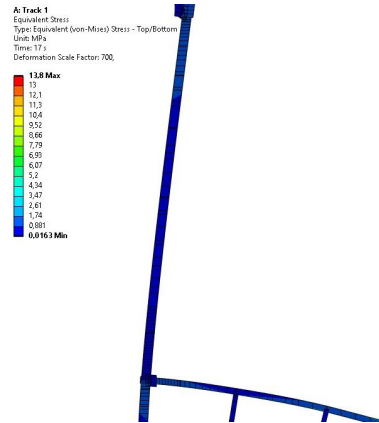


Figure E.32: Zoomed in, equivalent stress and deformed shape, $H_{mg} = 2400 \text{ [mm]}$ and $t = 17 \text{ [s]}$ [3]

E.4. The height of the main girder - same gap size

In this section, the plots of the parameter, the height of the main girder (same gap size), are shown. The figures show the deformed shape and equivalent stresses for a main girder height of 1900 [mm], and 2400 [mm]. Also, the normal stresses in the y-direction at the location of fatigue detail M1.1 are shown at $t = 2$ [s].

$$t = 2 \text{ [s]}$$

At $t = 2$ [s] a deformation scale factor of 1500 is applied.

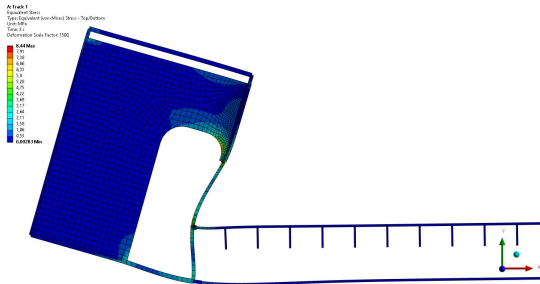


Figure E.33: Equivalent stress and deformed shape, $H_{mg} = 1900$ [mm] and $t = 2$ [s] [3]

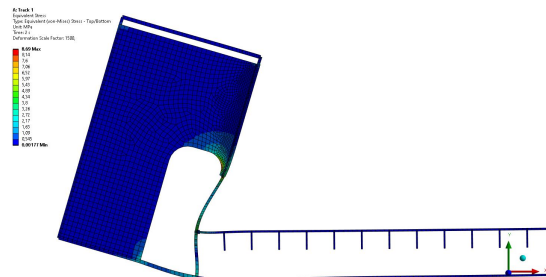


Figure E.34: Equivalent stress and deformed shape, $H_{mg} = 2400$ [mm] and $t = 2$ [s] [3]

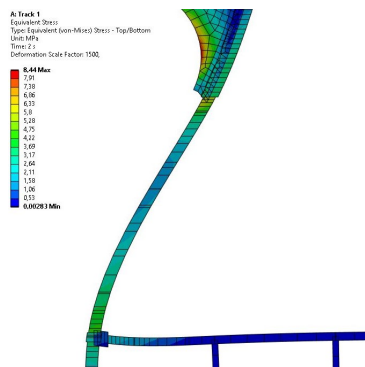


Figure E.35: Zoomed in, equivalent stress and deformed shape, $H_{mg} = 1900$ [mm] and $t = 2$ [s] [3]

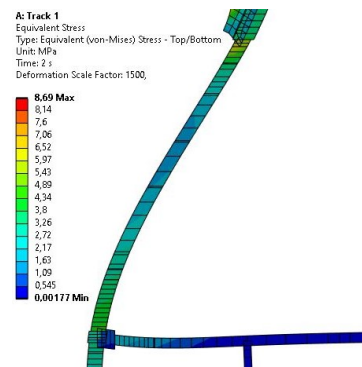


Figure E.36: Zoomed in, equivalent stress and deformed shape, $H_{mg} = 2400$ [mm] and $t = 2$ [s] [3]

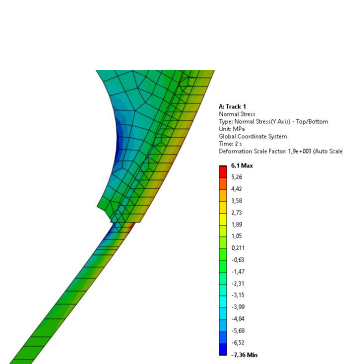


Figure E.37: Zoomed in at detail M1.1, normal stress in y-direction and deformed shape, $H_{mg} = 1900$ [mm] and $t = 2$ [s] [3]

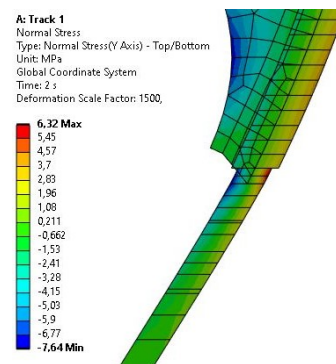


Figure E.38: Zoomed in at detail M1.1, normal stress in y-direction and deformed shape, $H_{mg} = 2400$ [mm] and $t = 2$ [s] [3]

$t = 17 [s]$

At $t = 17 [s]$ a deformation scale factor of 700 is applied.

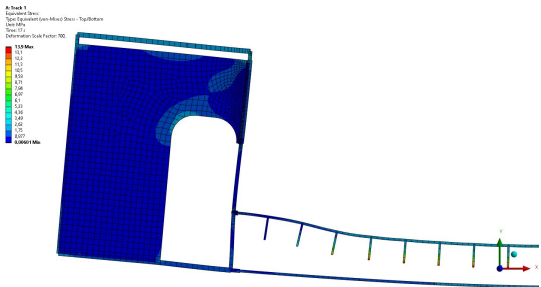


Figure E.39: Equivalent stress and deformed shape, $H_{mg} = 1900 [mm]$ and $t = 17 [s]$ [3]

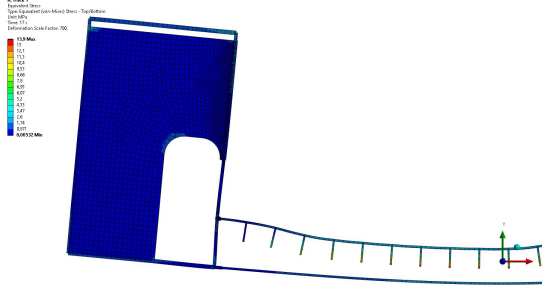


Figure E.40: Equivalent stress and deformed shape, $H_{mg} = 2400 [mm]$ and $t = 17 [s]$ [3]

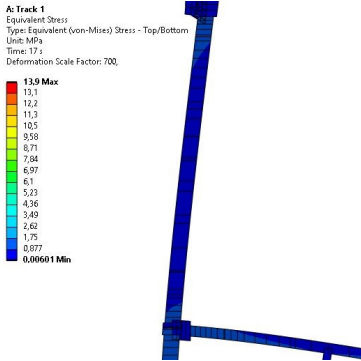


Figure E.41: Zoomed in, equivalent stress and deformed shape, $H_{mg} = 1900 [mm]$ and $t = 17 [s]$ [3]



Figure E.42: Zoomed in, equivalent stress and deformed shape, $H_{mg} = 2400 [mm]$ and $t = 17 [s]$ [3]

E.5. The thickness of the inner web of the main girder

In this section, the plots of the parameter, the thickness of the inner web of the main girder, are shown. The figures show the deformed shape and Von Mises stresses for a main girder inner web thickness of 10 [mm], and 50 [mm]. Also, the normal stresses in the y-direction at the location of fatigue detail M1.1 are shown at $t = 2$ [s].

$$t = 2 \text{ [s]}$$

At $t = 2$ [s] a deformation scale factor of 1500 is applied.

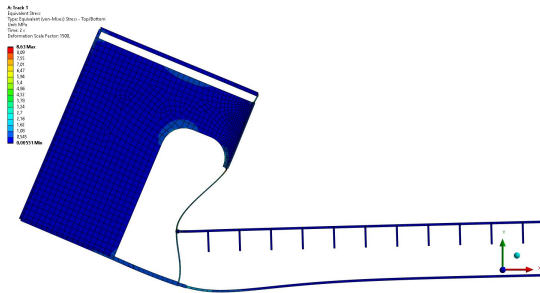


Figure E.43: Equivalent stress and deformed shape, $T_{mg} = 10$ [mm] and $t = 2$ [s] [3]

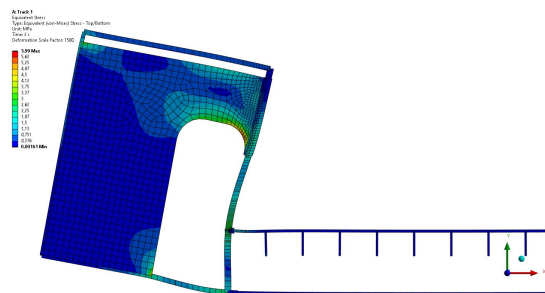


Figure E.44: Equivalent stress and deformed shape, $T_{mg} = 50$ [mm] and $t = 2$ [s] [3]

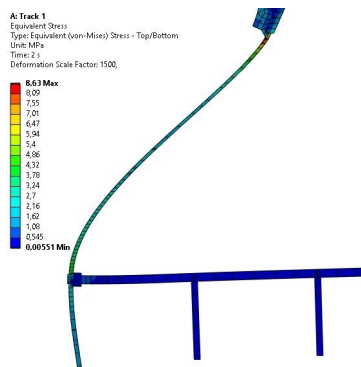


Figure E.45: Zoomed in, equivalent stress and deformed shape, $T_{mg} = 10$ [mm] and $t = 2$ [s] [3]

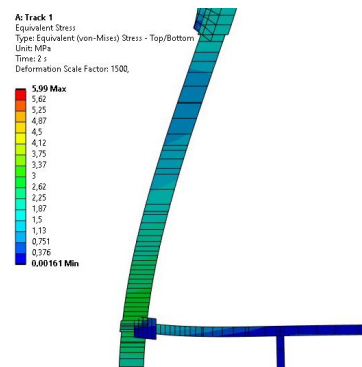


Figure E.46: Zoomed in, equivalent stress and deformed shape, $T_{mg} = 50$ [mm] and $t = 2$ [s] [3]

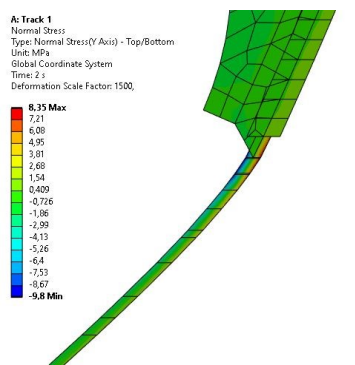


Figure E.47: Zoomed in at detail M1.1, normal stress in y-direction and deformed shape, $T_{mg} = 10$ [mm] and $t = 2$ [s] [3]

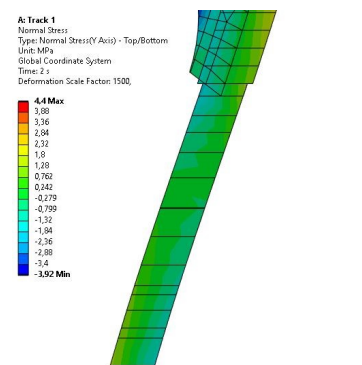


Figure E.48: Zoomed in at detail M1.1, normal stress in y-direction and deformed shape, $T_{mg} = 50$ [mm] and $t = 2$ [s] [3]

$t = 17 [s]$

At $t = 17 [s]$ a deformation scale factor of 700 is applied.

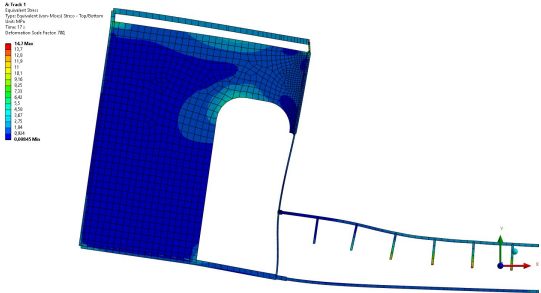


Figure E.49: Equivalent stress and deformed shape, $T_{mg} = 10 [mm]$ and $t = 17 [s]$ [3]

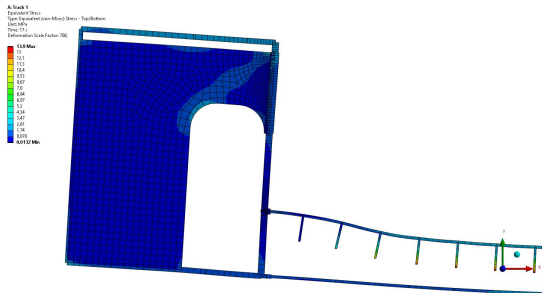


Figure E.50: Equivalent stress and deformed shape, $T_{mg} = 50 [mm]$ and $t = 17 [s]$ [3]

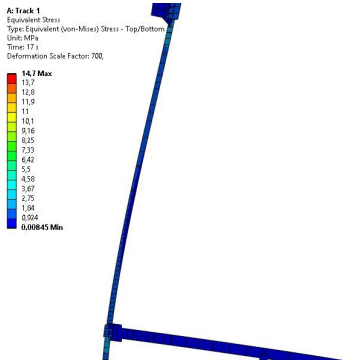


Figure E.51: Zoomed in, equivalent stress and deformed shape, $T_{mg} = 10 [mm]$ and $t = 17 [s]$ [3]

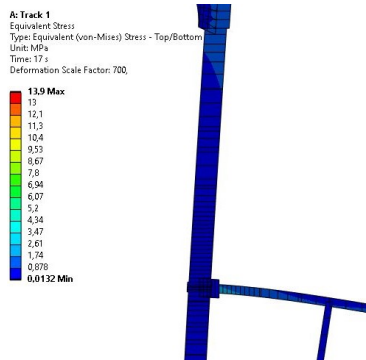


Figure E.52: Zoomed in, equivalent stress and deformed shape, $T_{mg} = 50 [mm]$ and $t = 17 [s]$ [3]

E.6. The thickness of the diaphragm

In this section, the plots of the parameter, the thickness of the diaphragm, are shown. The figures show the deformed shape and equivalent stresses for a diaphragm thickness of 10 [mm], and 30 [mm]. Also, the normal stresses in the y-direction at the location of fatigue detail M1.1 are shown at $t = 2$ [s].

$$t = 2 \text{ [s]}$$

At $t = 2$ [s] a deformation scale factor of 2000 is applied.

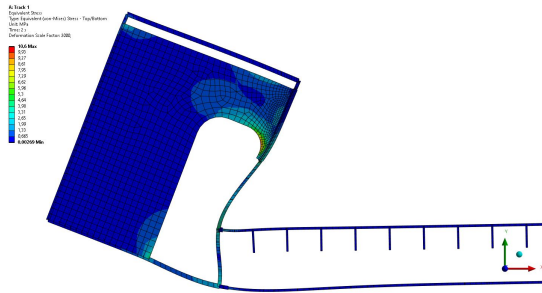


Figure E.53: Equivalent stress and deformed shape, $T_{dia} = 10$ [mm] and $t = 2$ [s] [3]

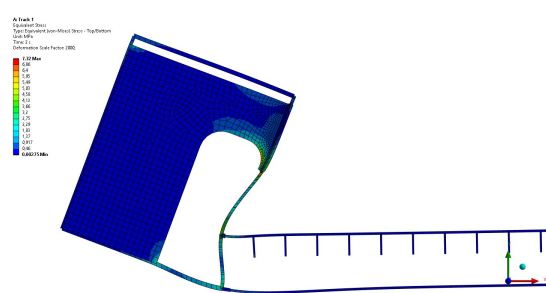


Figure E.54: Equivalent stress and deformed shape, $T_{dia} = 30$ [mm] and $t = 2$ [s] [3]

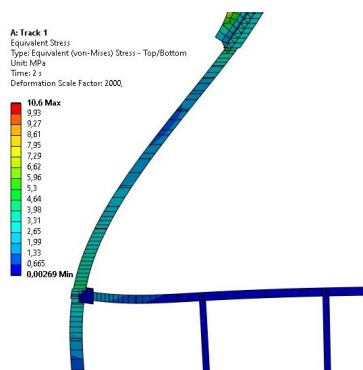


Figure E.55: Zoomed in, equivalent stress and deformed shape, $T_{dia} = 10$ [mm] and $t = 2$ [s] [3]

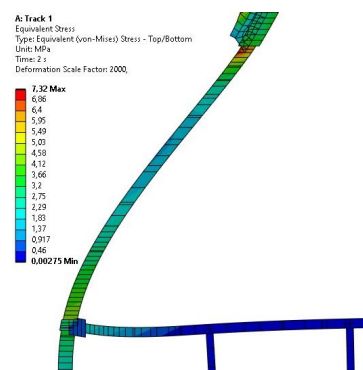


Figure E.56: Zoomed in, equivalent stress and deformed shape, $T_{dia} = 30$ [mm] and $t = 2$ [s] [3]

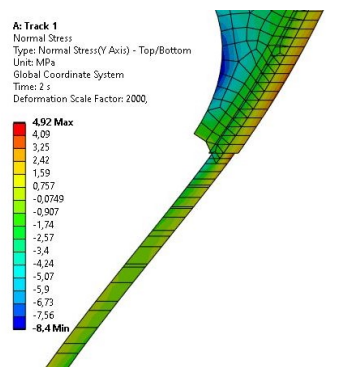


Figure E.57: Zoomed in at detail M1.1, normal stress in y-direction and deformed shape, $T_{dia} = 10$ [mm] and $t = 2$ [s] [3]

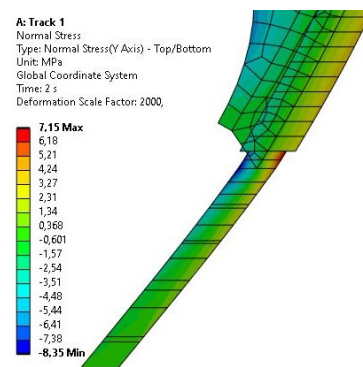


Figure E.58: Zoomed in at detail M1.1, normal stress in y-direction and deformed shape, $T_{dia} = 30$ [mm] and $t = 2$ [s] [3]

$t = 17 [s]$

At $t = 17 [s]$ a deformation scale factor of 700 is applied.

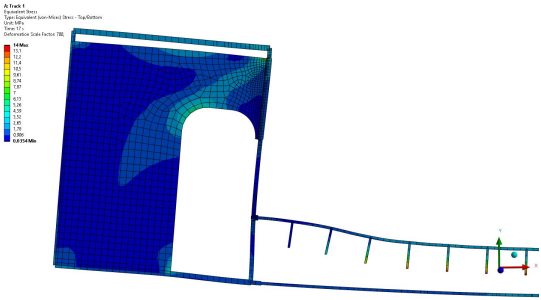


Figure E.59: Equivalent stress and deformed shape, $T_{dia} = 10 [mm]$ and $t = 17 [s]$ [3]

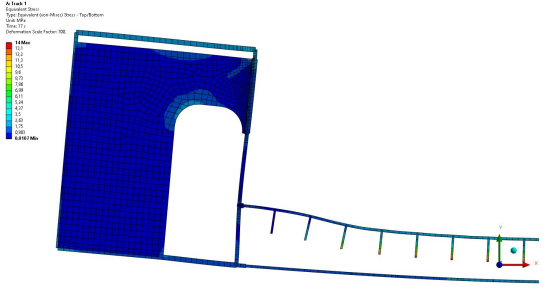


Figure E.60: Equivalent stress and deformed shape, $T_{dia} = 30 [mm]$ and $t = 17 [s]$ [3]



Figure E.61: Zoomed in, equivalent stress and deformed shape, $T_{dia} = 10 [mm]$ and $t = 17 [s]$ [3]



Figure E.62: Zoomed in, equivalent stress and deformed shape, $T_{dia} = 30 [mm]$ and $t = 17 [s]$ [3]

E.7. The thickness of the steel deck plate

In this section, the plots of the parameter, the thickness of the steel deck plate, are shown. The figures show the deformed shape and equivalent stresses for deck plate thickness of 10 [mm], and 40 [mm]. Also, the normal stresses in the y-direction at the location of fatigue detail M1.1 are shown at $t = 2$ [s].

$$t = 2 \text{ [s]}$$

At $t = 2$ [s] a deformation scale factor of 2000 is applied.

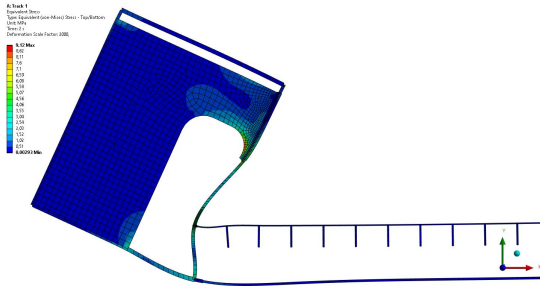


Figure E.63: Equivalent stress and deformed shape, $T_{deck} = 10$ [mm] and $t = 2$ [s] [3]

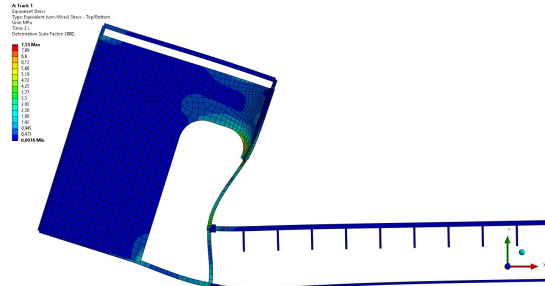


Figure E.64: Equivalent stress and deformed shape, $T_{deck} = 40$ [mm] and $t = 2$ [s] [3]

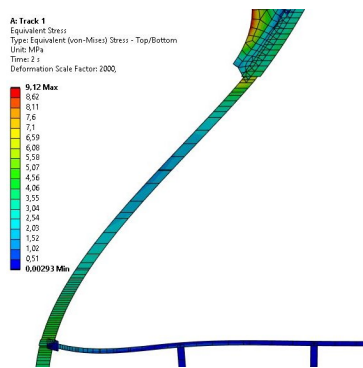


Figure E.65: Zoomed in, equivalent stress and deformed shape, $T_{deck} = 10$ [mm] and $t = 2$ [s] [3]



Figure E.66: Zoomed in, equivalent stress and deformed shape, $T_{deck} = 40$ [mm] and $t = 2$ [s] [3]

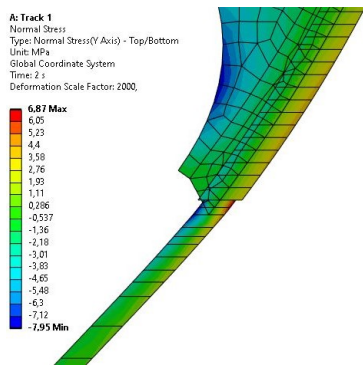


Figure E.67: Zoomed in at detail M1.1, normal stress in y-direction and deformed shape, $T_{deck} = 10$ [mm] and $t = 2$ [s] [3]

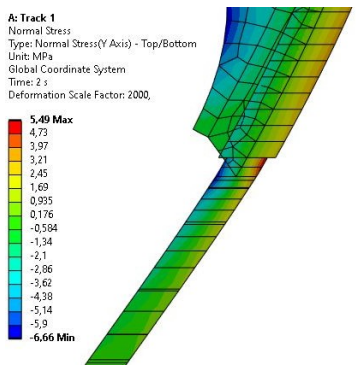


Figure E.68: Zoomed in at detail M1.1, normal stress in y-direction and deformed shape, $T_{deck} = 40$ [mm] and $t = 2$ [s] [3]

$$t = 17 \text{ [s]}$$

At $t = 17 \text{ [s]}$ a deformation scale factor of 700 is applied.

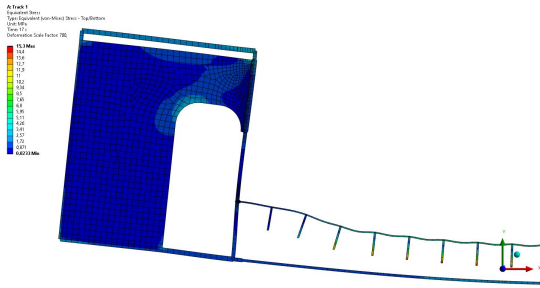


Figure E.69: Equivalent stress and deformed shape, $T_{deck} = 10 \text{ [mm]}$ and $t = 17 \text{ [s]}$ [3]

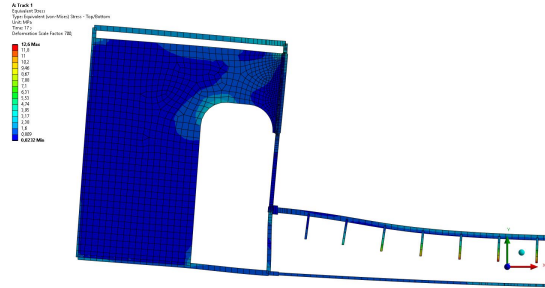


Figure E.70: Equivalent stress and deformed shape, $T_{deck} = 40 \text{ [mm]}$ and $t = 17 \text{ [s]}$ [3]

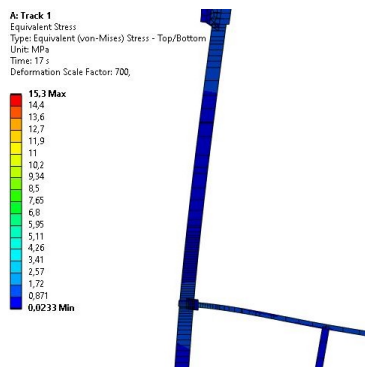


Figure E.71: Zoomed in, equivalent stress and deformed shape, $T_{deck} = 10 \text{ [mm]}$ and $t = 17 \text{ [s]}$ [3]

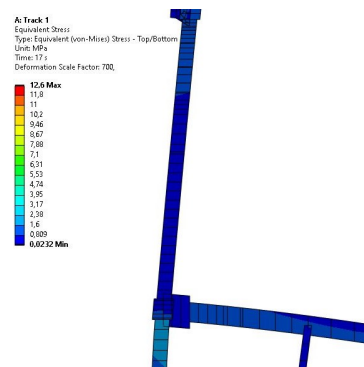


Figure E.72: Zoomed in, equivalent stress and deformed shape, $T_{deck} = 40 \text{ [mm]}$ and $t = 17 \text{ [s]}$ [3]

F

Results fatigue detail M3

Figure F.1 visualizes the location of fatigue detail M3 and the parameters. Section F.1 to F.6 show the fatigue damage results for each parameter. The hot spot stress method is used. The detail category considered is 100, see Figure 3.12.

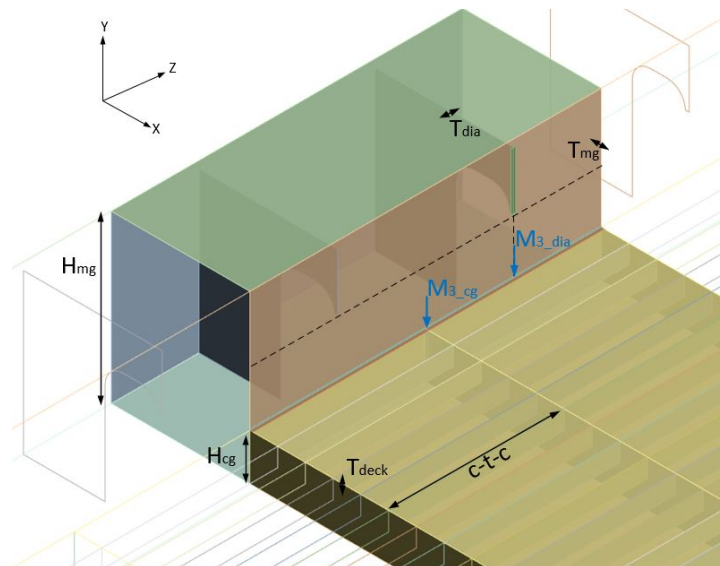


Figure F.1: Visualisation of the parameters and fatigue detail M3 [3]

The dynamic factor considered in the parametric study is given in Table F.1.

Table F.1: Dynamic factor, fatigue detail M3 [53]

Fatigue detail	L_ϕ [m]	K [-]	φ' [-]	φ'' [-]	$\phi = 1 + \frac{1}{2} \cdot (\varphi' + \frac{1}{2} \varphi'')$ [-]
M3	20	0.14	0.16	0.01	1.08

Concentrated nominal surface stresses are measured at detail M3 in the y-direction, see Figure F.2.

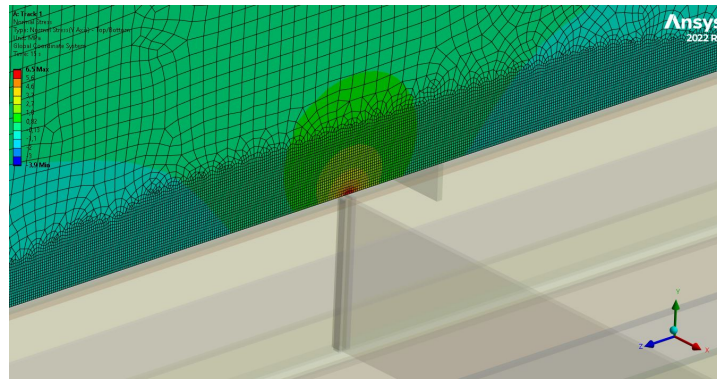


Figure F.2: Concentrated stress in y-direction at detail M3 at $t = 15$ [s], reference model [3]

F.1. The center-to-center distance between the cross-girders

The fatigue damage is determined for 4, 8, and 10 cross-girders. The numerical results are shown in Table F.2.

In Figure F.3 the line of best fit between the measured data points is shown. The linear regression lines of all considered fatigue details are combined in Figure F.4. The m - and R^2 -value of the best linear fit for fatigue detail M3, based on three measured data points, are: $m = -0.9907$ and $R^2 = 0.9493$.

The damage value decreases with an increasing number of cross-girders. An increasing number of cross-girders decreases the deformation of the deck plate. The main girder inner web has to deform less at detail M3, which reduces the concentrated stresses.

Table F.2: Damage detail M3, parameter: the center-to-center distance between the cross-girders

No. of cg	c-t-c cg [mm]	Damage M3 [-]	Location M3
4	3420	10.31	cg
8	1900	5.29	cg
10	1555	4.63	cg

Abbreviations: no. = number, c-t-c= center-to-center, cg = cross-girder
 Elaboration: in bold = the results of the reference model

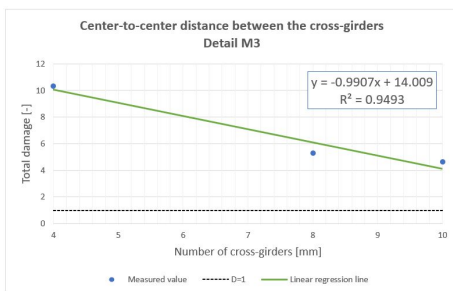


Figure F.3: Linear regression detail M3: c-t-c

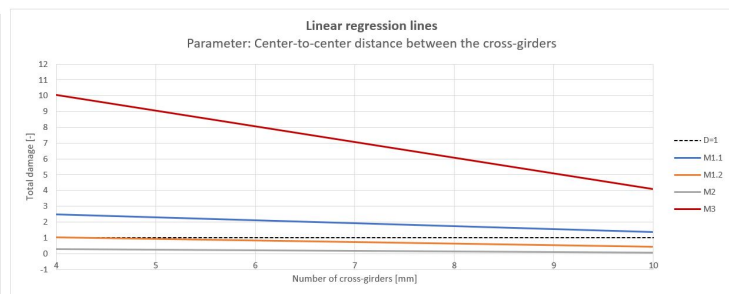


Figure F.4: Linear regression lines: c-t-c

F.2. The height of the cross-girder

The total fatigue damage is determined for a cross-girder height of 300, 500, and 1000 [mm]. The numerical results are shown in Table F.3.

In Figure F.5 the line of best fit between the measured data points is shown. The linear regression lines of all considered fatigue details are combined in Figure F.6. The m - and R^2 -value of the linear regression line are: $m = -0.0121$ and $R^2 = 0.9378$.

The less deformation of the cross-girder by increasing the height causes the inner web of the main girder to deform less. This decreases the stresses at detail M3.

Table F.3: Damage detail M3, parameter: the height of the cross-girder

Height of cg [mm]	Damage M3 [-]	Location M3
300	9.88	cg
500	5.29	cg
1000	0.85	dia

Abbreviations: cg = cross-girder, dia = diaphragm
 Elaboration: in bold = the results of the reference model

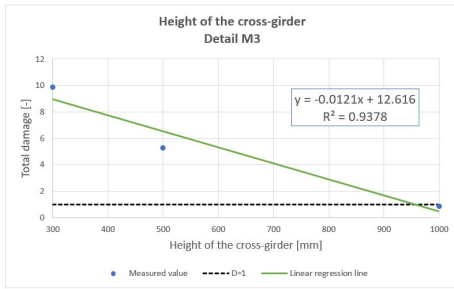


Figure F.5: Linear regression detail M3: H_{cg}

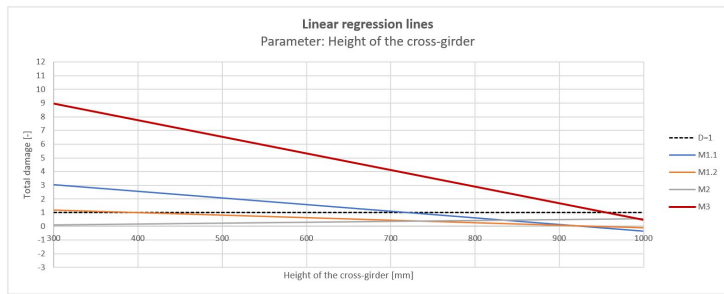


Figure F.6: Linear regression lines: H_{cg}

F.3. The height of the main girder - increasing gap size

The total fatigue damage is determined for a main girder height of 1600, 1800, and 2400 [mm]. The numerical results are shown in Table F.4.

In Figure F.7 the line of best fit between the measured data points is shown. The linear regression lines of all considered fatigue details are combined in Figure F.8. The m - and R^2 -value of the linear regression line are: $m = -0.0031$ and $R^2 = 0.9457$.

Increasing the height of the main girder results in more flexibility of the main girder inner web reducing the stresses at detail M3.

Table F.4: Damage detail M3, parameter: the height of the main girder- increasing gap size

Height main girder [mm]	Damage M3 [-]	Location M3
1600	5.31	cg
1800	5.29	cg
2400	2.98	cg

Abbreviations: cg = cross-girder
 Elaboration: in bold = the results of the reference model



Figure F.7: Linear regression detail M3: H_{mg}

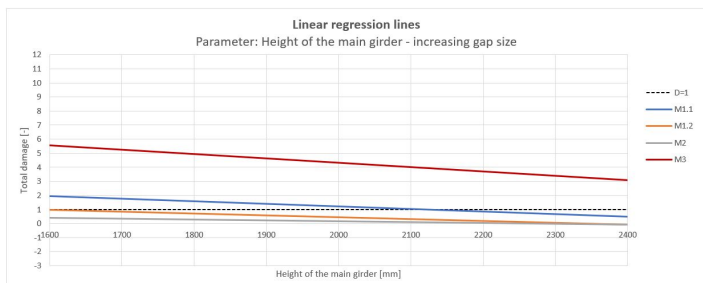


Figure F.8: Linear regression lines: H_{mg}

F.4. The thickness of the inner web of the main girder

The total fatigue damage is determined for a main girder inner web thickness of 10, 30, and 50 [mm]. The numerical results are shown in Table F.5.

In Figure F.9 the linear line of best fit between the measured data points is shown. The linear regression lines of all considered fatigue details are combined in Figure F.10 for the parameter the thickness of the inner web of the main girder. The m - and R^2 -value of the linear regression line are: $m = -0.1583$ and $R^2 = 0.9948$.

The results show a decrease in the total fatigue damage when increasing the thickness of the inner web of the main girder. A thicker web has a larger cross-sectional area and is stiffer from itself. There is less difference in stiffness over the height of the main girder web which reduces concentrated stresses. The deck, however, can deform less at the attachment to the main girder, which increases stresses at detail M2. In addition, because the hot spot stress method is used, the stresses are read at a location further from the weld toe location ($0.4t$ and $1.0t$). This reduces also the measured stresses at detail M3.

Table F.5: Damage detail M3, parameter: the thickness of the inner web of the main girder

Thickness inner web [mm]	Damage M3 [-]	Location M3
10	8.85	cg
30	5.29	cg
50	2.52	cg

Abbreviations: cg = cross-girder

Elaboration: in bold = the results of the reference model

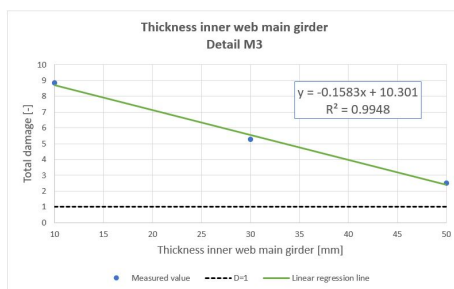


Figure F.9: Linear regression detail M3: T_{mg}



Figure F.10: Linear regression lines: T_{mg}

F.5. The thickness of the diaphragm

The total fatigue damage is determined for a diaphragm thickness of 10, 20, and 30 [mm]. The numerical results are shown in Table F.6.

In Figure F.11 the linear line of best fit between the measured data points is shown. The linear regression lines of all considered fatigue details are combined in Figure F.12. The m - and R^2 -value of the linear regression line are: $m = 0.0245$ and $R^2 = 0.9316$. The diaphragm thickness does not influence the fatigue damage of detail M3 a lot. The overall stability of the main girder influences slightly the stresses at M3. The position of the diaphragm is at a distance from the critical location, so will not locally influence the results.

Table F.6: Damage detail M3, parameter: the thickness of the diaphragm

Thickness diaphragm [mm]	Damage M3 [-]	Location M3
10	4.93	cg
20	5.29	cg
30	5.42	cg

Abbreviations: cg = cross-girder

Elaboration: in bold = the results of the reference model

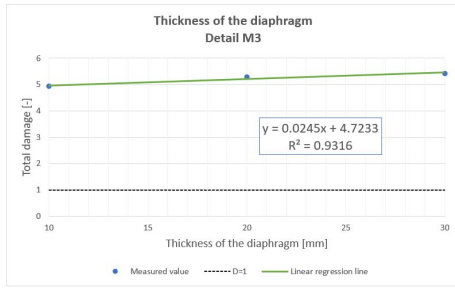


Figure F.11: Linear regression detail M3: T_{dia}

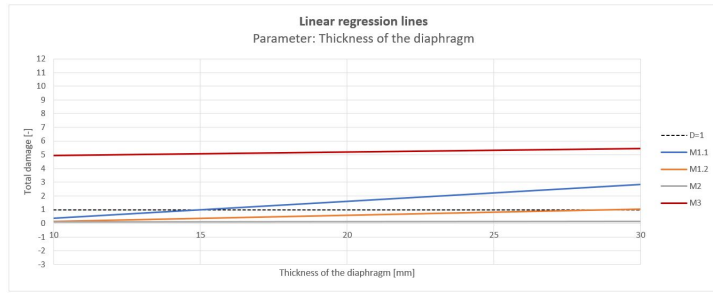


Figure F.12: Linear regression lines: T_{dia}

F.6. The thickness of the steel deck plate

The total fatigue damage is determined for a deck plate thickness of 10, 20, and 40 [mm]. The numerical results are shown in Table F.7.

In Figure F.13 the line of best fit between the measured data points is shown. The linear regression lines of all considered fatigue details are combined in Figure F.14. The m - and R^2 -value of the linear regression line are: $m = -0.3326$ and $R^2 = 0.8998$.

increasing the thickness of the deck plate will reduce the deformation of the deck. As a result, the main girder inner web has to deform less which reduces the stresses at detail M3.

Table F.7: Damage detail M3, parameter: the thickness of the steel deck plate

Thickness deck plate [mm]	Damage M3 [-]	Location M3
10	11.82	cg
20	5.29	cg
40	1.2	cg

Abbreviations: cg = cross-girder
Elaboration: in bold = the results of the reference model

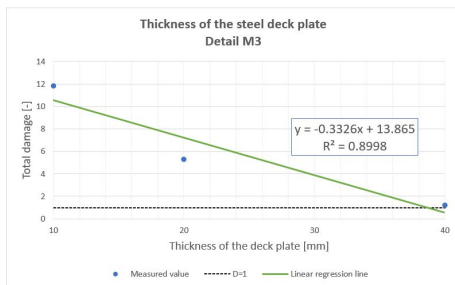


Figure F.13: Linear regression detail M3: T_{deck}

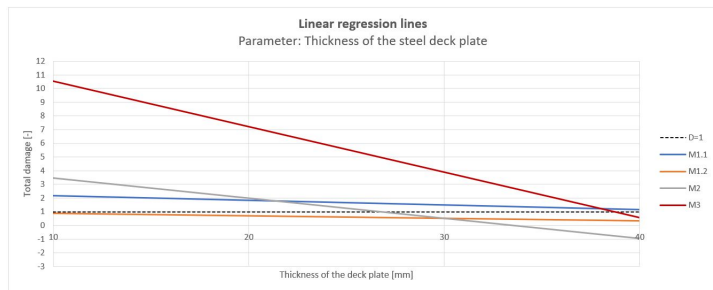


Figure F.14: Linear regression lines: T_{deck}

F.7. Cost-effectiveness of the parameters for detail M3

In Table F.8, the costs per damage change for each parameter are sorted by magnitude. The costs are determined using the same method as in Section 4.2. The parameter offering the most cost-effective means of reducing damage by 1 unit will be most interesting to change when designing for fatigue. In the case the thickness of the diaphragm is optimized for fatigue design of detail M3, costs will be saved. For the remaining parameters, costs need to be incurred to reduce the damage at detail M3. The most cost-effective methods are increasing the cross-girder height, reducing the center-to-center distance between the cross-girders, and increasing the thickness of the inner web of the main girder. However, these methods will not reduce the damage value to below 1.

Table F.8: Sorted costs per damage detail M3, in bold: results that require attention

Parameter	Costs [€] / damage	€↑ D↓
<i>H_{cg}</i>	2357	+
<i>c-t-c</i>	1299744	+
<i>T_{mg}</i>	 3570436 	+
<i>T_{deck}</i>	4251594	+
<i>H_{mg}</i>	4532942	+
<i>T_{dia}</i>	15179776	-

Abbreviations: €↑ D↓ = increase (+) or decrease (-) of the costs when reducing the damage value